REPORT DOCUMENTATION PAGE

Form Approved
OMB No. 0704-0188

Public reporting burden for this collection of information is estimated to average 1 hour per response, including the time for reviewing instructions, searching existing data sources, gathering and maintaining the data needed, and completing and reviewing the collection of information. Send comments regarding this burden estimate or any other aspect of this collection of information, including suggestions for reducing this burden, to Washington Headquarters Services, Directorate for Information Operations and Reports, 1215 Jefferson Davis Highway, Suite 1204, Arlington, VA 22202-4302, and to the Office of Management and Budget, Paperwork Reduction Project (0704-0188), Washington, DC 20503.

1. AGENCY USE ONLY (Leave blank)	2. REPORT DATE	3. REPORT TYPE AND DATES COVERED
	August 31, 1995	Final Technical 1/15/92-6/30/95

4. TITLE AND SUBTITLE

VORTEX DYNAMICS AND SEPARATION OVER PITCHING WINGS

5. FUNDING NUMBERS

F49620-92-J-0146

AFOSR-TR
95-0645

6. AUTHOR(S)

B. R. Ramaprian

7. PERFORMING ORGANIZATION NAME(S) AND ADDRESS(ES)

School of Mechanical and Materials Engineering
Washington State University
Pullman, WA   99164-2920

8. PERFORMING ORGANIZATION REPORT NUMBER

9. SPONSORING / MONITORING AGENCY NAME(S) AND ADDRESS(ES)

Dr. Leonidas Sakell/NA
AFOSR/NA
110 Duncan Avenue, Suite B115
Bolling AFB, DC   20332-0001

NA

10. SPONSORING / MONITORING AGENCY REPORT NUMBER

F49620-92-J-0146

11. SUPPLEMENTARY NOTES
The views, opinions and/or findings contained in this report are those of the author(s) and should not be construed as an official Department of the Army position, policy, or decision, unless so designated by other documentation.

12a. DISTRIBUTION / AVAILABILITY STATEMENT

Approved for public release; distribution unlimited.

12b. DISTRIBUTION CODE

DTIC ELECTE
OCT 17 1995
F

13. ABSTRACT (Maximum 200 words)

This project, aimed at an extensive study of the unsteady vortex dynamics and separation of pitching wings, started on January 15, 1992 and terminated on June 30, 1995. However, there was a reduction in the scope of the Project after January 1994 because of a cut in the budget. Even so, significant accomplishments were made in the project. These included extensive documentation of the 2-D velocity and vorticity field around a pitching NACA 0015 wing at a Reynolds number of 150,000, and extensive surface pressure and velocity data in the 3-D flow over a pitching swept wing of the same profile. The velocity data were obtained using the technique of Particle Image Velocimetry (PIV) developed during a prior AFOSR Grant. The data have been used to understand the physics of 2-D and 3-D vortex dynamics/separation in unsteady flows. The data have been archived carefully and will be made available to any interested user. This Final Technical Report gives a very brief summary of the Project activities. More details can be found in several publications that have resulted from this project.

14. SUBJECT TERMS

Unsteady Aerodynamics, Dynamic Stall, Supermaneuverability, Vortex Dynamics

15. NUMBER OF PAGES
75

16. PRICE CODE

17. SECURITY CLASSIFICATION OF REPORT	18. SECURITY CLASSIFICATION OF THIS PAGE	19. SECURITY CLASSIFICATION OF ABSTRACT	20. LIMITATION OF ABSTRACT
UNCLASSIFIED	UNCLASSIFIED	UNCLASSIFIED	UL

NSN 7540-01-280-5500

Standard Form 298 (Rev. 2-89)
Prescribed by ANSI Std. Z39-18
298-102

19951013 028

DTIC QUALITY INSPECTED 5

VORTEX DYNAMICS AND SEPARATION OVER PITCHING WINGS

B.R. Ramaprian
Principal Investigator

A. ABSTRACT

This project, aimed at an extensive study of the unsteady vortex dynamics and separation of pitching wings, started on January 15, 1992 and terminated on June 30, 1995. However, there was a reduction in the scope of the Project after January 1994 because of a cut in the budget. Even so, significant accomplishments were made in the project. These included extensive documentation of the 2-D velocity and vorticity field around a pitching NACA 0015 wing at a Reynolds number of 150,000, and extensive surface pressure and velocity data in the 3-D flow over a pitching swept wing of the same profile. The velocity data were obtained using the technique of Particle Image Velocimetry (PIV) developed during a prior AFOSR Grant. The data have been used to understand the physics of 2-D and 3-D vortex dynamics/separation in unsteady flows. The data have been archived carefully and will be made available to any interested user. This Final Technical Report gives a summary of the Project activities. More details can be found in several publications that have resulted from this project.

B. SUMMARY OF RESEARCH ACCOMPLISHMENTS

I. Introduction

This projected started on January 15, 1992, as a continuation of an earlier AFOSR-supported 2-year project during which the flow facility and PIV instrumentation were developed and a part of the pressure and velocity measurements were made over a 2-dimensional pitching airfoil. The main tasks of the present project were to first to complete the PIV measurements in the 2-D flow and later study, in detail, the unsteady 3-D flow produced by imparting a small backsweep of 15 degrees to the same airfoil. In all the experiments, the airfoil was pitched at constant angular velocity about an axis perpendicular to the freestream direction. The objective of the study was to understand the vorticity dynamics and the physics of separation and stall in unsteady flows. The flow over the mildly swept wing represents a small departure from two-dimensionality and hence, the experiments over the swept wing were expected to elucidate the effect of three-dimensionality on the dynamics of unsteady flows.

II. Experimental Facility and Instrumentation

The Water Channel and Model

The experiments were performed in a free-surface, water channel which has a test section 4 m long and 1m x 0.7 in cross-section. The channel is constructed from PVC and stainless steel to prevent rust formation. The water quality is controlled by a combination of softening,

filtering and pH management. The flow in the test section is uniform to within 1%. The freestream turbulence level is about 1.2 % at a test section velocity of 0.3 m/s and about 2% at 0.1 m/s. For more details and a complete description of the water channel, reference may be made to the departmental report on this subject by Conger and Ramaprian (1992), cited in Section C.

The test model used in the 2-D experiments was a NACA 0015 airfoil of 0.3 m chord (c) and 0.6m span (s) cut from an extruded aluminum stock. The details of construction of this model has been described in earlier reports. In the 3-D experiments, the wing model used was of the same NACA 0015 profile, but had a backsweep angle of 15 degrees, with $c'= 0.305$ m and $s'= 0.61$ m (measured perpendicular and parallel to the leading edge respectively). A schematic of this model is shown in Fig.1. It is constructed in 5-cm wide airfoil sections of aluminum machined on a numerically controlled milling machine and anodized for corrosion protection. The wing is assembled from these sections of which one is instrumented with pressure taps. The sections slide on two guide rods such that the instrumented section can be repositioned to varying spanwise locations. This construction allows one to make pressure measurements in several finely spaced spanwise locations without having to provide an impractically large number of pressure taps. The assembled wing has a chord (c) of 32 cm and a span (s) of 59 cm. Each end of the wing is fitted with a 1.2-cm thick Plexiglas end plate of 64 cm diameter. Surface pressure measurements were made over the central 19 cm of the span, which was found to be free from significant end effects. PIV data were obtained over the central 10 cm of span.

Both in the 2-D and 3-D experiments, the wing assembly is suspended in the 0.9 m (width) x 0.62 m (water depth) test section of the water channel, as shown schematically (for the 3-D case) in Fig.2. When mounted in place, the centers of the end plate are located on a vertical axis passing through the c/4 point at midspan of the wing. The upper Plexiglas end plate is bolted into the recess of a PVC pipe which rides on a 64 cm bearing. The bearing is positioned at the center of a rectangular aluminum plate located above the water level. This plate is supported by a large frame (not shown in Fig.2) independent of the water channel and designed to damp out vibrations generated by the pumps.

Pitching of the airfoil at constant angular velocity, about the vertical axis through the center of the end plate, is accomplished by a chain attached to the outside of the PVC pipe and driven by a servo-controlled microstepping motor. A digital encoder on the motor shaft provides information on the angular position of the airfoil. The encoder and controller communicate with an IBM-compatible personal computer, which also acquires the pressure data.

Instrumentation for pressure measurement

The pressure measurement system used in both the 2-D and 3-D experiments utilizes a diaphragm-type pressure transducer connected between a reference static tap and a surface pressure port via a scanning valve capable of switching among 48 channels. The transducer and scanning valve are carried on an aluminum bar which is mounted on the end plate (see Fig.2). A Pitot tube immersed in the flow upstream of the wing provides the reference static pressure and stagnation pressure for all experiments. A swivel ball joint mounted above the center of the rotating aluminum bar provides leak-proof communication between the stationary pressure tubing from the Pitot tube and the transducer moving with the end plate.

PIV instrumentation

The entire water channel was seeded with polystyrene particles of 20 μm diameter and specific gravity of 1.04. These were used as the tracer particles for the PIV measurements. They were illuminated by a horizontal laser light sheet of approximately 1-2 mm thickness. The light source used was a pulsed copper vapor laser pulsing at a uniform rate of 6 kHz and operating at an average power of approximately 10 watts. The optical arrangement for the light sheet is shown in Fig.3. A Nikon F3 35-mm camera was mounted directly above the 65 cm bearing and was focused through the top Plexiglas end plate onto the illuminated spanwise plane of interest. The camera moved with the rotating end plate, so that photographs were obtained in a frame moving with the wing. Multiple exposures of the tracer particles were produced by the use of a rotating slotted disk operating at 254 Hz and placed in the optical path of the laser (see Fig.1). The width of the slot was such as to provide an exposure period of about 1/2000 s. As an example, in the experiments at a test section velocity of 30 cm/s, the camera shutter was set to remain open for 1/30 sec., thus making it possible to capture eight exposures of the particles in each picture. The above settings correspond to a maximum particle travel of about 4 mm in the streamwise direction between exposures, and an effective averaging time of 1/30 s. These can be compared with the chord length of 300 mm and the total pitching time of about 9s. The camera shutter itself was triggered by the computer to open at the rate of one frame per degree in the incidence interval of 0 to 33 degrees, so that 34 pictures could be obtained during one pitching realization. The camera settings were proportionately adjusted for other test section velocities.

It should be noted that the PIV system used can measure only two components of the velocity, in this case the streamwise (v_x) and cross-stream (v_y) components. Thus, the spanwise component of the velocity could not be measured in the case of the swept-wing experiments. Also, the two-dimensional PIV system can, in principle, be used only in a two-dimensional flow. However, the mild spanwise flow present in the 3-D experiments did not introduce any major difficulties in the measurement of the flow field using the two-dimensional PIV system.

Each photographic negative was digitized using a microscope objective, a CCD camera, and a digital image processor. A rectangular area 2.4 cm long and 1.85 cm high was analyzed on each negative. This represents an area of approximately 17 cm by 13 cm in the actual flow. This rectangular area was divided into a checkerboard pattern with 40 divisions per side, for a total of 1600 square segments to be analyzed. The velocity vector was computed at the center of each segment by evaluating the two-dimensional autocorrelation function of the digitized image of the particles, using a high-speed array processor installed inside the PC. The entire process was automated, and a computer controlled two-axis traverse moved the film from one position to another.

After the velocity vectors were obtained in the above manner, the results were examined for missing and spurious values, which were then either corrected (where possible), or interpolated from reliable neighboring values (where not possible). Such corrections/interpolations were usually limited to about 10% of the total number of vectors. The details of this procedure are reported in the Ph.D. thesis of Oshima (1994). Also, after determining the velocity vectors, corresponding vorticity and stream function values were obtained using a series of post-processing programs described in the theses of Oshima (1994) and Rymarz (1995).

III. Experimental Procedure

Pressure Measurements in 3-D Flow

All the measurements were made at a Reynolds number of 130,000. Phase-locked pressure data were obtained at four different nondimensional pitching rates, α^+ $(=c/U_\infty)= 0.037$, 0.075, 0.104 and 0.207. Measurements were made at 22 z'-locations extending over about 22 cm. These data were subsequently interpolated to obtain pressure distributions C_p vs x/c at 19 spanwise locations (i.e., z-direction) extending over a distance of 19 cm. These pressure data were integrated to obtain the lift, pressure-drag and moment about the pitching axis, following standard procedure. The details of calculation are described in the M.S. thesis of Patterson (1994). Pressure gradients along the x' and z' directions were computed from the original 22 sets of data. These results were subsequently used to evaluate the pressure gradients (or, equivalently the vorticity fluxes) in the x- and z- directions. The experimental uncertainties are estimated to be 6% for C_p and the aerodynamic coefficients, and ± 0.07 degree for α. The surface vorticity fluxes (or equivalently, the surface pressure gradients) obtained from smoothed, phase-locked surface pressure distributions are estimated to be accurate to within 12% .

PIV Measurements

In the 2-D experiments, PIV data were obtained at two Reynolds numbers, namely 54,000 and 150,000 and a single pitch rate, α^+ =0.075 . This was in addition to the data obtained at a Reynolds number of 18,000 in the earlier Project. The PIV data in the 3-D experiments were obtained at a single freestream velocity of about 32 cm/s (corresponding to a Reynolds number Re= 135,000) and a pitch rate α^+ of 0.075. It was insured that between the present and the earlier projects, surface pressure and velocity data for the 2-D airfoil were available for this combination of Reynolds number and pitch rate. In order to achieve a higher spatial resolution of the velocity field, only 1/3 of the chord (forward, middle, or aft) was photographed during a pitching realization. The results thus obtained for the three regions from three separate pitching realizations were then combined to obtain the composite flow field over the entire wing.

Each realization consisted of a pitching maneuver from 0 to 33 degrees, with photographs being taken in one degree increments. In the swept-wing experiments, PIV data were obtained in the midspan plane, as well as at two off-midspan planes, 5 cm above and 5 cm below the midspan plane. Although the somewhat small aspect ratio of the swept wing model does not allow it to truly represent an "infinite" wing, this region around the mid-span plane was judged to be nearly free from end effects (based on the results from the pressure measurements reported in the thesis of Patterson 1994, and also in the paper by Patterson, Rymarz and Ramaprian cited in Section C), and hence was considered to be satisfactory for studying the three-dimensional effects introduced by sweep and pitch axis location.

A detailed discussion of the estimation of uncertainties associated with the present PIV measurements is provided in the thesis of Rymarz (1995). These estimates indicate that, v_x and v_y have an uncertainty of 4% over all the regions of the flow except in the immediate vicinity of the wall where the uncertainty is about 8%, and the vorticity and stream function values estimated from the velocity data have an uncertainty of 8% (16% immediately next to the wall)

and 4% respectively.

III. Conclusions

The important conclusions arrived at, from the experiments mentioned above are listed below. The three key papers that led to these conclusions are attached as appendices I, II and III to this report. Detailed discussions of the experimental results can be found in these papers, as well as, various other publications and student theses that have resulted from this Project. The publication details of these are listed in Section C of this Report.

2-D Unsteady Flow over a Pitching Airfoil

A comprehensive set of velocity data have been obtained on a pitching airfoil. These data complement the surface pressure data obtained earlier on the same airfoil in the same facility. A detailed study of these data has led to the following important conclusions (See Appendix 1).

(1)   The increase in lift of a pitching airfoil is due to the influx of vorticity from the surface by the presence of strong favorable pressure gradient near the leading edge. Lift continues to increase so long as vorticity is generated and remains close to the airfoil surface. Infusion of counter-clockwise vorticity from the airfoil surface due to local adverse pressure gradient forces the shear layer to lift up and thus creates the Leading Edge Vortex (LEV). Also, the continued influx of counter-clockwise vorticity from the surface produces a secondary counter-clockwise vortical structure underneath the LEV, which causes the shear layer to roll up. The rolled up shear layer along with several vortices generated by the shear-layer instability forms the so called Dynamic Stall Vortex (DSV). The DSV grows in size and is eventually ejected abruptly at a large angle with respect to the airfoil surface leading to the dynamic stall.

(2)   Early transition to turbulence at high Reynolds numbers causes the LEV to form at larger incidences, but more abruptly than at low Reynolds numbers. Also, the DSV at high Reynolds numbers is more compact, better defined and contains fewer vortices formed from the instability of the shear layer before it is ejected from the surface. The DSV is clearly separated from an other dominant vortical structure, the so-called shear-layer vortex (SLV), which occupies the mid-to-aft region of the airfoil.

(3)   Several pairs of topological critical points have been identified in the flow pattern obtained from the PIV data. However, all these critical points are characterized by non-zero shear strain rate and hence do not represent unsteady separation points in the MRS sense. Computation of particle trajectories may help to understand the mechanism underlying the unsteady separation from the Lagrangian point of view. This requires additional work and may require improvement in the temporal resolution of the PIV.

3-D Unsteady Flow over the Pitching Swept Wing

Even though the geometry studied represented a small departure from two-dimensionality, significant three-dimensional and pitch-axis location effects were observed in the present experiments. The conclusions based on the pressure (See Appendix 2) and velocity

measurements (See Appendix 3) are separately listed below.

Conclusions from pressure measurements

1. The onset of the dynamic stall vortex in three-dimensional flow over the swept wing is associated with a long pressure plateau (or very mild second suction peak) in the surface pressure distribution, which replaces the strong second suction peak observed over an unswept wing. Thus, there does not appear to be a rapid ejection/lift-off of the DSV from the surface, but a rather gradual spreading of the vortex across the wing surface. This is believed to be due to the occurrence of more gradual, open-type, three-dimensional, flow separation in the presence of the spanwise velocity component. Consequently, sweep increases unsteady C_{lmax}, as well as the incidence at which it occurs. It causes C_m about the pitching axis to increase at an earlier incidence but less drastically than in two-dimensional flow.

2. The aerodynamic coefficients follow a trend that is an extension of the quasi-steady behavior to post-static stall incidences. This is true at all spanwise locations and at all except the highest pitch rate studied. Of these, the pitching moment coefficient departs the earliest from the quasi-steady behavior and shows a large increase well before the occurrence of dynamic stall, whereas the lift and drag coefficients continue to follow quasi-steady trend almost up to the occurrence of dynamic stall. These characteristics are qualitatively similar to those observed in two-dimensional flows.

3. Lift curve slope and maximum lift increase from the bottom towards the top part of the wing. Pitching moment increases in a similar manner, except that the increase begins to appear earlier during the pitching maneuver. The pressure-minimum wave front (usually associated with the stall vortex) convects obliquely along the wing surface from the bottom towards the top of the wing with a longitudinal convection velocity of about $0.17U_0$. All these effects can be related to the pitch-axis geometry studied in the present experiments.

4. There is strong evidence of spanwise modulation in the production of vorticity at the wing surface, especially in the downstream regions of the wing. In fact, some spanwise modulation can be observed even in the lift distribution. The precise cause of this periodicity is unknown. This aspect requires further study.

Conclusions from the PIV measurements

1. The vortex structures remained close to the surface of the swept airfoil. In fact, the DSV was never actually washed away from the swept wing even at the highest post-stall incidence of 34 degrees studied in the present experiments. Hence, post-stall loss of circulation and lift was gradual rather than catastrophic.

2. The DSV at the larger incidences over the swept wing is really a conglomeration of a number of smaller vortex structures that spread out over the entire wing surface. The swept wing stalls as the vortical structures begin to move away one by one from the surface. The unswept wing, in contrast, stalls after the DSV is abruptly swept away as a single structure. The distributed vortex structure, as well as the noncatastrophic nature of stall are believed to be the general characteristics of all three dimensional flows.

3. The trailing edge flow of the swept wing does not seem to influence the lift-off of the

leading-edge vortex structure. Rather, the LEV seems to be pushed away from the surface of the wing by a localized build-up of low energy fluid. While this feature can be observed over the unswept wing also, it is more clearly observed over the swept wing.

4.   A strong spatial periodicity was observed in the rate of accumulation of vorticity along the swept wing. This periodicity is caused essentially by periodic convection of vorticity in both the chordwise and spanwise directions. The origin of this periodicity is unknown. It is also not clear whether this periodicity is peculiar to the specific mildly three-dimensional geometry studied in the present experiments, or whether it is a characteristic feature of all three-dimensional flows.

5.   There is strong evidence that aftward movement of the pitch axis delays the dynamic stall process, as well as slightly increasing the maximum lift produced by the wing. The present data trend (strong monotonic variation with z) suggest that this is primarily a pitch-axis location effect, and should be observable in two-dimensional flows also.

Based on the detailed study reported in Conger and Ramaprian (1992), there is strong reason to believe that the present results (especially those obtained at the Reynolds number of 1.5×10^5) are representative of flow behavior at "high" Reynolds numbers of practical interest. The PIV data, along with the surface pressure data, have been archived and are available to any interested reader. These data form a comprehensive database suitable for use in the development and verification of computational fluid dynamics codes for pitching airfoils.

C. PERSONNEL, DEGREES AWARDED AND PUBLICATIONS

1. Personnel and Degrees Awarded

Name	Participated as	Degree	Awarded
B.R. Ramaprian	PI		
Rand N. Conger	Graduate Research Assistant	M.S.	Jun 1992
April K. Patterson	Graduate Research Assistant	M.S.	Dec 1993
Hideya Oshima	Graduate Research Assistant	Ph.D.	Aug 1994
Paul B. Rymarz	Graduate Research Assistant	M.S.	June 1995

II. Publications

1.   Oshima, H., and Ramaprian, B.R., ``Measurements of the Velocity and Vorticity Fields over a Pitching Airfoil," AIAA Paper No. 92-226, 1992.

2.   Oshima, H., and Ramaprian, B.R., ``Experimental Study of the Spatio-Temporal Structure of K'arman Vortex Shedding," *Proc. of the Intl. Symp. on Aerospace Sciences and Engrg.,* Indian Institute of Science, Bangalore, Dec. 12-15, 1992, pp.

3.   Conger, R.N., Oshima, H., and Ramaprian, B.R., "Experimental Studies of the Unsteady Vortex Dynamics of a Two-Dimensional Pitching Airfoil", Proc. of the *11th Australasian Fluid Mechanics Conference*, University of Tasmania, Hobart, Australia, 14-18,

Dec. 1992, p 1117-1120.

4.   Oshima, H., Conger, R.N., and Ramaprian, B.R., ``Flow Measurements Over a Pitching Airfoil," Proc. of the *Ninth Intl. Symposium on Turbulent Shear Flows*, Kyoto, Japan, Aug.16-18, 1993, pp. 7.5.1- 7.5.5

5.   Conger, R., and Ramaprian, B.R., ``Pressure Measurements on a Pitching Airfoil in a Water Channel," AIAA paper No. 93-0184.

6.   Conger, R.N., and Ramaprian, B.R., ``Pressure Measurements on a Pitching Airfoil in a Water Channel," *AIAA Journal*, Vol.32, No.1, Jan 1994, pp.108-115.

7.   Conger, R.N., and Ramaprian, B.R., ``Correcting for Response Lag in Unsteady Pressure Measurements in Water," *J. Fluids. Engrg.*, Vol.115, Dec 1993, pp.676-679.

8.   Rymarz, P.B., and Ramaprian, B.R., "Measurements of Velocity and Vorticity Fields around a Pitching Swept Wing," AIAA paper No.95-2161.

9.   Patterson, A.K., Rymarz, P.B., and Ramaprian, B.R., "Surface Pressure Measurements on a Pitching Swept Airfoil in a Water Channel", AIAA Paper No. 94-2254; to appear in the *AIAA Journal*, April 1996.

10.   Oshima,H., and Ramaprian, B.R., "Velocity Measurements over a Pitching Airfoil," submitted to the *AIAA Journal*.

III. Reports

1.   Conger, R.N., and Ramaprian, B.R., ``The WSU-MME 1 m x 1 m Water Channel," Washington State University, Department of Mech. and Materials Engineering, Report No. MME-TF-92-1, May 1992.

2.   Conger, R.N., and Ramaprian, B.R., ``Correcting for Response Lag in Unsteady Pressure Measurements in Water," Washington State University, Department of Mech. and Materials Engineering, Report No. MME-TF-92-2, May 1992.

3.   Conger, R.N., and Ramaprian, B.R., ``Pressure Measurements on a Pitching Airfoil in a Water Channel," Washington State University, Department of Mechanical and Materials Engineering, Report No. MME-TF-92-3, May 1992.

IV. Dissertations

1.   Oshima, H. (1994) " The Use of Particle Image Velocimetry for the Study of the Vortex Dynamics of a Pitching Airfoil", Ph.D. Thesis, Mechanical and Materials Engineering Department, Washington State University, Pullman, WA, July 1994.

2.   Conger, R.N. (1992) "Pressure Measurements on a Pitching Airfoil in a Water Channel," M.S. Thesis, Department of Mechanical and Materials Engineering, Washington State University, Pullman, WA, May 1992.

3.   Patterson, A.K. (1993) "Surface Pressure Measurements on a Pitching Swept Airfoil in a Water Channel," M.S. Thesis, Department of Mechanical and Materials Engineering, Washington State University, Pullman, WA, Dec 1993.

4.   Rymarz, P.B. (1995) " Measurements of Velocity and Vorticity Fields around a Pitching Swept Wing," M.S. Thesis, Mechanical and Materials Engineering Department, Washington State University, Pullman, WA, May 1995.
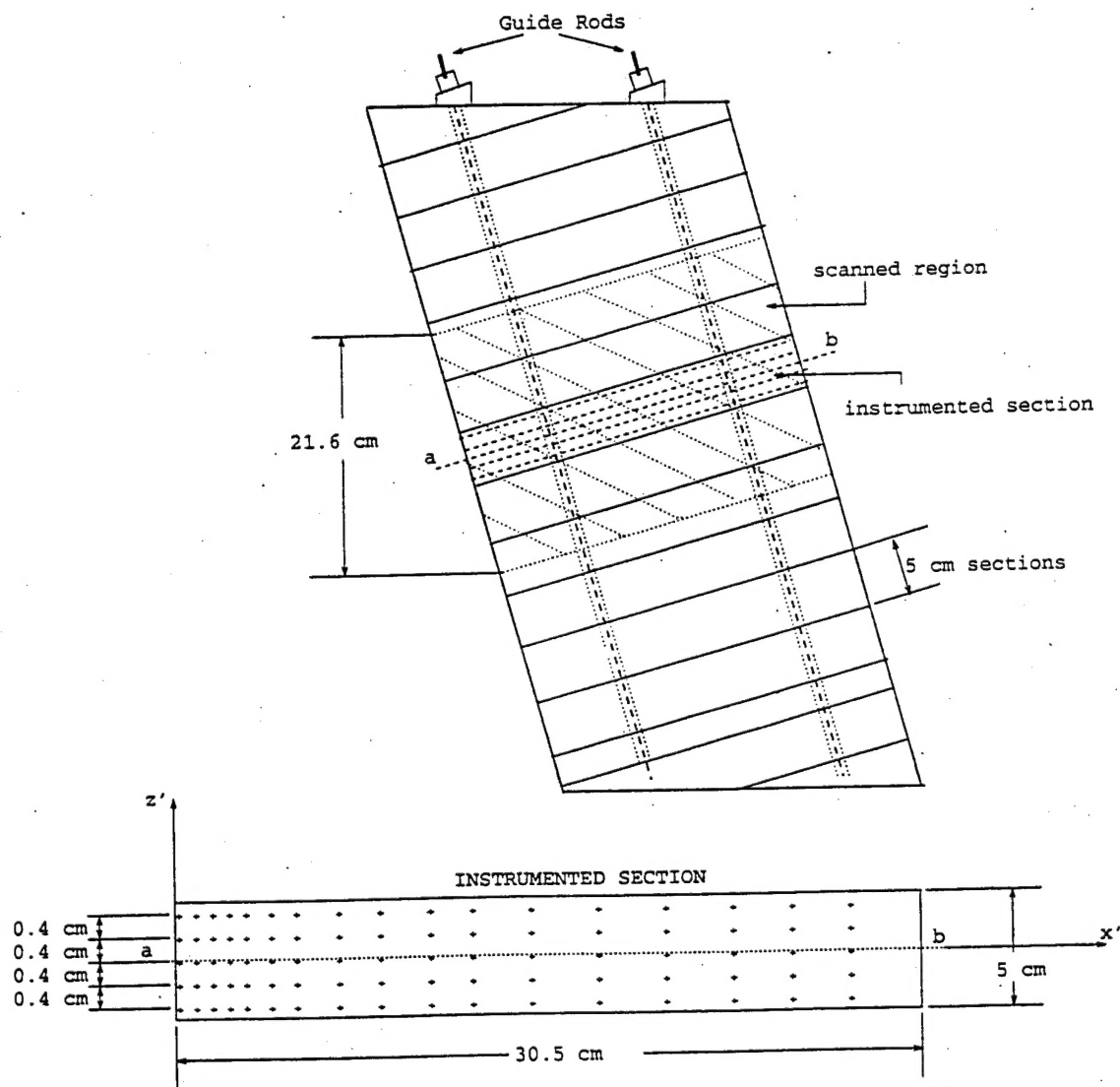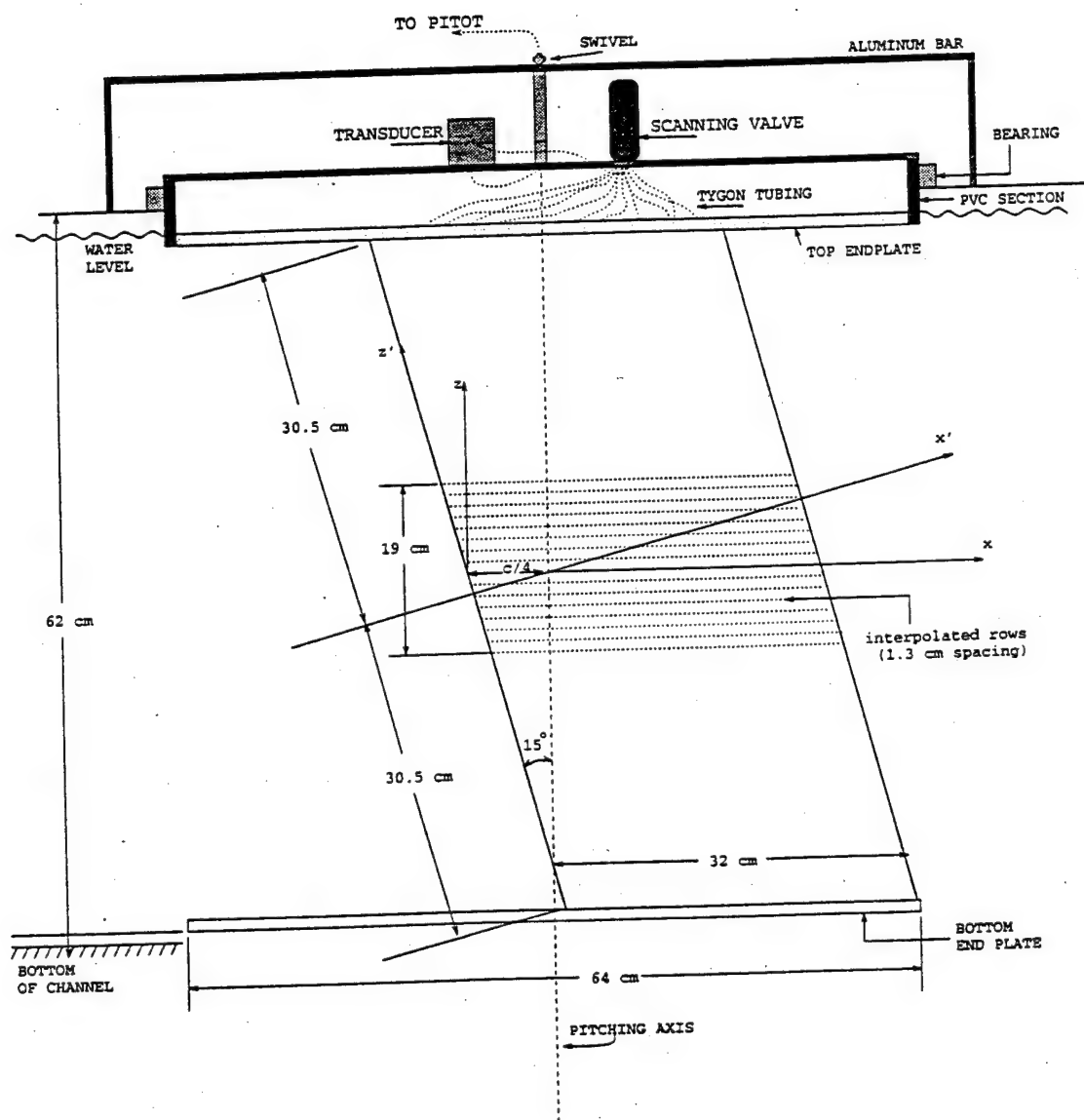
Figure 1 Construction of the Swept Wing

Figure 2 Details of Wing Model mounting in the Water Channel
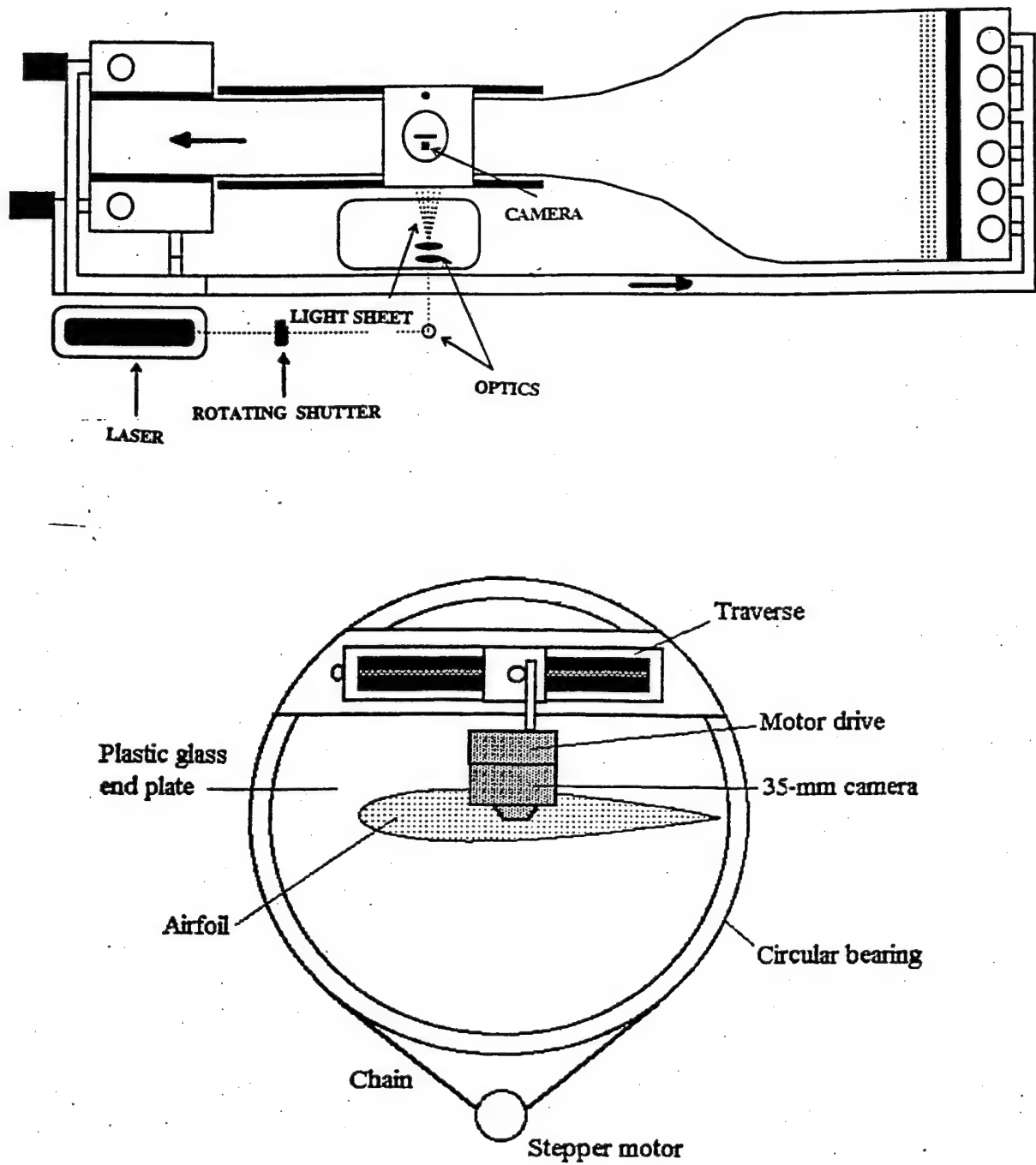
LASER

ROTATING SHUTTER

LIGHT SHEET

OPTICS

CAMERA

Traverse

Motor drive

35-mm camera

Circular bearing

Stepper motor

Chain

Airfoil

Plastic glass end plate

Figure 3   Schematic of the Optical set up for PIV

APPENDICES

VELOCITY MEASUREMENTS OVER A PITCHING AIRFOIL

H.Oshima
Graduate Student, School of Electrical Engineering and Computer Science,
Washington State University, Pullman, WA
and
B.R. Ramaprian
Professor, School of Mechanical and Materials Engineering, Washington State University,
Pullman, WA

Abstract

This paper presents the results of velocity measurements on the suction side of a two-dimensional NACA 0015 airfoil pitching at constant angular velocity about its quarter-chord spanwise axis. The object of the study was to obtain quantitative information on vortex dynamics and stall in the unsteady flow over the pitching airfoil. The experiments were performed in an open-surface water channel using the technique of Particle Image Velocimetry (PIV) for the measurement of the instantaneous velocity field. Two features that distinguish the present work from earlier studies are (i) the flow conditions in the present experiments appear to simulate very high Reynolds number behavior, and (ii) the velocity (hence vorticity) data are accompanied by surface pressure data, obtained earlier on the same model in the same facility under the same flow conditions. The study has shown that the dynamic-stall vortex (DSV) still consists of the rolled-up shear layer along with several vortices generated by the shear layer instability, as observed in earlier studies at low Reynolds numbers, and that the increase of lift at post-static stall incidences is still due to the presence of vortical structures close to the surface, till they are eventually ejected prior to the occurrence of dynamic stall. However, the DSV at high Reynolds numbers is more compact, has fewer discrete vortical structures and is ejected abruptly from the airfoil surface in a direction almost normal to the surface. It therefore appears that the flow at high Reynolds numbers would be less responsive to control techniques that attempt to alter the stability characteristics of the shear layer. The detailed quantitative experimental data have been archived and will be available to any interested user.

Introduction

The unsteady flow over a two-dimensional airfoil pitching at a constant angular velocity about a spanwise axis has been studied by a number of investigators in recent years. The interest in this flow configuration has primarily been driven by the desire to understand unsteady vortex dynamics and the phenomenon of dynamic stall. However, practically all experimental studies of these flows have so far been limited to qualitative flow visualization, measurement of surface pressure distribution or a limited amount of near-surface velocity measurements over the wing. A few exceptions to these is the unsteady velocity field measurements around a NACA 0012 airfoil by Shih

et al[1] and our own recent experiments on a NACA 0015 airfoil[2].   On the other hand computational studies such as those of Oswald *et al*[3], Visbal and Shang[4] and Visbal[5] have resulted in a detailed description of the surface pressure as well as the flow field around the airfoil. However, a complete set of experimental data are not available for the verification or further development of such numerical models.

The present work formed a part of an extensive research program on the study of the unsteady aerodynamics and dynamic stall of a pitching airfoil of NACA 0015 profile. The studies under this program were performed in an open-surface water channel specially designed and constructed for this purpose. The experiments were conducted at several Reynolds numbers Re (defined as $U_\infty c/\upsilon$, where U_∞ is the freestream velocity, c the airfoil chord and υ the kinematic viscosity of the fluid) in the range $1.8 \times 10^4 - 2.3 \times 10^5$. In all the experiments, the airfoil was pitched about its spanwise c/4-axis at constant nondimensional pitching rates of $0.036 < \alpha^+ < 0.2$, where α^+ is defined as $\dot{\alpha}c/U_\infty$. The velocity measurements at the lowest Reynolds number of 1.8×10^4, which were made using the technique of Particle Image Velocimetry (PIV) in the very early phase of the research program, have been reported separately[2]. The surface pressure data for several Reynolds numbers and pitch rates in the above range have also been reported in an earlier publication[6]. The present paper describes PIV measurements at two of the highest Reynolds numbers (5.4×10^4 and 1.5×10^5) in the above range. These correspond to nominal test section velocities of 10 cm/s and 30 cm/s respectively. The value of α^+ was 0.072 in both these experiments. Surface pressure data corresponding to these flow conditions are available from Ref.6. It has therefore become possible to study the PIV data in these two cases in conjunction with the corresponding surface pressure data. This is a distinguishing feature of the present work.

The earlier pressure measurements in the water channel (especially those obtained at Reynolds numbers larger than 300,000) revealed interestingly that the boundary layer over the airfoil model undergoes very early transition from laminar to turbulent flow near the leading edge. The early transition resulted in almost complete elimination of the so-called leading-edge separation bubble. The pressure distribution and lift data indicated that, under these conditions, the flow behavior closely resembled that at much higher Reynolds numbers (say, of the order of 2×10^6). There is a strong evidence (see Ref.6) that this accelerated transition is caused by the combination of the relatively high level of freestream turbulence (about 1.5-2%) and externally imposed unsteadiness. The fact that the flow field mimics closely the flow at significantly higher Reynolds numbers, combined with the fact that both velocity and pressure data have been obtained, makes the present study unique and particularly useful from a practical point of view. A further important feature of the present work is that PIV data have been obtained with spatial and temporal resolution higher than has been achieved in the past. This became possible because of the relatively large size of the test section (1 m x 0.7 m) and the model (35 cm chord), and the use of water as the working fluid.

Experimental Details

Experimental facility

The experiments were performed in a free-surface water channel with a test section 4 m long

and 1 m x 0.7 m in cross-section. The test section velocity in this facility can be varied from 0-0.5 m/s. The freestream turbulence level is about 1.5%, at a test section velocity of 30cm/s, and 2.5 % at a velocity of 5 cm/s. For a complete description of the facility, see Conger and Ramaprian[7]. The entire channel is seeded with micron size particles of controlled size to allow PIV measurements.

The airfoil studied is a NACA 0015 profile of 35 cm chord and 67 cm span. This is the same model on which pressure measurements were made in the earlier study reported in Ref.6. It is formed from extruded aluminum stock and painted dull black to prevent glare and reflection during flow visualization. The airfoil is mounted with its span vertical in the test section. It is provided with a circular transparent end plate which just dips into the water. The end plate prevents wave effects at the free surface and also provides an unobstructed and distortion-free view of the flow field around the airfoil. The end plate is mounted in a circular bearing of 65cm diameter carried by a rectangular aluminum plate. The bearing allows the end plate to be rotated about its vertical axis clockwise or counterclockwise at any desired angular velocity over an angle of 90 degrees, via a chain drive, by a computer-controlled stepper motor. The chain drive arrangement leaves the top of the end plate optically clear, for flow visualization from the top. An encoder mounted on the shaft of the stepper motor measures the angle of incidence of the airfoil. The airfoil is mounted with its quarter-chord ($c/4$) axis passing through the center of the end plate. Hence the rotation of the end plate about its center causes the airfoil to pitch about its c/4 axis. A schematic of the airfoil pitching mechanism is shown in Fig.1(a). More details of the model assembly are provided in Ref.7.

Instrumentation

Since phenomena of interest to this study occur primarily on the suction side of the airfoil, PIV measurements were obtained only on this side of the airfoil. However, surface pressure data are available for both sides of the airfoil. The PIV data were obtained at the midspan plane of the airfoil. This was achieved by illuminating this plane by a laser light sheet. Figure 1(b) shows the schematic of the optical set-up used. In the lower Reynolds number experiment, fluorescent polystyrene particles of 2 microns diameter were used for seeding the flow and a 4-watt argon ion laser was used as the light source. Since a shorter exposure time was required in the higher Reynolds number experiment, this source was replaced by a more powerful 20-watt copper-vapor laser in that experiment. Also, the seed particles were replaced by 20 micron nonflourescent particles (supplied by Optimage Company of England). These particles were found to be less expensive and superior in performance. In both the experiments, a rotating shutter was used in the path of the laser beam to obtain laser pulses at the desired frequency. A Nikon F-3 35-mm camera equipped with a motor drive was used for taking the multiple-exposure particle image photographs. The motor drive allowed photographs to be obtained at a rate of up to 4 frames per second. Kodak Tri-X ASA 400 B/W film was used for the photography. The camera was mounted on top of the circular end plate, aiming directly downward (see Fig.1a) and was moved with the airfoil. The velocity data were thus obtained in a coordinate frame moving with the airfoil. The movement of the airfoil was synchronized with the camera control and in both the experiments, a total of 36 photographs were obtained at equal intervals over the pitching range of 0 to about 35 degrees. The angular resolution was thus approximately 1 degree. The rotating shutter was set to provide four exposures during each opening of the camera shutter. For details on camera and shutter settings and the experimental

procedure, reference may be made to Oshima[8].

As in the first PIV experiments reported in Oshima and Ramaprian[2], in order to achieve good spatial resolution and reach points closer to the airfoil surface, the flow field on the suction side of the airfoil was subdivided into three regions, namely - front, mid and aft regions, and each region was zoomed in and photographed during separate pitching realizations. This procedure provided a spatial resolution of approximately 0.5% of the chord. However, the measured flow fields in the three regions do not correspond to the same pitching realization. The velocity fields computed for the three regions were later combined to obtain the entire flow field. Although this may introduce some mismatch of the velocity fields between two adjacent regions, it was a trade-off needed to achieve higher spatial resolution. It was found that the flow structure becomes simpler and more organized as the Reynolds number increases. Therefore, the problem of the mismatch was less severe at the higher Reynolds number of 1.5×10^5.

The multiple-exposed photographs were scanned and processed using the PIV interrogation system developed in-house at WSU. This system uses the well-known auto-correlation method to obtain the velocity vectors. Velocity vectors were obtained at 1600 points over the photograph to achieve a spatial resolution of 0.009c and 0.007c in the streamwise (x) and cross-stream (y) directions respectively. Separate post-processing programs were used later to remove/replace bad vectors, compute vorticity, stream function, strain rate and other quantities of interest. The PIV system and the details of the entire procedure are described briefly in Ref.2, and in more detail in the Ph.D. thesis of Oshima[8].

The overall uncertainty in the velocity measurements is about 2 percent of the maximum velocity in the flow. Based on the observed scatter in the velocity data, it is reasonable to assume an uncertainty of 10% in the vorticity calculations. It is also important to state that velocity data could not be obtained closer than 2.4 mm from the wall, though they can be estimated approximately from extrapolation to the wall. The uncertainties in velocity and vorticity estimates are higher in this region. The uncertainty in the estimation of the stream function is not more than 10%.

PIV Results

Because of the early triggering of transition at both the Reynolds numbers studied, the basic features of the flow were quite similar in the two experiments. For this reason and also in the interest of brevity, results will be presented mostly for the higher Reynolds number experiment. It is also important to note that while the velocities were measured in a non-inertial co-ordinate system (spinning at a constant angular velocity about the pitching axis of the airfoil), the effect of rotation of the co-ordinate axes has negligible effect on the results at the very low pitching rate of $\alpha^+ = 0.072$ studied.

Velocity and vorticity fields

Figure 2 displays a few typical velocity and vorticity fields on the suction side over the entire airfoil. The examples cover the interval from $\alpha = 20.9$ degrees to 27.8 degrees. Figures 3(a)-3(c) show the corresponding pressure and lift data, taken from Conger and Ramaprian[6]. At incidences

below 21 degrees, the flow features evolve slowly and are qualitatively similar to those at 20.9 degrees. The contours of very high negative vorticity are very narrow, stretched out and are nearly parallel to the airfoil surface. Pressure distributions and the lift-slope curve behave essentially as in steady flow, except that the peak suction pressure and lift continue increasing with incidence. The vorticity contours spread out a little towards the trailing edge indicating a general decrease in the magnitude of vorticity. It can be seen from the velocity field at α =20.9 degrees that, in the mid to aft regions of the airfoil, the flow is lightly separated and a thin layer of reverse flow is present near the airfoil surface. In fact, this region of separation appears first at an incidence of about 18 degrees and begins to spread from the trailing edge in the upstream direction thickening the shear layer in the mid to aft regions as the airfoil pitches up from α =18 degrees to 20.9 degrees. The thickened boundary layer can be clearly seen at the incidence of 20.9 degrees.

Beyond α = 20.9 degrees, vorticity contours at around x/c = 0.1 start to bulge out, producing a locally closed set of vorticity contours, which is indicative of the inception of the so-called Leading-Edge Vortex (LEV). The LEV then continues to grow in size as can be seen typically from Fig.2 for α = 22.6 degrees. The reverse flow from the trailing edge does not, however, seem to be the cause of the LEV formation in the front region of the airfoil, since it is physically separated from the LEV as seen clearly from the vorticity contours at this incidence. The shear layer in the front region starts to bulge out because of the large adverse pressure gradient, which infuses positive (counter-clockwise) vorticity at the surface. This causes the vorticity maximum to move away from the wall causing the vorticity contours to form locally closed curves. A region of flow reversal seems to edge in between the negative vorticity contours convected from the leading edge and the airfoil surface, causing the shear layer of negative vorticity to lift up. Simultaneously, a plateau begins to appear in the pressure distributions near the leading edge. This can be seen typically form the pressure distribution for α = 22.24 degrees in Fig.3(a). However, the vorticity still remains concentrated close to the wall. The lift therefore continues to increase with incidence, as seen from Fig.3(b). As the incidence increases further beyond 22 degrees, the reverse flow carrying vorticity of opposite sign grows between the shear layer and the airfoil surface causing the shear layer to roll up. Also, during this period the shear layer appears to breakdown due to instability forming several smaller vortices. A conglomeration of such shear layer vortices can typically be seen at α = 24.4 degrees in Fig.2. The rolled up shear layer and the conglomeration of shear-layer vortices can together be described as the dynamic-stall vortex (DSV). As the incidence increases, the DSV begins to grow very rapidly and move slightly downstream. The downstream convection of the DSV is, however, minimal and most part of the vortex stays in the front region (x/c < 0.3). A second suction peak corresponding to the signature of the DSV begins to appear in the pressure distributions in the region during this incidence range. The location of the suction peak moves downstream with the DSV, as can be seen from Fig 3(a). Earlier flow visualization studies and surface pressure measurements (Walker et al[9,10]) have also indicated that the location of the DSV center coincides approximately with the location of the secondary peak in C_p distribution. The lift curve appears a little erratic during this period. Further increase in the incidence angle causes the dynamic-stall vortex to enlarge rapidly, as can be seen from the results for α=25.2 degrees. The dynamic-stall vortex seems to be eventually ejected into the cross-stream direction at an incidence of about 26 degrees. A secondary vortical structure with positive vorticity grows beneath it as seen from the vorticity contours for α=26.1 degrees. The lift reaches a maximum value at about this incidence. At the incidence of 27.8 degrees, the DSV leaves our view

and only a thin shear layer with a pair of shear layer vortices emanating from the leading edge can be seen. The dynamic stall has already occurred and the lift has dropped significantly from its maximum value. (Note the second peak in the lift curve is most probably due to blockage effects that becomes significant after the occurrence of dynamic stall.)

Meanwhile, in the mid to aft regions, the separated layer originating from the trailing edge starts to form a second vortex, the so-called "Shear-Layer Vortex" (SLV). Beyond an incidence of about 23 degrees, the spacing between the two vortical regions increases and the two vortices become more distinct from each other. This can be clearly seen from both the velocity and vorticity results for α=24.4 to 26.1 degrees. These flow structures observed in the present experiments confirm the results of earlier flow visualization studies (eg. Walker, Helin and Strickland[9] and Lavato[11], as well as numerical analyses (eg. Visbal[5]).

Effects of Reynolds Number

As already mentioned, detailed PIV data were also obtained at a Reynolds number of 5.4 x 10^4. These results were very similar to those at the higher Reynolds number, the LEV forming at only a fraction of a degree less than 20 degrees, and dynamic stall occurring slightly beyond 25 degrees. However, these results differ considerably from the values of about 14 degrees for LEV formation and about 24 degrees for dynamic stall, observed in Ref.2 at a Reynolds number of 1.8 x10^4. The detailed flow structure observed at the three Reynolds numbers also exhibit the same trend. This can be seen from Fig.4 which compares the vorticity contours just prior to the occurrence of dynamic stall for each of these three Reynolds numbers. The most striking difference is in the extent of the wing surface over which the DSV has spread before it leaves the surface. At the lowest Reynolds number, the rolled-up shear layer contains a number of vortices, generated by the shear-layer instability. The shear layer has been just pinched off in this figure but the DSV consisting of the conglomeration of the vortices is still within the view of the camera. In fact, the release of the DSV from the surface can be considered to be "gradual" and is in a direction approximately along the airfoil surface. In contrast to this, the release of the DSV at the highest Reynolds number is more in the nature of an abrupt "ejection" in a direction almost normal to the airfoil surface. The DSV in this case is also more compact and its severance from the shear layer is sharper. One can still observe several instability vortices inside the DSV but these are fewer in number than at the lowest Reynolds number. Apparently, at the highest Reynolds number, the breakdown of the shear layer due to instability occurs more slowly relative to the roll up and ejection process. The latter is completed very rapidly even though it *starts* at a slightly larger incidence than at lower Reynods numbers. Since the nondimensional pitching rate was the same at all the Reynolds numbers, this indicates that the shear-layer breakdown and roll-up/ejection are two different processes each characterized by a different time scale. The rapidity with which the shear layer ejection occurs compared to the rate of formation of the instability vortices suggests that at high Reynolds numbers, the process of dynamic stall is likely to be less sensitive to any attempt to alter the stability characteristics of the shear layer. Another significant feature that can be seen from Fig.5 is that as the Reynolds number increases, the DSV is more clearly separated from the SLV occupying the aft region of the airfoil.

Figure 4 shows that the flow structure at the intermediate Reynolds number is somewhat similar to that at the highest Reynolds number. Some similar features are that the there are only a

small number of *strong* discrete vortices in the shear layer and that the latter is ejected at a fairly large angle to the airfoil surface in both the cases. This similarity is consistent with the observed trends in surface pressure distribution and lift generation at these two Reynolds numbers and is due to the triggering of early transition over the airfoil by the high freestream turbulence (and consequent elimination of the laminar separation bubble) at these Reynolds numbers, as discussed in Ref.6. This early triggering of transition did not occur at the Re=$1.8x10^4$. It is therefore reasonable to expect that the present PIV results (especially those obtained at the higher Reynolds number) are closely representative of the behavior that can be expected at very high Reynolds numbers.

Discussion of the Detailed Flow Structure

The detailed PIV data can be used to study the kinematic and dynamic aspects of the vortex structure over the pitching airfoil. For this purpose, these data have been further processed to obtain quantities such as vortex trajectory, velocity/vorticity distributions in the cross-stream direction, strain rates, streamfunctions and vorticity fluxes. These will be presented and discussed below. In view of the comments made earlier, results will be presented only for Re=$1.5x10^5$.

Velocity and vorticity profiles

Figures 5 and 6 show typical cross-stream distributions of the velocity components u_s, u_n and the spanwise vorticity ω_z at a few instantaneous angles of incidence. The co-ordinates s and n measured along and normal to the airfoil surface and centered at the nose of the airfoil are used for this purpose. The jaggedness and the abrupt changes in slope of the velocity profiles are primarily due to the presence of a number of vortices in the flow. Multiple peaks and changes in sign in the vorticity distributions indicate the possible existence of several positive and negative vortices in the flow. No flow reversal was observed in the leading-edge region at incidences of less than 20 degrees. However, a very small reverse flow can be seen creeping upstream from the trailing edge region as the incidence increases. At incidence of 20.9 degrees, the distributions of u_s in the aft region of the airfoil resemble Moore's[12] model of upstream-moving unsteady separation. Indeed the trailing-edge separation point has moved upstream into the mid region at an incidence of 21.8 degrees. In addition at this incidence, the shear strain rate (which, in this case, is nearly equal to vorticity) vanishes at the n-location of the maximum flow reversal, as seen from Fig.6. At α= 20.9 degrees vorticity profiles at around x/c = 0.1 indicate the presence of the LEV. Notice also that at several regions of the flow, the n-component of the velocity is quite significant in magnitude. Because of this reason and also because of the presence of flow reversal, boundary-layer models are not appropriate for describing this flow.

The LEV rapidly grows during the incidence range 21.8 - 22.6 degrees. It can be seen that during this period, the streamwise component of velocity at the upstream edge of the LEV also exhibits a distribution similar to Moore's upstream-moving unsteady separation with flow reversal. Thus, both the reverse flow from the trailing-edge region and the reverse flow associated with the LEV fit in to the upstream-moving unsteady separation model.

As the angle of attack increases further, one can observe rapid growth of the LEV into the dynamic-stall vortex in the front region and consolidation of the SLV in the aft region of the

airfoil.

Strain Rate and Velocity Gradients

Figure 7(a) shows the shear strain rate, while Figs.7(b) and 7(c) show the individual velocity gradients $S_{s,n}(=dV_s/dn)$ and $S_{n,s}$ $(=dV_n/ds)$, for an incidence of 25.2 degrees (just prior to the occurrence of dynamic stall). Note that the sum of these velocity gradients represents the shear strain rate and their difference represents the vorticity which is shown in Fig.3. In all the cases, the outermost contours have the same magnitude (of about 7 units) and the contour intervals are the same (about 14 units). It is seen that in the front region, $S_{n,s}$ (showing 1 to 2 contour lines and a maximum value of about 21 units) is quite significant (about 60%) compared to $S_{s,n}$ (showing up to 3 contours and a maximum value of about 35 units). This results in the vorticity and shear strain rates to differ significantly from each other, as can be seen form a comparison of the vorticity contours in Fig.3 with the shear strain contours in Fig. 7(a). The shear strain rate contours are stretched out longer along the airfoil. On the other hand, in the rear part of the airfoil (occupied by the SLV), $S_{n,s}$ is, at least, less than 7 units in magnitudes (since its contours are not seen in Fig.7c), whereas $S_{s,n}$ has a maximum magnitude of about 21 units. In fact, $S_{n,s}$ is substantially less than 7 units since, the vorticity, shear strain rate and $S_{s,n}$ contours are all nearly identical to one another in this region. Note however, that in all regions of the flow, the values of $S_{n,s}$ are still significant enough to invalidate boundary-layer approximations at his incidence.

Vortex Trajectory

Figure 8 shows the coordinates $(x_c/c, y_c/c)$ of the center of the dynamic-stall vortex and the vortex trajectory. The center of the vortex was determined by assuming it to coincide with the centroid of the vorticity distribution associated with the DSV. For this purpose, the domain of the DSV was subjectively inferred from observing the streamline pattern of the flow. The dynamic-stall vortex first becomes clearly recognizable with its center located at (0.07c, 0.05c) at an incidence of about 21 degrees. Its trajectory subsequently seems to follow nearly a straight line as the angle of incidence increases, till the flow is close to dynamic stall (i.e., till about 26 degrees). The effective chordwise convection velocity of the vortex relative to the airfoil (obtained from the slope of this line) is about $0.24U_\infty$ during this period. Beyond the incidence of 26 degrees, the DSV is rapidly ejected in a direction almost normal to the airfoil surface into the free-stream. Since the vortex is either partially or fully outside the field of view at these incidences, its trajectory could not be calculated beyond the incidence of 26 degrees.

Topology of the Flow Field

The topology of the flow field computed numerically for a pitching NACA 0012 airfoil at Re= 10^4 and $\alpha^+ = 0.2$, was studied by Visbal[13] in the light of the critical point theory. The critical point theory on flow patterns has been extensively reviewed by Perry and Chong[14] (1987). In this section, the topological features of the streamline patterns obtained in the present study are studied in the light of the above.

As stated by Perry and Chong[14], critical points are points in the flow field where the streamline slope is indeterminate and the velocity is zero relative to an appropriate observer. Normally the critical point theory is applied to the flow field with no-slip boundaries. In the case of a pitching airfoil, the flow field represented in the coordinate system moving with the airfoil represents such a situation. For incompressible flows, following Ref.14, the critical points in the flow can be described in terms of the Jacobian J defined as

$$J = \frac{\partial u}{\partial x}\frac{\partial v}{\partial y} - \frac{\partial u}{\partial y}\frac{\partial v}{\partial x} \tag{1}$$

The critical point is a saddle for $J < 0$ and a center for $J > 0$. $J=0$ represents pure shear.

The detailed process of formation of a primary recirculation (or the LEV) in the front region of the airfoil ($x/c = 0.18$) is revealed in Visbal's[13] calculations by the appearance of a pair of critical points (a center and a saddle downstream of the center). This process occurs within a thin layer of 0.0025c from the surface and is beyond the spatial resolution of the present PIV measurements, at small incidences. However, the subsequent development of the LEV can be observed from the PIV data at the higher angles. Figures 9(a) - 9(f) show some selected streamline patterns from the experiment at Re=1.5x10^5 of the present study. At the incidence of 20.9 degrees (Fig.9a), it can be seen that a recirculation or reverse flow is crawling upstream from the trailing edge while the streamlines next to the surface in the front region also start to thicken. This stage corresponds to the formation of the primary recirculation (center) near the leading edge within the thin layer next to the surface, even though the PIV data could not capture the recirculation in detail, due to the limited spatial resolution. However, a distinctive "half-saddle" point (S1 in the figure) can be observed between the primary recirculation (in this case bulged up streamlines in the front region, C1 in the figure) and the flow reversal from the trailing edge. The pair of critical points (a center C1 and a saddle S1) associated with the formation of the clockwise primary recirculation (or the LEV) can be clearly observed in Fig.9(b) at the incidence of 21.8 degrees. During the incidence interval of 20.9 to 21.8 degrees, the saddle point moves downstream to the mid region and a secondary recirculation region with counter-clockwise rotation can be observed upstream of the LEV. The secondary recirculation has a center C2 (which is very close to the surface and hence can not be seen very well from the PIV data) and an another half-saddle point S2 upstream of the center. At the incidence of 22.6 degrees (Fig.9c), a third pair of critical points (C3 and S3) appear upstream of the other two recirculation regions to form a tertiary recirculating region associated with clockwise rotation. The saddle S3 associated with the third recirculating region is a full saddle located above the secondary recirculation. Streamlines emanating from the leading edge encompass the three recirculating regions. Up to this incidence, streamline patterns in the aft region are relatively complex and it is hard to describe them using the critical point theory. At the incidence of 24.4 degrees, the primary recirculation region rapidly increases in size to form the dynamic-stall vortex. Three pairs of critical points ((C4, S4), (C5, S5) and (C6, S6)) can also be seen in the aft region of Fig.9(d) as the coherent vortical structure of the SLV begins to form. The saddle point S4 associated with the SLV must be

in the wake and is not seen in the figure. At 25.2 degrees (Fig.9e), the half-saddle point **S1** associated with the primary recirculation detaches from the surface and forms a full-saddle point. In the aft region, the vortical structures seem to settle into two recirculating regions. At the incidence of 26.1 degrees (Fig.9f), the center of the primary recirculation **C1** (the dynamic-stall vortex) is about to leave the view, approaching dynamic-stall. The full saddle point **S1** associated with the vortex can be clearly seen in the mid region. The secondary recirculating region (or the secondary vortex) with counter-clockwise rotation has also moved away from the surface. The flow fields are heavily influenced by interactions of these recirculating regions and the airfoil surface.

Conclusions

A comprehensive set of velocity data have been obtained on a pitching airfoil. These data complement the surface pressure data obtained earlier on the same airfoil in the same facility. A detailed study of these data has led to the following important conclusions.

(1)   The increase in lift of a pitching airfoil is due to the influx of vorticity from the surface by the presence of strong favorable pressure gradient near the leading edge. Lift continues to increase so long as vorticity is generated and remains close to the airfoil surface. Infusion of counter-clockwise vorticity from the airfoil surface due to local adverse pressure gradient forces the shear layer to lift up and thus creates the LEV. Also, the continued influx of counter-clockwise vorticity from the surface produces a secondary counter-clockwise vortical structure underneath the LEV, which causes the shear layer to roll up. The rolled up shear layer along with several vortices generated by the shear-layer instability forms the DSV. The DSV grows in size and is eventually ejected abruptly at a large angle with respect to the airfoil surface leading to the dynamic stall.

(2)   Early transition to turbulence at high Reynolds numbers causes the LEV to form at larger incidences, but more abruptly than at low Reynolds numbers. Also, the DSV at high Reynolds numbers is more compact, better defined and contains fewer vortices formed from the instability of the shear layer before it is ejected from the surface. The DSV is clearly separated from an other dominant vortical structure, the so-called shear-layer vortex (SLV), which occupies the mid-to-aft region of the airfoil.

(3)   Several pairs of critical points have been identified in the flow pattern obtained from the PIV data. However, all these critical points are characterized by non-zero shear strain rate and hence do not represent unsteady separation points in the MRS sense. Computation of particle trajectories may help to understand the mechanism underlying the unsteady separation from the Lagrangian point of view[16]. This requires additional work and may require improvement in the temporal resolution of the PIV.

There is strong reason to believe that the present results (especially those obtained at the Reynolds number of 1.5×10^5) are representative of flow behavior at "high" Reynolds numbers of practical interest. The PIV data, along with the surface pressure data, have been archived and are available to any interested reader. These data form a comprehensive database suitable for use in the development and verification of computational fluid dynamics codes for pitching airfoils.

References

[1]Shih, C., Lourenco, L.,, Van Dommelen, L., and Krothapalli, A., "Unsteady Flow Past an Airfoil Pitching at a Constant Rate," *AIAA.Journal*, Vol.30, No.5, p.1153.

[2]Oshima, H., and Ramaprian, B. R., "Measurement of the Velocity and Vorticity Fields around a Pitching Airfoil," AIAA Paper No.92-2626, June 1992.

[3]Oswald, G., Ghia, K. and Ghia, U., "Simulation of Dynamic Stall Phenomenon Using Unsteady Navier-Stokes Equations," Proceedings of IMACS First International Conference on Computational Physics, June 1990.

[4]Visbal, M. R. and Shang, J., "Investigation of the Flow Structure Around a Rapidly Pitching Airfoil," *AIAA J.*, Vol. 27, No. 8, 1989, pp.1044-1051.

[5]Visbal, M., "On Some Physical Aspects of Airfoil Dynamic Stall," Proc. of the Int.Symp. on Nonsteady Fluid Dynamics, ASME, FED, Vol.92, eds. J.A. Miller and D.P. Telionis, 1990, pp.127-148.

[6]Conger, R. C. and Ramaprian, B. R., "Pressure Measurements on a Pitching Airfoil in a Water Channel," *AIAA Journal*, Vol.32, NO.1, 1994, pp.

[7]Conger, R. C. and Ramaprian, B. R., "The WSU-MME 1m x 0.7m Water Channel," Department of Mechanical and Materials Engineering Report, No. MME-TF-92-1, Washington State University, Pullman, WA, December 1992.

[8]Oshima, H., "PIV Studies of the Unsteady Vortex Dynamics of a Two-Dimensional Pitching Airfoil," Ph.D. Thesis, Department of Mechanical and Materials Engineering, Washington State University, Pullman, WA, December 1994.

[9]Walker, J. M., Helin, H. E., and Strickland, J.H., " An Experiential Investigation of an Airfoil Undergoing large Amplitude Pitching Motions," AIAA Paper No. 85-039, 1985.

[10]Walker, J. M., Helin, H. E., and Chou, D.C., "Unsteady Surface Pressure Measurements on a Pitching Airfoil," AIAA Paper no. 85-0532, 1985.

[11]Lovato, J. A., "Active Control of the Separation Region on a Two-Dimensional Airfoil," Ph.D thesis, Department of Mechanical and Materials Engineering, Washington State University, Pullman WA, June 1992.

[12]Moore, F. K., "On the Separation of the Unsteady Laminar Boundary Layer," IUTAM Symposium Unsteady Boundary Layers, H. Gortler ed., pp.296-311, 1958.

[13]Visbal, M. R., "Two-Dimensional Unsteady Leading-Edge Separation on a Pitching Airfoil," *AIAA J.*, Vol. 32, No. 4, 1994, pp.673-681.

[14]Perry, A. E. and Chong, M.S., "A Description of Eddying Motions and Flow Patterns using Critical-Point Concepts," *Ann. Rev. Fluid Mech.*, Vol. 19, pp.125-55, 1987.

[15]Sears, W. R. (1956) "Boundary Layer Growth near a Rear Stagnation Point," *Q. Appl. Maths.*, Vol 13, 1956, pp.444-51.

[16]Panton, R.L., "Incompressible Flow," Wiley-Interscience, 1984, Ch.13.
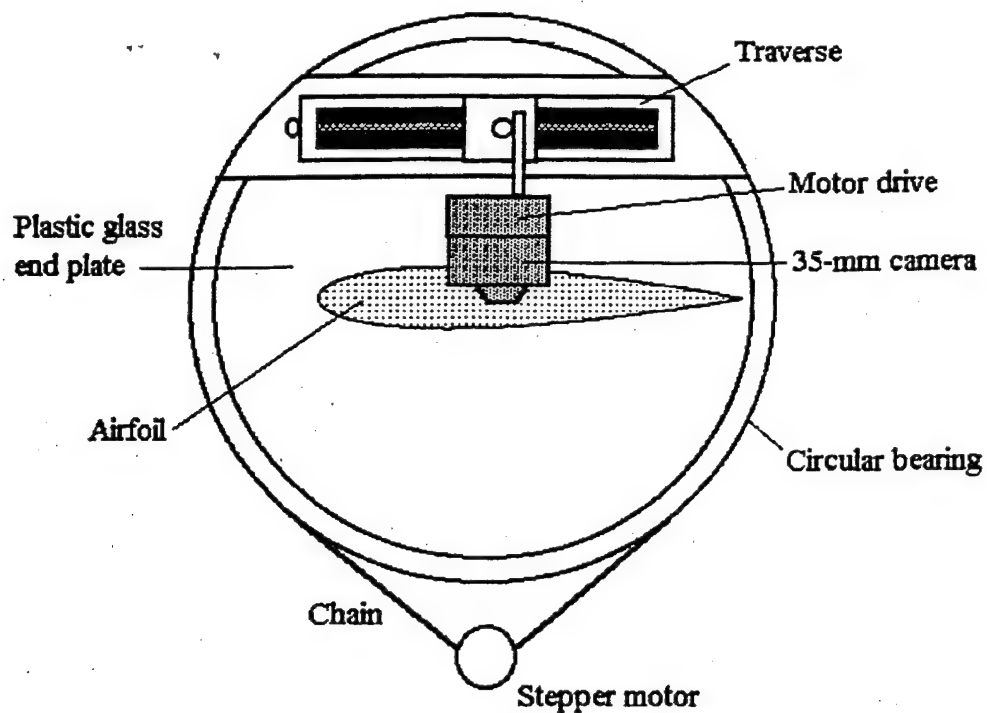
Figure 1(a) Schematic of the Airfoil Pitching Mechanism
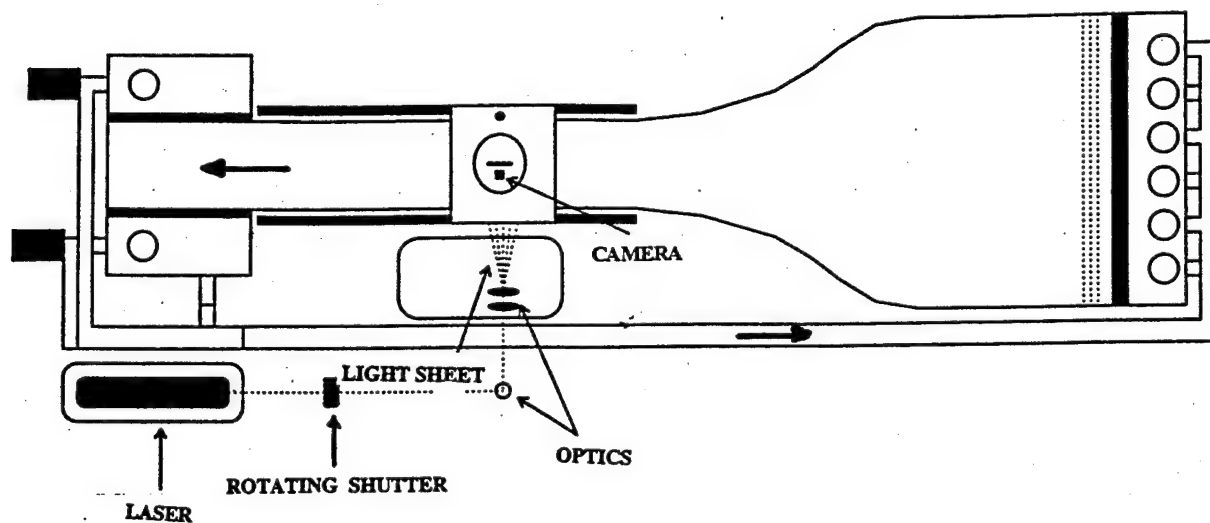
Figure 1(b) Schematic of the Optical Set-Up used for PIV

20.9 degrees

20.9 degrees

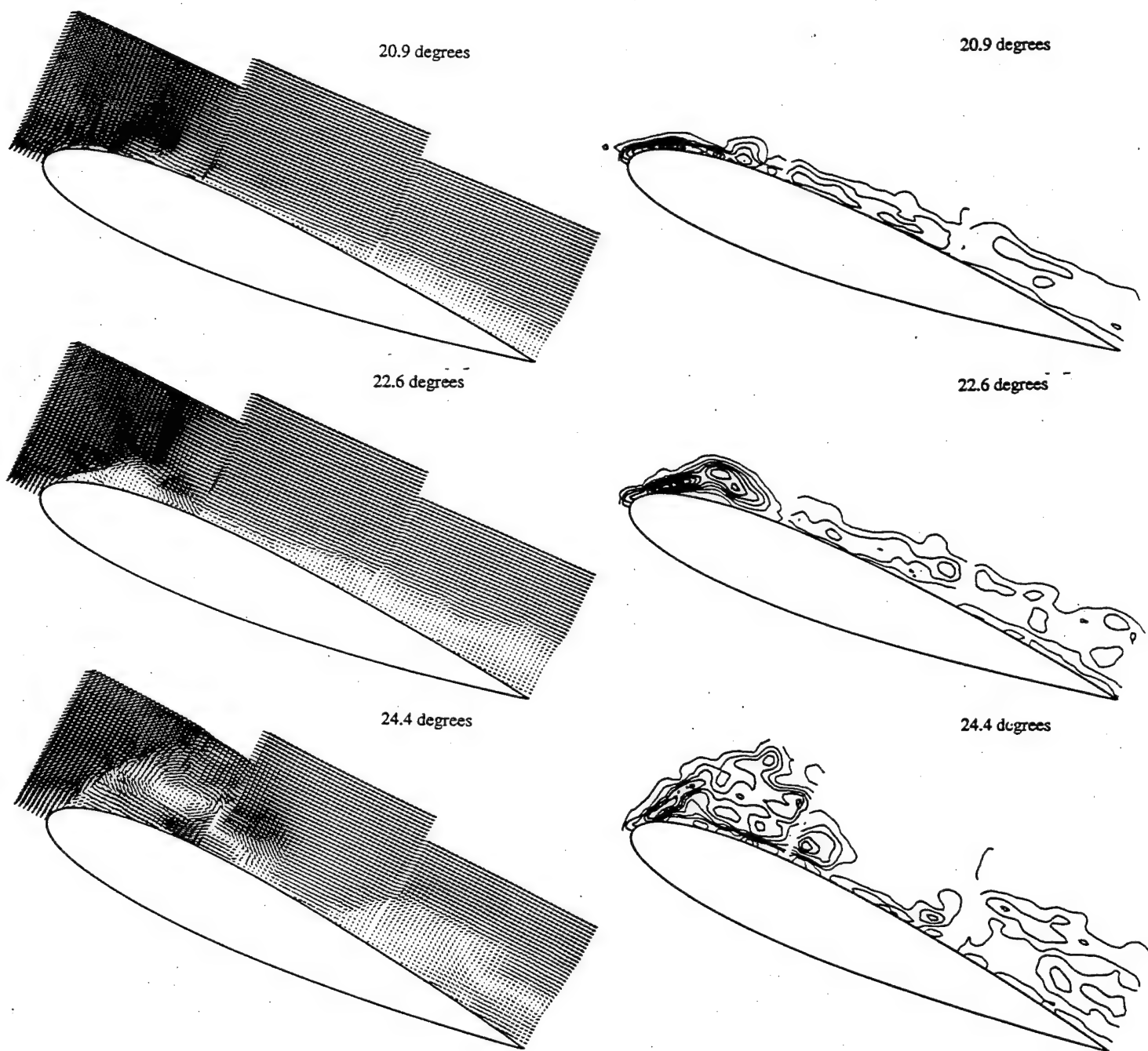22.6 degrees

22.6 degrees

24.4 degrees

24.4 degrees

Figure 2   Typical Velocity and Vorticity Fields over the Airfoil. Velocity vectors are shown
on the lefthand side.   Vorticity contours are shown on the righthand side.   The numbers
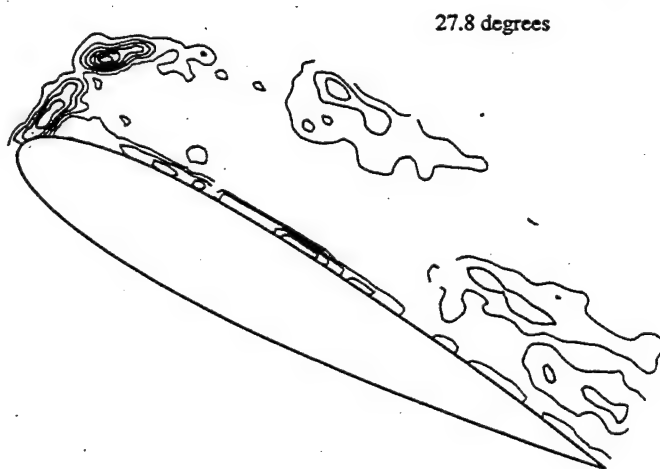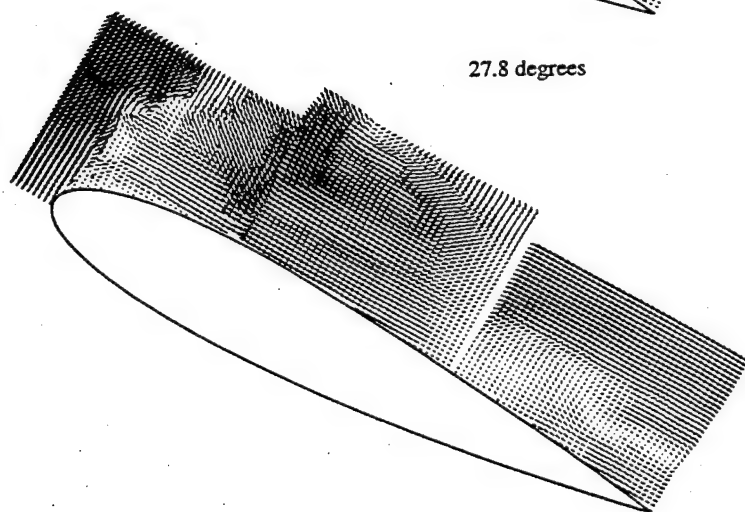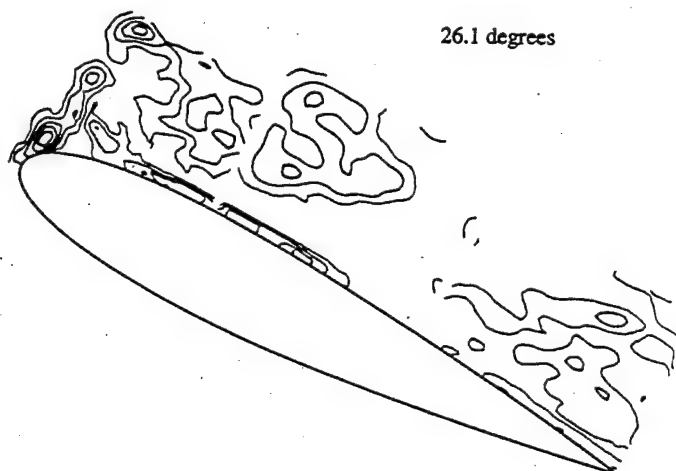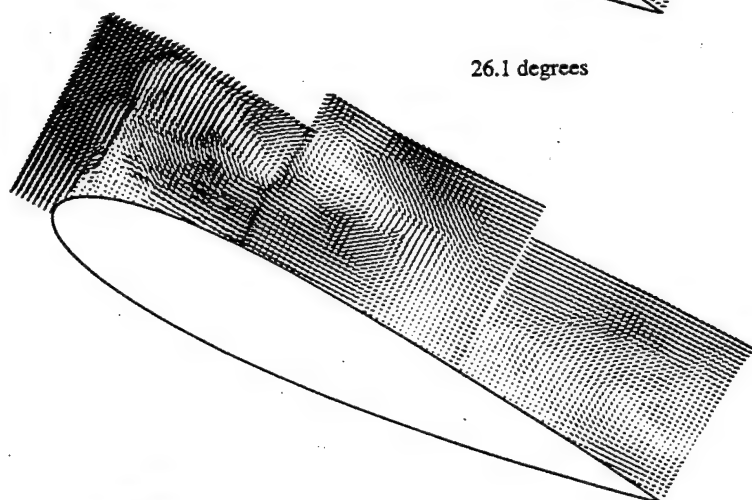shown are the instantaneous incidences.

25.2 degrees

25.2 degrees

26.1 degrees

26.1 degrees

27.8 degrees

27.8 degrees
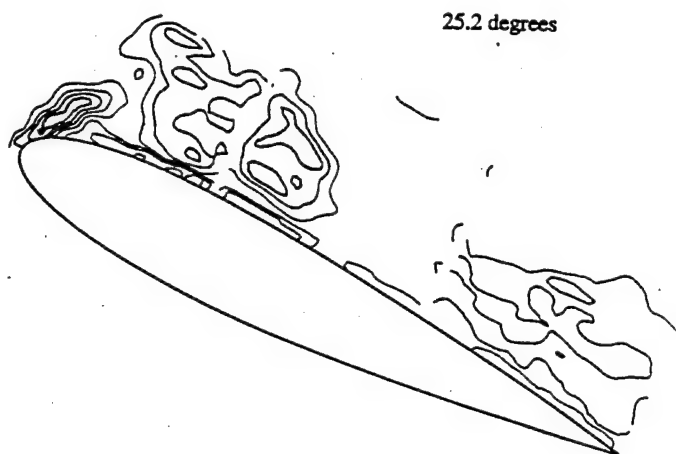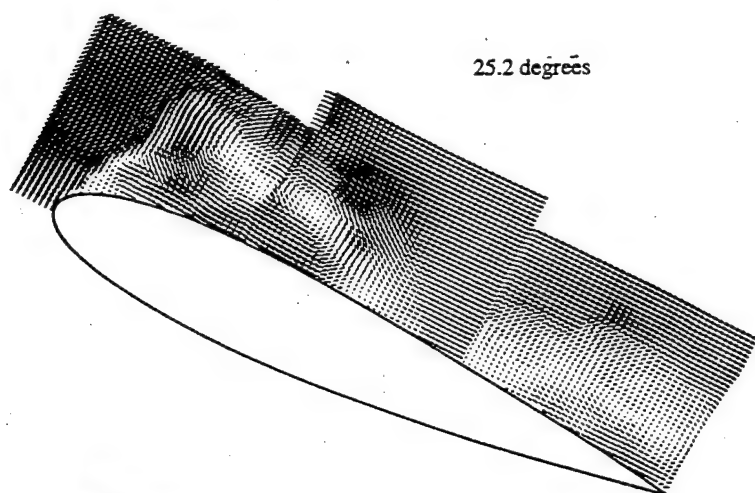
Figure 2 (Contd)
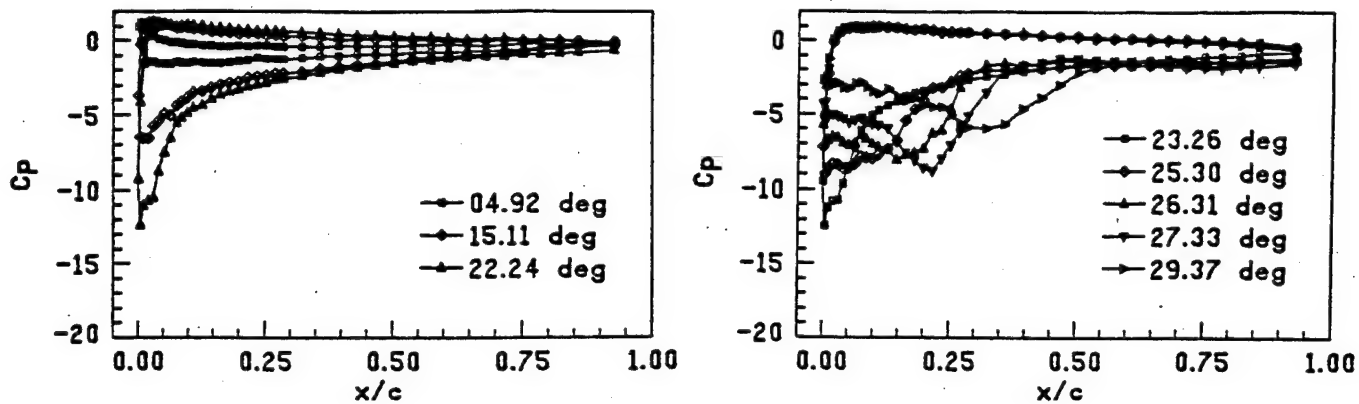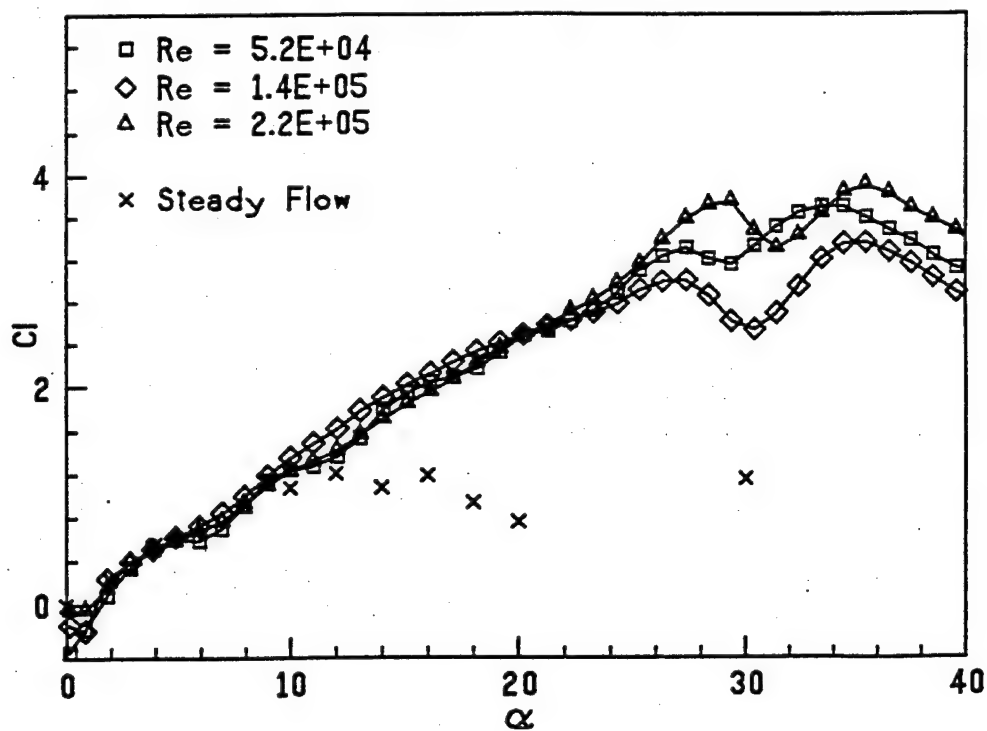
Figure 3 Phase-locked surface pressure distributions and lift. (a) C_p distributions at different incidences. Re=150,000 (b) Effect of Reynolds number on Lift in unsteady flow. α^+=0.075. Steady flow results are for Re=150,000.

24.2 degrees

(a)

25 degrees

(b)

26.1 degrees

(c)
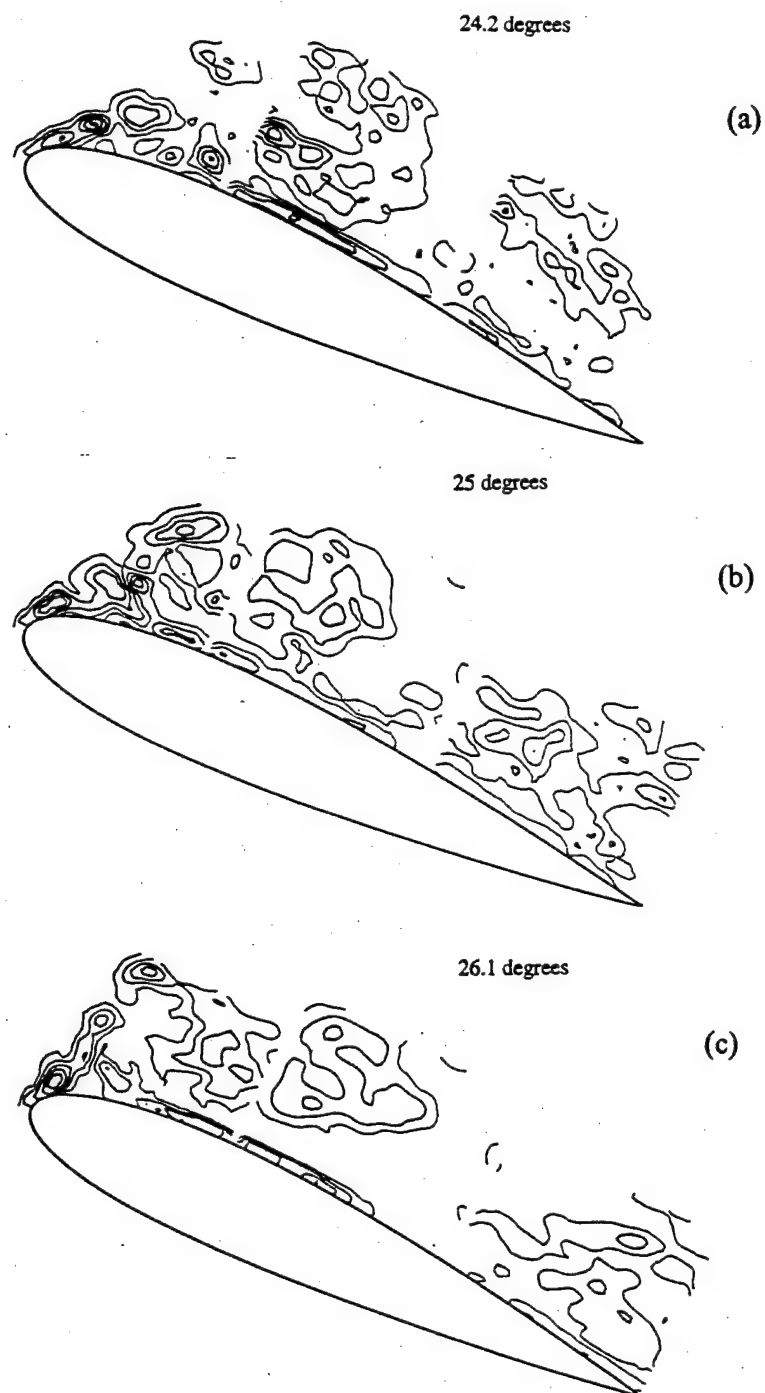
Figure 4 Effect of Reynolds number on the unsteady vorticity field. $\alpha^+ = 0.075$.
(a) Re=18,000 (b) Re= 54,000 (c) Re=150,000
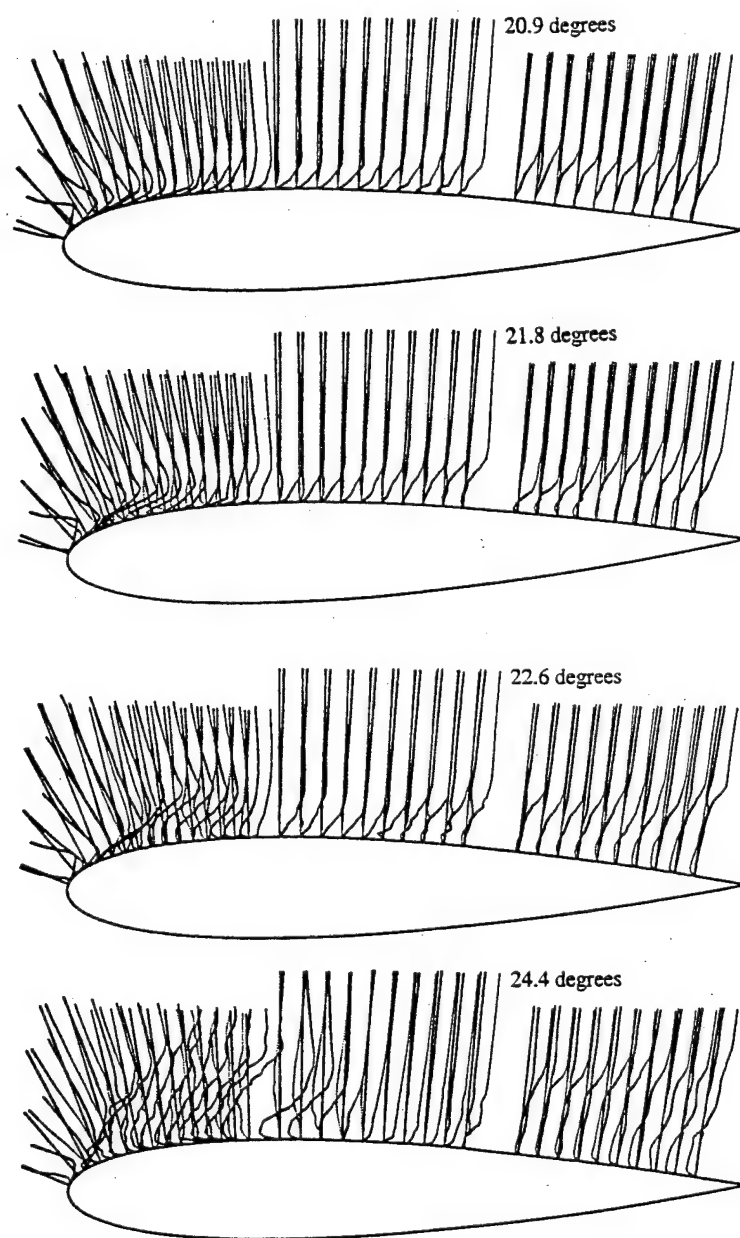
Figure 5 Typical cross-stream distributions of the velocity components u_s (shown as full libes) and u_n (shown as dotted lines). Re=150,000, α^+= .075.
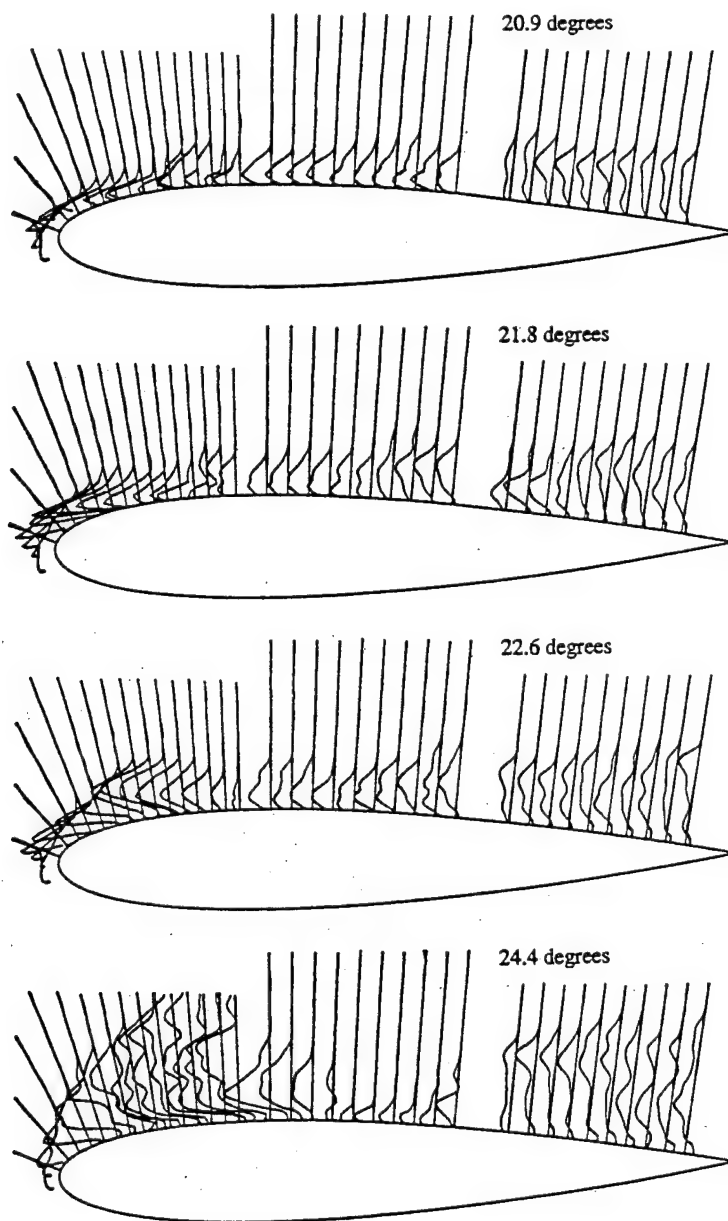
Figure 6 Typical cross-stream variations of the spanwise vorticity ω_z. Re=150,000, α^+=0.075.

25.2 degrees

(a)

25.2 degrees

(b)

25.2 degrees

(c)
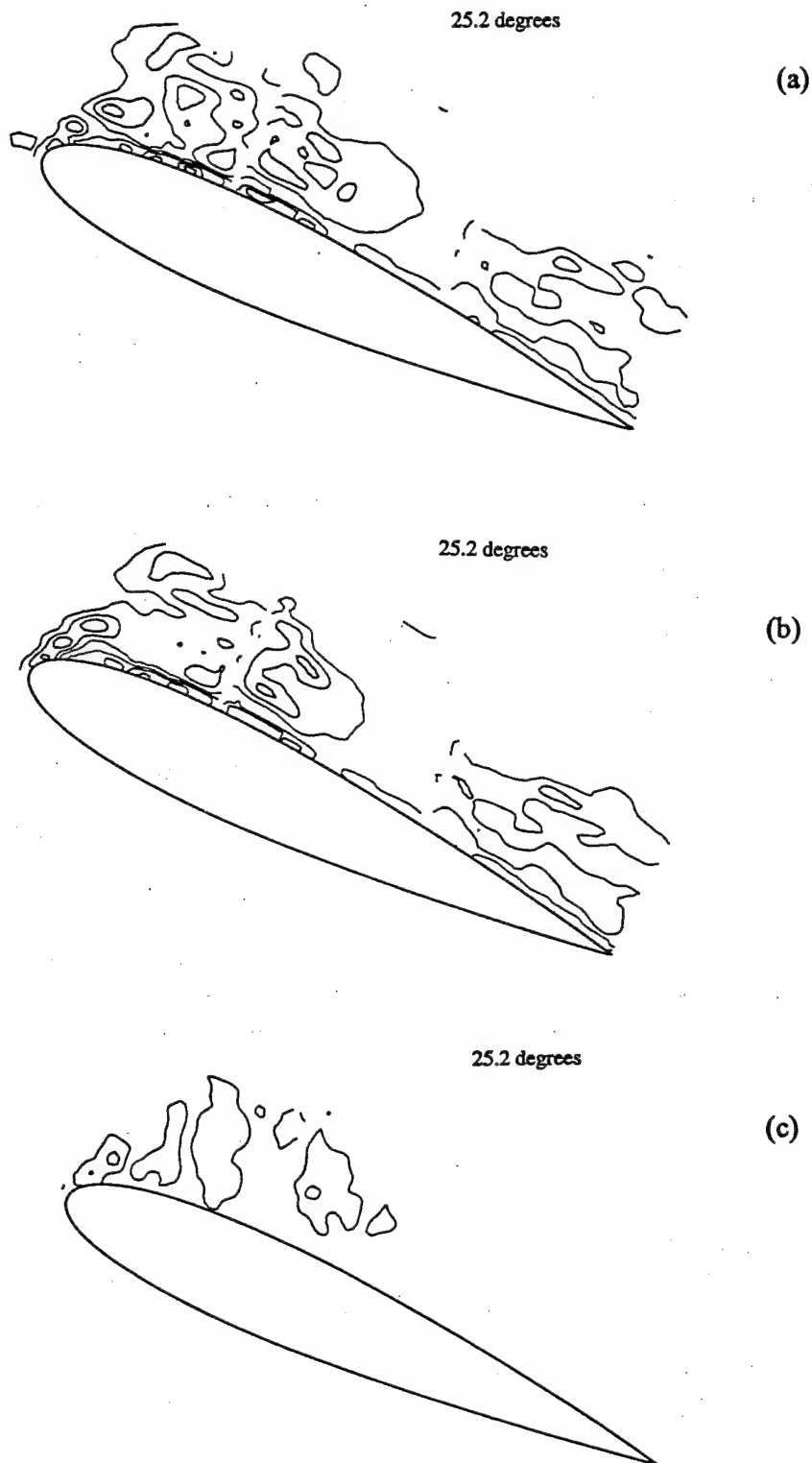
Figure 7 Contours of the various velocity gradients at the incidence of 25.2 degrees (just prior to dynamic stall). Re=150,000. α^+=0.075. (a) shear strain rate (b) $S_{s,n}$ (c) $S_{n,s}$
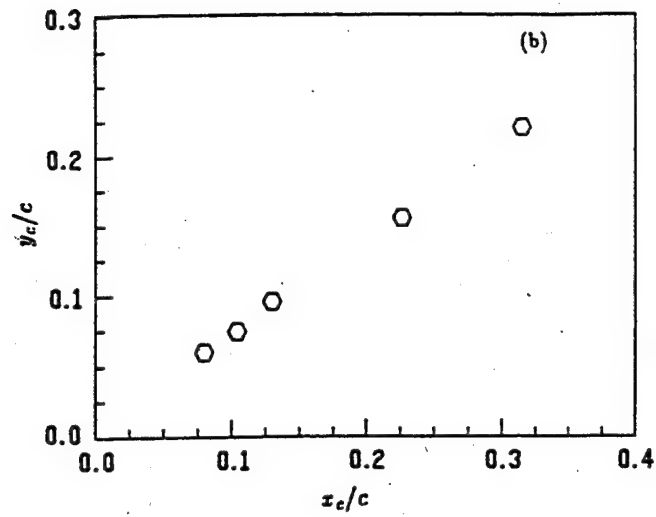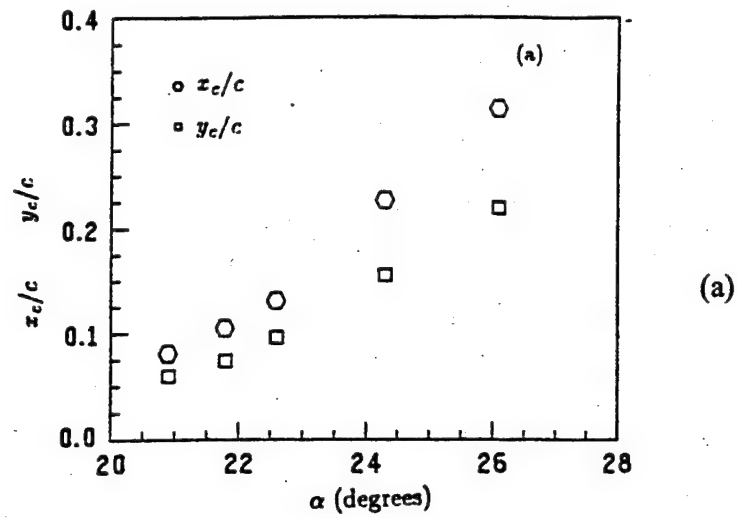
Figure 8 Motion of the DSV. (a) Co-ordinates x_c/c and y_c/c of the center of the vortex at different incidences (b) Trajectory of the vortex center
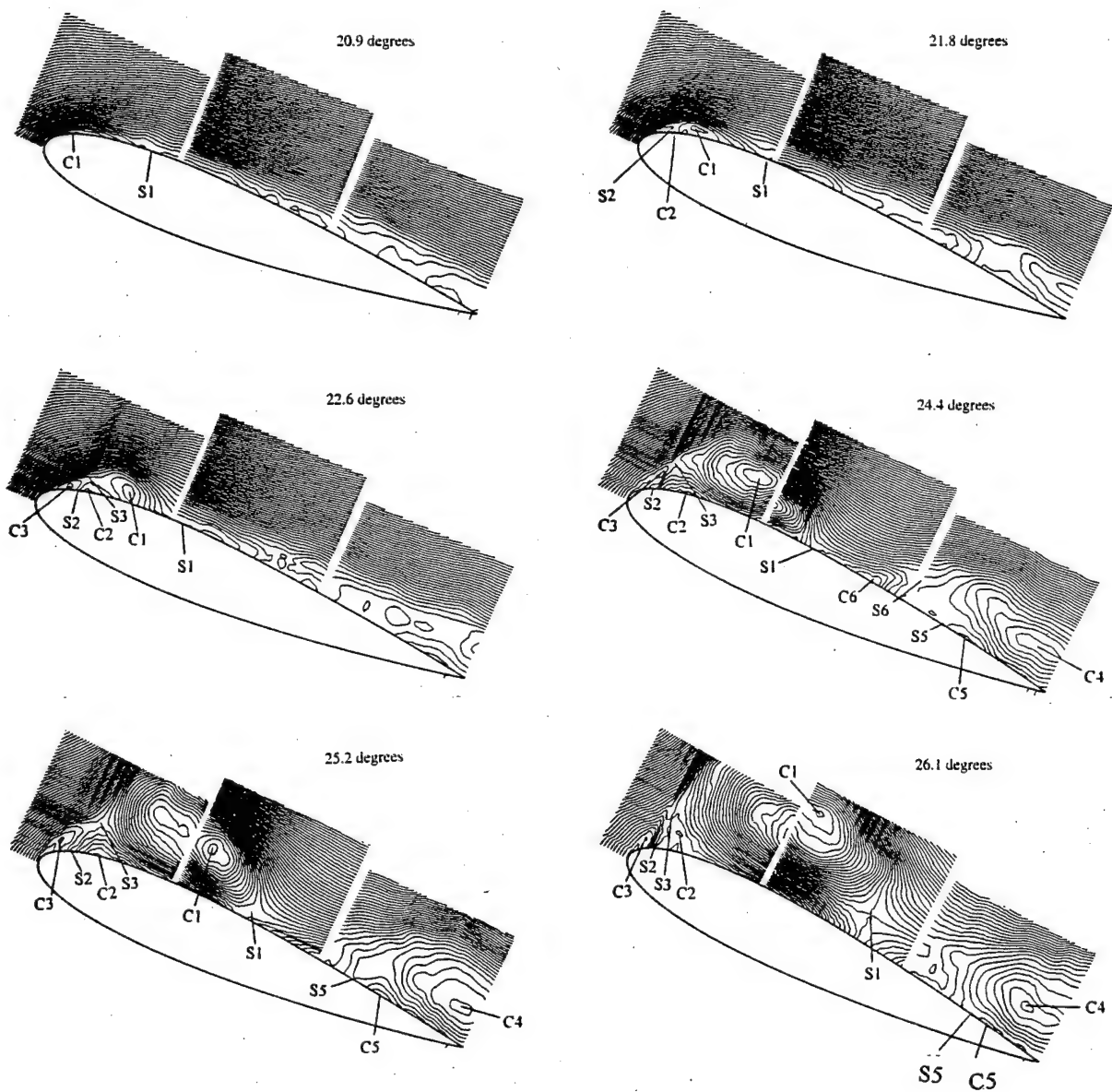
Figure 9 Topological features of the unsteady flow at selected incidences. Re=150,000, α^+=0.075.

APPENDIX II

SURFACE PRESSURE MEASUREMENTS ON A PITCHINGSWEPT WING IN A WATER CHANNEL

by
April Patterson[1]
U.S. Army Corps of Engineers
Hydroelectric Division Center, Portland, OR.,

Paul Rymarz[2] and B.R. Ramaprian[3]
Department of Mechanical and Materials Engineering
Washington State University, Pullman, WA 99164-2920

Abstract

This paper presents the results of surface pressure measurements on a swept wing of NACA 0015 profile and a back sweep angle of 15 degrees, which was pitched at a uniform angular velocity. The pitching axis was perpendicular to the flow direction so that the experiment simulated the pitch-up maneuver of a fixed-wing aircraft. The experiments were performed in an open-surface water channel. The object of the study was to understand the mechanics of vorticity production and dynamic stall in three-dimensional unsteady flows. The phase-locked pressure data which were obtained at several closely spaced spanwise locations of the wing were used to obtain information on the fluxes of spanwise and chordwise vorticity components, in addition to the usual information on the aerodynamic coefficients. The study showed that the three-dimensional dynamic stall over the slightly swept wing is less catastrophic and more gradual than the two-dimensional process over an unswept wing. Other important effects observed were a spanwise variation of the aerodynamic coefficients and the presence of spanwise periodicity in the production of vorticity following the onset of dynamic stall. The experimental data have been archived and are available to any interested user.

Nomenclature

b   span (measured along z)
c   chord length (measured along x)
C_p pressure coefficient
C_l sectional lift coefficient
C_m moment coefficient
C_l^* reduced lift coefficient, defined as $C_l / \cos^2 \Lambda$

---

[1]Mechanical Engineer

[2]Graduate Research Assistant

[3]Professor, Member AIAA

p	distance of the pitch axis from nose
Re	Reynolds number, $U_0 c / \vartheta$
s	longitudinal surface coordinate
U_0	freestream velocity
x	co-ordinate along the free stream
y	co-ordinate normal to chord
z	co-ordinate perpendicular to the free stream
α	angle of attack
α^+	nondimensional pitch rate, $\omega c / U_0$
Λ	back sweep angle
ω	angular velocity of pitching
ω_x	axial vorticity
ω_z	spanwise vorticity
W_x	flux of ω_x
W_z	flux of ω_z
ρ	density
ϑ	kinematic viscosity
'	denotes coordinate system perpendicular to leading edge. See Fig.1.

Introduction

The unsteady vortex dynamics of an airfoil pitched at a uniform angular velocity about its c/4-axis has been studied with interest in recent years. Most of these studies relate to two-dimensional flows. Studies reported on the unsteady aerodynamics of three-dimensional flows have, so far, largely pertained to the flow over Delta wings. Some studies have recently been reported on the three-dimensional flow associated with pitching/oscillating rectangular wings of finite aspect ratio[1-10]. These include flow visualization as well as pressure/force measurements..

The three-dimensional flows mentioned above represent extremely complex situations. To understand some of the characteristics of the unsteady, three-dimensional vortex dynamics and flow separation, it will be useful to conduct experiments which represent *small* departures from two-dimensional flows. In fact, this has been the approach used successfully in the past, to understand steady three-dimensional flows. A very comprehensive study of the pressure and velocity field associated with a pitching two-dimensional NACA 0015 airfoil has been completed at Washington State University, using a water channel specially constructed for this purpose (see Conger and Ramaprian[11,12]). This study has now been extended to the investigation of the flow over a pitching wing of the same profile, but with a small back sweep angle of 15 degrees. Three-dimensionality, characterized by a small cross flow, is introduced into the unsteady flow by pitching this wing about an axis perpendicular to the free stream. This paper presents the results of the first phase of this ongoing program of study. In this phase, phase-locked surface pressure distributions were measured at different spanwise locations on the wing while it was pitched at constant angular velocity. Data have been obtained at a Reynolds number Re= 130,000 and at four different non-dimensional pitching rates in the range $0.037 \le \alpha^+ \le 0.21$. Previous studies[11] on the two-dimensional airfoil (unswept wing) have shown that under these

conditions existing in the water channel, the flow mimics very closely the behavior representative of much higher Reynolds numbers (~ 10^6). The pressure data from the swept wing have been used to obtain information on the aerodynamic coefficients, and the production of vorticity by pressure gradients in the spanwise and chordwise directions.

Experimental Particulars

Experimental Set-Up

One of the distinguishing features of the present experiments is the unique design of the wing model. The wing is of NACA 0015 profile with c'= 0.305 m and s'= 0.61 m (measured perpendicular and parallel to the leading edge respectively). A schematic of the model is shown in Fig.1. It is constructed in 5-cm wide airfoil sections of aluminum machined on a numerically controlled milling machine and anodized for corrosion protection. The wing is assembled from these sections of which one is instrumented with pressure taps. The sections slide on two guide rods such that the instrumented section can be repositioned to varying spanwise locations. This construction allows one to make pressure measurements in several finely spaced spanwise locations without having to provide an impractically large number of pressure taps. The assembled wing has a chord (c) of 32 cm and a span (s) of 59 cm. Measurements are reported over the central 19 cm of the span which was found to be free from significant end effects.

The instrumented wing section has a total of 85 pressure taps of 1.25 mm diameter arranged in five rows spaced approximately 1 cm apart (see Fig.1). The pressure taps are unequally spaced along x' and are provided only on one side of the airfoil surface. "Suction" and "pressure" side data are obtained by pitching the airfoil first in the clockwise and then in the counterclockwise direction. With the present design of the model, it is possible to obtain pressure distributions at 22 z'-locations at intervals of approximately 1 cm. These data can be used to obtain pressure gradients in the chordwise as well as spanwise directions with acceptable accuracy.

Each end of the wing is fitted with a 1.2-cm thick Plexiglas end plate of 64 cm diameter. The wing assembly is suspended in the 0.9 m (width) x 0.62 m (water depth) test section of the water channel, as shown schematically in Fig.1. When mounted in place, the centers of the end plate are located on a vertical axis passing through the c/4 point at midspan of the wing. The upper Plexiglas end plate is bolted into the recess of a PVC pipe which rides on a 64 cm bearing. The bearing is positioned at the center of a rectangular aluminum plate located above the water level. This plate is supported by a large frame (not shown in Fig.1) independent of the water channel and designed to damp out vibrations generated by the pumps. For more details and a complete description of the water channel, reference may be made to Conger and Ramaprian[11,12].

Instrumentation

Pitching of the airfoil at constant angular velocity, about the vertical axis through the center of the end plate, is accomplished by a chain attached to the outside of the PVC pipe and driven by a servo-controlled microstepping motor. A digital encoder on the motor shaft provides information on the angular position of the airfoil. The encoder and controller communicate with

an IBM-compatible personal computer, which also acquires the pressure data.

The pressure measurement system utilizes a diaphragm-type pressure transducer connected between a reference static tap and a surface pressure port via a scanning valve capable of switching among 48 channels. The transducer and scanning valve are carried on an aluminum bar which is mounted on the end plate. A Pitot tube immersed in the flow upstream of the wing provides the reference static pressure and stagnation pressure for all experiments. A swivel ball joint mounted above the center of the rotating aluminum bar provides leak-proof communication between the stationary pressure tubing from the Pitot tube and the transducer moving with the end plate.

Pressure vs. time records were obtained for each pressure tap, one at a time. Steady-flow data were time averaged. The unsteady pressure data were smoothed and corrected for any dynamic response lag effects using a method developed earlier in Conger and Ramaprian[13]. Results were phase averaged over 4 pitching realizations (which have been shown in Ref.11 to be repeatable, at prestall incidences, within $\pm 4.3\%$ in C_p) as a reasonable compromise between accuracy and experimental time. Phase-locked pressure distributions on the airfoil were later obtained from these individual pressure vs time (angle) records.

Experimental Conditions

As already mentioned, all the measurements reported in this paper were made at a Reynolds number of 130,000. Data were obtained at four different pitching rates, $\alpha^+ = 0.037$, 0.075, 0.104 and 0.207. Measurements were made at 22 z'-locations extending over about 22 cm. These data were subsequently interpolated to obtain pressure distributions C_p vs x/c and C_p vs s/c at 19 spanwise locations (i.e., z-direction) extending over a distance of 19 cm. These pressure data were integrated to obtain the lift, pressure-drag and moment about the pitching axis, following standard procedure (see for e.g. Ref.7). The details of calculation are described in Patterson[14]. Pressure gradients along the x' and z' directions were computed from the original 22 sets of data. These results were subsequently used to evaluate the pressure gradients (or, equivalently the vorticity fluxes) in the x- and z- directions. The experimental uncertainties are estimated to be 6% for C_p and the aerodynamic coefficients, and ± 0.07 degree for α. The surface vorticity fluxes (or equivalently, the surface pressure gradients) obtained from smoothed, phase-locked surface pressure distributions are estimated to be accurate to within 12% .

Results and Discussion

Steady Flow

Generally, spanwise flow near the wing surface tends to convect end effects to the midspan region of the wing. It is therefore necessary in principle to use much larger aspect ratios for the swept wing than for unswept-wing, if end effects are to be kept small. However, considerations of the physical limitations of the flow facility and a desire to use a large chord (to obtain more favorable Reynolds number, angular velocity of pitching and spatial resolution of pressure and velocity data) dictated the use of a relatively small aspect ratio and restricting the study to a small (but significant) spanwise region around the midspan plane. The steady-flow

data were used to assess the effect of the proximity to the end, on the uniformity of the flow conditions over this region of study. It was found from the C_p vs x' distributions measured at different (z') locations over the stationary wing, that typically, the overall variations in C_p along z' were on the order of ± 0.1 at an incidence of 14 degrees, in the region -0.33 < z'/c' < +0.33. The lift curves for three spanwise locations shown in Fig.2(a) also confirm that there is no significant spanwise variation in lift. This indicates that the spanwise region of interest can be regarded as being acceptably far away from the ends, at least so long as the flow is not significantly detached from the surface. Flow visualization studies conducted using dyes of different color (discussed in Rymarz[15]) also supported this observation. Since it is not easy to distinguish "end effects" from the *imposed* three-dimensional effects in the case of the pitching wing, we can only extrapolate from the steady-flow experiments and assume that, even over the pitching wing, the end effects are not significant over this spanwise region so long as the flow is not massively separated from the surface, i.e., almost close to the occurrence of dynamic stall. It should be noted, however, that end effects may become significant after separation both in steady and unsteady flow. The present results for the pitching wing at post-dynamic-stall incidences are therefore to be interpreted with some care.

Also, in view of the small variation of pressure in the spanwise direction, it is reasonable to use the span-averaged C_p vs x'/c' distribution to represent the steady-state results. Since x/c=x'/c', this average C_p vs x'/c' distribution, when transformed to the free-stream (x,y,z) coordinate system, yields an identical C_p vs x/c distribution. The lift curve obtained from the averaged C_p vs x/c distribution is shown in Fig.2(b) and compared with the results for un unswept wing from Conger and Ramaprian[11]. It can be seen that sweep results in a reduction of the lift coefficient. Also, the swept wing does not exhibit a drastic drop in lift beyond stall. This latter result is due to the presence of a spanwise component of velocity which causes the onset of separation to be gradual rather than catastrophic. With regard to the lift data at prestall incidences for the swept wing, it has been shown (see for eg. Lorber and Carta[2]) that a "reduced' lift coefficient C_l^* defined by normalizing the lift by 1/2 $\rho U_0^2 \cos^2\Lambda$, better collapses the lift curves for the swept and unswept wings. The result of this normalization is also shown in Fig. 2(b). It is seen that this normalization does not result in a complete collapse of the swept and unswept wing data, although the results are brought closer together. The residual discrepancy may be attributed to Reynolds number effects. In the two-dimensional experiments of Conger and Ramaprian[11], early laminar-turbulent transition seems to have occurred in the boundary layer over the leading-edge region of the wing surface, even at the moderate experimental Reynolds number of 1.3×10^5. The early triggering of transition was attributed in Ref.11 to the high freestream turbulence of about 1% in the water channel. The early transition would result either in the total elimination of the so-called leading-edge separation bubble (characteristic of low Reynolds number flows over airfoils) or in the formation of a very small bubble, thereby producing larger lift coefficients characteristic of flows at much higher Reynolds numbers. Apparently, such early transition and consequent "simulation" of high-Reynolds number effects did not occur at the Reynolds number of 1.3×10^5 in the present *steady-flow* experiments over the swept wing, in spite of the high freestream turbulence. This is presumably because of the presence of the spanwise flow, which is known to delay transition. The resulting formation of a separation bubble would explain the observed reduction in lift relative to the unswept wing. The presence of a small separation bubble could, in fact, be inferred from a mild plateau

observable in the pressure distribution curves for the steady swept wing, shown in Patterson[14]. However, the introduction of unsteadiness in to the flow changes the entire dynamics as will be seen from the corresponding results for the pitching wing, which are presented later.

Unsteady Flow

Phase-locked pressure data for the pitch-up maneuver will be presented in the x - z coordinate plane. Note that the location of the pitch axis with respect to the leading edge varies with z thus introducing three dimensionality, and hence spanwise variation, in the unsteady flow. In fact, based on the observations in steady flow, we believe that all systematic spanwise variations of flow properties observed in the unsteady flow are almost entirely due to the pitch-axis geometry, and not significantly due to end effects. A typical experimental condition of $\alpha^+=$ 0.075 is used for a detailed presentation of results. Effects of nondimensional pitch rate are then explored with $\alpha^+=$ 0.037, 0.104, and 0.207.

Surface pressure: A typical set of suction side pressure-angle traces is presented in Fig.3. The traces for different s/c-locations are off-set vertically for the sake of clarity. A three-dimensional plot of the pressure-angle history for all s/c values is shown typically for the midspan plane z/c=0 in Fig.4. It is seen that over most of the pressure side (s/c <0) except near the nose, no significant changes occur in C_p during the pitching process. However, large variations occur on the suction side. Specifically, the suction pressure exhibits a steady increase in magnitude with incidence, leading to the appearance of a local pressure minimum at some incidence, beyond which it begins to decrease. At the nose, $C_{p(min)}$ has a magnitude of about 9 and occurs at an incidence of about 23 degrees. The pressure minima grow weaker and occur later during pitch-up, at the more downstream locations, as is clearly seen from Fig.3. The behavior of these pressure-angle traces is qualitatively similar to that observed in the case of unswept wings[11].

The occurrence of $C_{p(min)}$ has been usually associated with the formation/arrival of the leading-edge vortex at the particular location. The chordwise movement of $C_{p(min)}$ can, therefore, be related to the convection of the leading-edge vortex, as has been done in Lorber and Carta[2], and Green, Galbraith, and Niven[16]. In the present studies, the angle α_{min} at which the local pressure minimum occurs at each chordwise location (s/c) was obtained from the pressure-angle records. The variation of α_{min} with s/c at the midspan plane, during the period $\alpha \approx 22$ degrees (when the vortex first appears on the wing) to $\alpha \approx 28$ degrees (approximate incidence for maximum lift) is shown by the full line drawn on the pressure contour map displayed at the bottom of Fig.4. It was found that this curve can be approximated by a straight line, the slope of which gives the convection velocity of the suction maximum point in the chordwise direction, as 0.17 U_0. A similar result was obtained for all spanwise locations. This value can be compared with $0.25U_0$ and $0.09U_0$ reported for the inboard and tip region, respectively, of a rectangular wing in Ref.4. From the α_{min} vs s/c results obtained at different spanwise locations, it is possible to draw the contours of α_{min} in the s-z plane, in the range of 22 to 36 degrees. These contours are shown in Fig.5. The contour for each α_{min} in this figure represents the line on the wing surface on which $C_{p(min)}$ (and hence the dynamic stall vortex) first appears at that incidence. Hence, each contour line can be regarded as the signature of the instantaneous axis (or a "wave front") of the stall vortex on the surface of the wing. The contour lines have a jagged

appearance which is due to the uncertainty in the determination of α_{min} from the pressure-angle traces. However, it is still possible to observe two overriding trends. These are:

(i) $C_{p(min)}$ moves along the wing surface, as indicated by the arrow in Fig.5, with a generally oblique wave front shown by the bold dashed line for each incidence. More specifically, $C_{p(min)}$ first occurs at the lower spanwise positions ($z/c<0$) and spreads upwards ($z/c>0$) during pitching.

(ii) this average wave front is modulated by what appears to be spanwise periodicity which is evident over the background noise.

These results bear qualitative resemblance to the observations of Lorber[3] in his studies of unsteady flow near the tip of a rectangular wing. However, no spanwise waviness was apparent in his data. It should be noted though that the two flows are not similar, even though they are both three-dimensional. While the baseline steady flow near a wing tip is three-dimensional, three dimensional unsteadiness is imposed in the present case (via the geometry of the pitching axis) on what is essentially a quasi-two-dimensional steady baseline flow.

The movement of the wave front in Fig.5 can however be identified only up to a certain incidence, beyond which it gets blurred. The full line drawn across Fig.5 approximately represents this limiting line in the s-z plane, to the left of which the contour lines can be distinguished. Thus, pressure minima can be identified only up to an incidence of about 22 degrees (and $s/c\approx0.1$) at $z/c=-0.3$ whereas they can be identified even up to 36 degrees (and $s/c\approx0.8$) at $z/c=+0.3$. It will be seen later that these angles approximately represent the incidence for maximum sectional lift at each spanwise position. The issue of spanwise modulation will be discussed later.

Figure 6 shows typical phase-locked pressure distributions in the midspan plane at three selected instantaneous angles of attack. The suction peak (the maximum magnitude of the phase-locked pressure) increases with increasing incidence and is located within 5% of the nose up to the stall angle. The suction peak reaches a maximum at 22.24 degrees in this case, after which it collapses. A slight bulge also appears just down stream of the suction peak at this incidence. It then develops to an approximate constant-pressure plateau and the suction side curve distorts to that seen at 26.31 degrees. The figure also shows corresponding results at the same angle of incidence for an unswept wing. The appearance of the long plateau (with a barely noticeable mild hump) in the pressure distribution for the unswept wing, is a contrast from a sharper second suction peak observed in the case of the unswept wing. However, like the second suction peak in the latter case, the appearance of the plateau indicates the presence of a stall vortex, which is eventually to be followed by the occurrence of C_{lmax} and dynamic stall. The difference in the pressure distributions observed prior to the onset of dynamic stall in the two cases is due to the difference in the nature of boundary-layer separation in the two cases. In the two-dimensional unsteady flow over the unswept wing, separation is catastrophic with the shear layer being ejected from the surface in the form of a compact and well-defined stall vortex. In the three-dimensional flow over the swept wing, separation occurs more gradually, resulting in a less well-defined, stretched-out dynamic stall vortex.

<u>Aerodynamic Coefficients:</u> The effects of sweep and unsteadiness on the coefficients of lift and pitching moment are shown in Figs. 7(a) and 7(b) by comparing the present data with those at the same Reynolds number from Conger and Ramaprian[11], for the unswept wing pitched at nearly the same rate ($\alpha^+ =0.072$) about its c/4-axis. To eliminate the effect of pitch axis location,

swept-wing results at midspan ($z/c= 0.000$) where the pitch axis is located at $c/4$, are used for comparison. Also presented for comparison are the present steady-flow swept-wing data. Note that the data have not been corrected for blockage effects. The unsteady lift curve for the swept wing departs from the steady lift curve at $\alpha \approx 8$ degrees and continues to increase nearly with the same slope up to an incidence of about 25 degrees. Beyond this incidence, the lift curve flattens out and reaches a maximum value of about 3.5 at an incidence of about 27 degrees after which the lift begins to decrease gradually due to the occurrence of dynamic stall. The lift data for the swept and unswept wings coincide up to an incidence of about 10 degrees, beyond which the swept wing seems to produce a slightly higher lift. This trend continues until dynamic stall occurs with the swept wing displaying maximum lift at a slightly larger incidence. Note that the larger maximum lift associated with the second peak in the unswept-wing data in Fig.7 is suspected to be caused by blockage effects (see Ref.11 for a discussion on the blockage effects) and hence is likely to be spurious. The smaller size of the model and three-dimensional features of the flow resulted in smaller blockage effects (estimated to be less than 18% at an incidence of 30 degrees) in the present case. Once again, as in steady flow, the more gradual decrease in lift at post-stall incidences, in the case of the swept wing, is a result of the less catastrophic nature of separation.

The closer behavior of the swept and unswept wings in the prestall region of unsteady flow (which is in contrast to the relatively lower lift slope observed for the swept wing in steady flow in Fig.2b) is attributed to the occurrence of (similar) early transition (resulting in the elimination/attenuation of the separation bubble) in both cases. The combination of imposed unsteadiness and high freestream turbulence is apparently adequate to trigger early transition over the swept wing even in the presence of the spanwise flow. The elimination/attenuation of the separation bubble leads to "simulation" of high-Reynolds number behavior and hence comparable lift characteristics for the swept and unswept wings in unsteady flow.

The results for drag coefficient, obtained from integration of the pressure distribution over the wing, showed little effect of sweep even up to the incidence of maximum lift. Beyond this, the swept-wing drag was found to increase more gradually and remained less than for the unswept wing even at large incidences. These results are not presented here for the sake of brevity. They are described in detail in Ref.14.

Figure 7(b) shows results for the coefficient of pitching moment about the pitching axis. These results also show that there is very little effect of sweep on the pitching moment up to an incidence of about 10 degrees. Beyond that incidence, sweep slightly increases the magnitude of the negative pitching moment. Both swept and unswept wings exhibit an increase in pitching moment in unsteady flow at large post-static stall incidences. The swept wing experiences an earlier and larger increase in pitching moment but this increase beyond dynamic stall is not catastrophic. In fact, C_{mmax} is significantly smaller for the swept wing. All the above effects on the aerodynamic coefficients can be explained as being due to a less catastrophic modification in flow pattern accompanying a nonsingular, open-type of separation. Past studies of steady flows (e.g. Wang[17]) have identified this type of separation in three-dimensional flows.

Spanwise Variations: The three-dimensional plots in Figs.8(a) and 8(b) show the variations in C_l and C_m with incidence and spanwise location. There is no significant spanwise variation in C_l at incidences less than about 20 degrees, as can be seen from contour lines which are nearly

parallel to the z-axis (except for the blips seen at $z/c \approx 0.1$, which are suspected to be due to experimental errors). However, after the appearance of the stall vortex, spanwise variation becomes noticeable. The trend that is most clearly seen is an increase in C_{lmax} and a delay in the occurrence of C_{lmax} as z/c increases from the bottom ($z/c=-0.322$) to the top ($z/c=+0.322$) of the wing, as shown by the maximum-lift line (full line) drawn on the contour map at the bottom of Fig.8(a). A similar trend in spanwise variation, namely larger values and delayed occurrence towards the top of the wing, was seen in the drag data also (see Ref.14 for details).

The increasing moment arm lengths from bottom to top of the wing contribute to a larger and even more ordered spanwise variation in C_m about the pitch axis. An increase in the magnitude of the pitching moment accompanied by increasing negative slope towards the bottom of the wing is evident in Fig.8(b), even at pre-stall angles. Also the increase in the magnitude appears at earlier incidences toward the bottom of the wing.

Figures 7 and 8 very clearly show that the dynamic stall process over the swept wing is significantly different from that over the unswept wing. Furthermore, this difference is not merely a quasi-two-dimensional pitch-axis effect, as can be seen from the noncatastrophic behavior of the aerodynamic coefficients (especially C_m) at post-dynamic stall incidences in the former case. It is therefore reasonable to conclude that even a small sweep can produce significant three-dimensional effects in the case of a pitching wing.

Pitch Rate Effects: Data obtained at different pitch rates showed that the pressure distributions are qualitatively similar to those obtained at $\alpha^+=0.075$. However, suction peaks were larger and occurred at higher angles of incidence as the pitch rate was increased. The detailed pressure distributions at all the pitch rates studied are presented in Ref.14. Only the corresponding aerodynamic coefficients C_l and C_m are shown here, typically for the midspan location, in Figs.9 and 10. Note that these results are plotted in terms of an "effective angle of attack" α_{eff} defined on the basis of the relative freestream velocity vector at the nose of the pitching wing. It can be easily shown that this effective angle is given by the equation

$$\alpha_{eff} = \alpha - \alpha^+ \left(\frac{p}{c}\right)\cos\alpha \qquad (1)$$

The use of α_{eff} serves to minimize, even if not eliminate, the effect of the change in the relative orientation of the incident velocity vector with pitch rate. It can be seen from the figure that an increase in pitch rate, especially at the lower pitch rates, primarily results in higher C_{lmax} values at increasing incidence. This also means that the occurrence of dynamic stall is delayed at higher pitch rates. In fact, at the highest pitch rate studied ($\alpha^+ = 0.204$), dynamic stall did not occur within the range of incidence studied. An important feature to note is that, except at the highest pitch rate studied, the lift slope is not significantly affected by pitch rate until the flow is close to dynamic stall. Some reduction in the slope is, however, observed at the highest pitch rate. The higher lifts realized at prestall incidences at moderate pitch rates ($\alpha \leq 0.1$) thus appear to be essentially a quasi-steady (and nearly inviscid) effect resulting from wall motion (which tends to keep the boundary layer attached to the wall up to larger incidences) rather than a *direct* unsteady effect. This is the same conclusion as was reached in Ref.11 for the unswept wing. Once the stall vortex begins to form however, its growth, convection and shedding are no longer either

quasi-steady or inviscid.

Figure 10 shows that pitching moment coefficients for different pitch rates also overlap at incidences below the incidence corresponding to the onset of the stall vortex (i.e. the appearance of the pressure plateau in Fig.6) but increase in general with pitch rate at higher incidences. The drag coefficient (not shown here) was found to exhibit a similar trend. It may be noted that the large increase in the magnitude of C_m occurs earlier than the appearance of C_{lmax}, i.e, considerably earlier than the occurrence of dynamic stall. The dynamic effect on C_m is thus more significant than on C_l.

The results obtained at other spanwise locations at the above pitch rates were found to be qualitatively similar to those observed at midspan. The spanwise variations of the aerodynamic coefficients at the different pitch rates were qualitatively similar to those described for $\alpha+=0.075$ and were found to be significant only beyond the incidence corresponding to the inception of the stall vortex, i.e., at progressively larger incidences at higher pitch rates. In fact, there was little spanwise variation in the lift coefficient at the highest pitch rate of $\alpha+=0.204$, at which dynamic stall was not observed at all within the incidence range studied. On the other hand, spanwise variations in drag and pitching moment, which occurred earlier than the onset of the stall vortex, were observed at all pitch rates. See Ref.14 for details of the results at the higher pitch rates.

<u>Vorticity Fluxes:</u>   It can be shown (see Panton[18]) that at the wing surface, the Navier- Stokes equations reduce to the following form:

$$\frac{\partial C_p}{\partial (s/c)} = -\frac{vc}{U_\infty^2}\frac{\partial \omega_z}{\partial y} = W_z \tag{2}$$

and

$$\frac{\partial C_p}{\partial (z/c)} = \frac{vc}{U_\infty^2}\frac{\partial \omega_x}{\partial y} = -W_x \tag{3}$$

Thus the nondimensional pressure gradients in the spanwise and chordwise directions represent respectively the nondimensional surface fluxes $(-W_x)$ and W_z of the chordwise and spanwise vorticity components ω_x and ω_z. These fluxes were evaluated and are shown for the suction side of the wing typically in Figs.11(a)-11(f), for $\alpha^+=0.075$ and, in each case, for three angles of incidence. The three-dimensional plots are drawn at a view angle such that the aft region of the wing (where W_x is negative and W_z is positive) is brought into view. This is the region where interesting features of three dimensionality are observed. Note that negative values of W_z represent the infusement of negative (lift-producing) spanwise vorticity ω_z from the surface in to the flow. Large negative values of W_z occur very near the leading edge. Some of this can be seen around s/c=0 in Figs. 11(a)-(c), even though the maximum negative value ($\approx$ - 180 units) which occurs at a slightly negative value of s/c is off the scale and hence not seen in the figures.

x

At the more downstream locations in these figures, humps can be observed. The most upstream hump in each case corresponds to the plateau (or a mild second suction maximum) seen typically in Fig.6. It represents the stall vortex still staying very close to the surface. It is seen that the hump appears first at the lowest spanwise location and is seen at upper spanwise planes as the angle of incidence increases from 24 to 28 degrees. The hump gets elongated with time and also appears to break in to longitudinal subhumps. The subhumps in the longitudinal direction most likely represent signatures of the vortices arising from the instability of the shear layer separating from the surface during the early stages of the dynamic stall vortex evolution. The interaction of these vortices with the surface results in the wavy pressure distribution along the flow direction.

At 28-degree incidence, the stall vortex (identified by the modulated hump) is seen to be occupying the entire chord length of the wing at the lowest plane while it occupies only about half the chord length of the wing at the uppermost plane. One can thus conclude that the stall vortex structure propagates obliquely across the wing surface in a wavelike manner. The vortex is also oriented obliquely to the flow direction. The above statements refer to the average structure of the stall vortex. However, Figs.11 (a)-(c) also show that there is significant spanwise modulation of this structure and that this modulation is fairly periodic. Figures 11(d)-11(f) show the distributions of the flux $-W_x$, which essentially lead to the same conclusions as above, both with respect to the propagation of the vortex with an oblique wave front, and with respect to the spanwise periodicity. Figures 11(a)-11(f) complement Fig.5, which shows spanwise periodicity in the contours of α_{min}. Some evidence of this periodicity can also be seen in the post-stall distributions in Fig.8. The precise cause of this periodicity is not known. One speculation is that this periodicity is the result of some Taylor-Gortler type instability produced by the concavity of the streamlines over the suction side of the wing, especially under post-stall conditions. Unfortunately, post-stall pressure data in this spanwise detail are available only for the pitching swept wing, and not for other cases, such as stationary/pitching unswept wing or stationary swept wing. It is not, therefore, clear whether this periodicity is peculiar to the pitching swept wing, or is a general feature of all separating boundary layers over wing surfaces. It is also not clear whether and how a change in the aspect ratio of the wing will affect this periodicity. Further studies are clearly needed to understand this aspect of the flow.

Figures 12(a)-12(c) show a vector plot of the vorticity flux vector at the surface. The wing is shown in the swept-back position and the individual vectors shown correspond to data from the 22 rows of individual pressure taps in the region $0.17<s'/c' <1.0$ and $-0.33<z'/c'<0.33$. The direction of the arrows indicate the direction of the vorticity vector infused at the surface and the length of the arrow denotes the magnitude of its surface flux (or the pressure gradient). The figures correspond to the same incidences as in Fig.11. Once again, the region $s/c<0.17$ where the fluxes are very large is excluded from the figure in order that the interesting behavior of the flux vectors in the downstream region can be scaled and presented more clearly. Note that the vorticity vector generated at the surface is perpendicular to the pressure gradient vector.

At a low incidence of 20 degrees, the flux vectors appear to be organized and, in fact, exhibit a spanwise periodicity. At 24 degrees, the stall vortex begins to appear near the bottom left corner. This results in the flux vectors (or the pressure field) getting disorganized slightly in that region of the wing. The structure over the rest of the wing is undisturbed indicating that there is no influence of the stall vortex on the global pressure field. At 28 degrees, the stall

vortex has spread over a substantial part (southwestern half) of the wing as seen from Fig 12(c). However, flow structure in the remaining part of the wing still appears to be organized and periodic. This shows that the vortex has not lifted off the surface which would have resulted in massive stall. In fact, there was no evidence of such massive stall occurring in the flow even at higher incidences. This was also confirmed from flow visualization studies. The gradual, rather than a catastrophic drop in lift and pitching moment, at post-stall incidences is also consistent with this observation. The evolution and spreading of the stall vortex over the swept wing is thus very different from the evolution, quick growth, and rapid ejection from the surface, observed in the case of two-dimensional flow over an unswept wing. The difference is very striking even when the sweep angle is very small as in the present case.

Conclusions

1. The onset of the dynamic stall vortex in three-dimensional flow over the swept wing is associated with a long pressure plateau (or very mild second suction peak) which replaces the strong second suction peak observed over an unswept wing. Thus, there does not appear to be a rapid ejection/lift-off of the stall vortex from the surface, but a rather gradual spreading of the vortex across the wing surface. This is believed to be due to the occurrence of more gradual, open-type, three-dimensional, flow separation in the presence of the spanwise velocity component. Consequently, sweep increases unsteady C_{lmax}, as well as the incidence at which it occurs. It causes C_m about the pitching axis to increase at an earlier incidence but less drastically than in two-dimensional flow.

2. The aerodynamic coefficients follow a trend that is an extension of the quasi-steady behavior to post-static stall incidences. This is true at all spanwise locations and at all except the highest pitch rate studied. Of these, the pitching moment coefficient departs the earliest from the quasi-steady behavior and shows a large increase well before the occurrence of dynamic stall, whereas the lift and drag coefficients continue to follow quasi-steady trend almost up to the occurrence of dynamic stall. These characteristics are qualitatively similar to those observed in two-dimensional flows.

3. Lift curve slope and maximum lift increase from the bottom towards the top part of the wing. Pitching moment increases in a similar manner, except that the increase begins to appear earlier during the pitching maneuver. The pressure-minimum wave front (usually associated with the stall vortex) convects obliquely along the wing surface from the bottom towards the top of the wing with a longitudinal convection velocity of about $0.17U_0$. All these effects can be related to the pitch-axis geometry studied in the present experiments.

4. There is strong evidence of spanwise modulation in the production of vorticity at the wing surface, especially in the downstream regions of the wing. In fact, some spanwise modulation can be observed even in the lift distribution. The precise cause of this periodicity is unknown. This aspect requires further study.

Acknowledgments

References

1.   Ashworth, J., and Luttges, M., "Comparisons in Three-Dimensionality in the Unsteady Flows Elicited by Straight and Swept Wings," AIAA Paper 86-2280-CP, Aug. 1986.

2.   Robinson, M.C., and Wissler, J.B., "Unsteady Surface Measurements on a Pitching Rectangular Wing," AIAA Paper 88-0328, Jan 1988.

3.   Robinson, M.C., and Wissler, J.B., "Pitch Rate and Reynolds Number Effects on a Pitching Rectangular Wing," AIAA Paper 88-2577-CP, 1988.

4. Lorber, P.F., Carta, O., and Covino, Jr., A.F., "An Oscillating Three-Dimensional Wing Experiment: Compressibility, Sweep, Rate, Waveform, and Geometry Effects on Unsteady Separation and Dynamic stall," UTRC Report No. R92-958325-6, United Technologies Research center, East Hartford, CT, Nov 1992

5.   Lorber, P.F., Carta, O., and Covino, Jr., A.F., "Dynamic Stall Experiments on a Swept Three-Dimensional Wing in Compressible Flow," AIAA Paper 91-1795, June 1991

6. Lorber, P..F., "Tip Vortex, Stall Vortex and Separation Observations on Pitching Three-Dimensional Wings," Paper presented at the *AIAA 24th Fluid Dynamics Conference, Orlando FL, July 1993*

7 .McAlister, K.W., and Takahashi, R. K., "NACA 0015 Wing Pressure and Trailing Vortex Measurements," NASA Technical Paper 3151, NASA Ames Research Center, Moffett Field, CA, 1991

8.   Piziali, R., "Personal Communication," NASA Ames Research Center, Moffett Field, CA, 1993

9.   Zheng, Y., and Ramaprian, B.R., "LDV Measurements in the Three-Dimensional Near Wake of a Stationary and Oscillating Wing," AIAA Paper No. 92-2689, June 1992

10.   Szafruga, J., and Ramaprian, B.R., "Pressure Measurements Over the Tip Region of a Rectangular Wing. part II. Oscillating Wing," AIAA Paper No. 94-1949, June 1994

11.   Conger, R., N., and Ramaprian, B.R., "Pressure Measurements on a Pitching Airfoil in a Water Channel," *AIAA Journal,* vol.32, No.1, January 1994, pp.108-115

12.   Conger, R.N. and Ramaprian, B.R., "The WSU-MME 1 m x 0.7 m Water Channel," Report No. MME-TF-92-1, Mechanical and Matlerials Engineering Department, Washington State University, May 1992

13.   Conger, R.N., and Ramaprian, B.R., "Correcting for Response Lag in Unsteady Pressure Measurements in Water," *Journal of Fluids Engineering,* vol.115, Dec 1993, pp.676-679

14.   Patterson, A., "Surface Pressure Measurements on a Pitching Swept Airfoil in a Water Channel," M.S. Thesis, Mechanical Materials Engineering. Department, Washington State University, Pullman, WA, Dec 1993

15. Rymarz, P.B., "Measurements of Velocity and Vorticity Fields around a Pitching Swept Wing," M.S. Thesis, Department of Mechanical and Materials Engineering, Washington State University, Pullman, WA, May 1955.

16. Green, R.B., Galbraith, R.A.McD., and Niven, A.J., "Measurement of the Dynamic Stall Vortex Convection Speed," *Aeronautical Journal,* Vol.96, Oct 1992, pp.319-325

17. Wang, K.C., "Separation Patterns of Boundary Layer Over an Inclined Body of Revolution," *AIAA Journal,* Vol.10, No.8, 1972, pp.1044-1050

18. Panton, R.L., "Incompressible Flow," John Wiley & Sons, New York, 1984
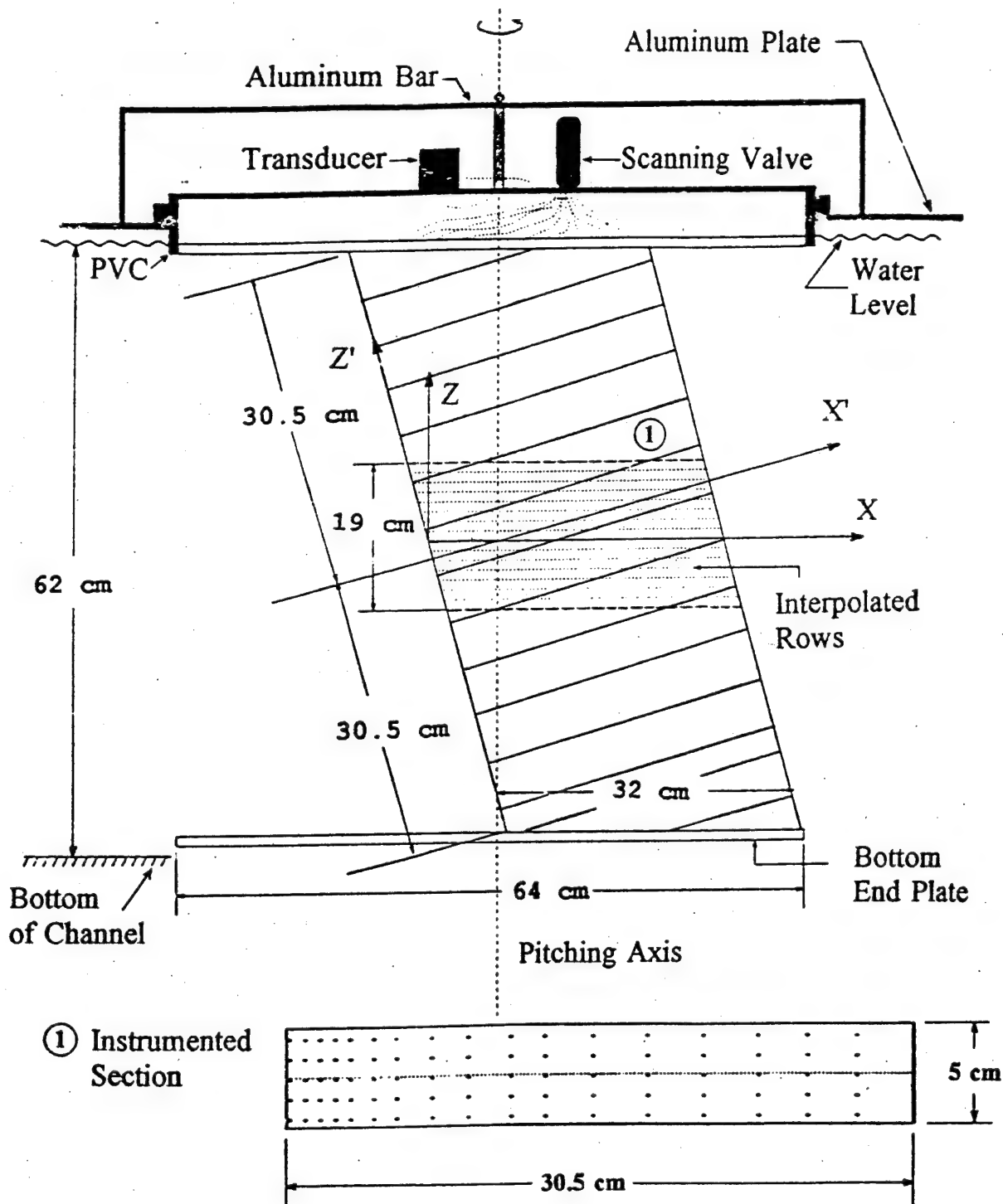
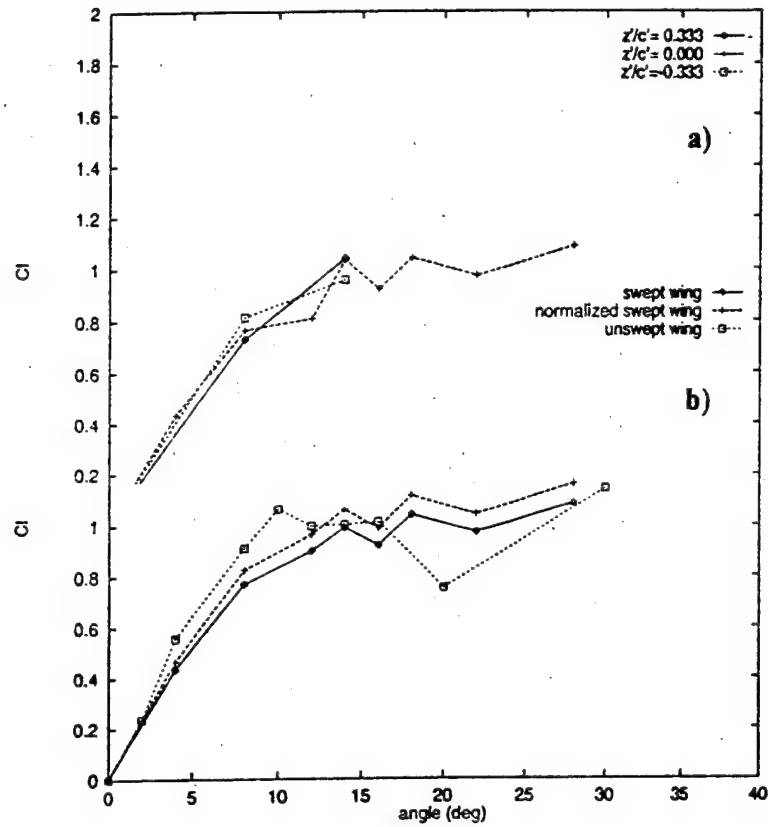Figure 1. Schematic of the wing model and experimental set-up in the water channel

Figure 2. Lift data for the stationary wing. (a) Results for different spanwise locations (b) Comparison with unswept-wing data from Ref.8. Normalized results correspond to $C_l^{\bullet}$.
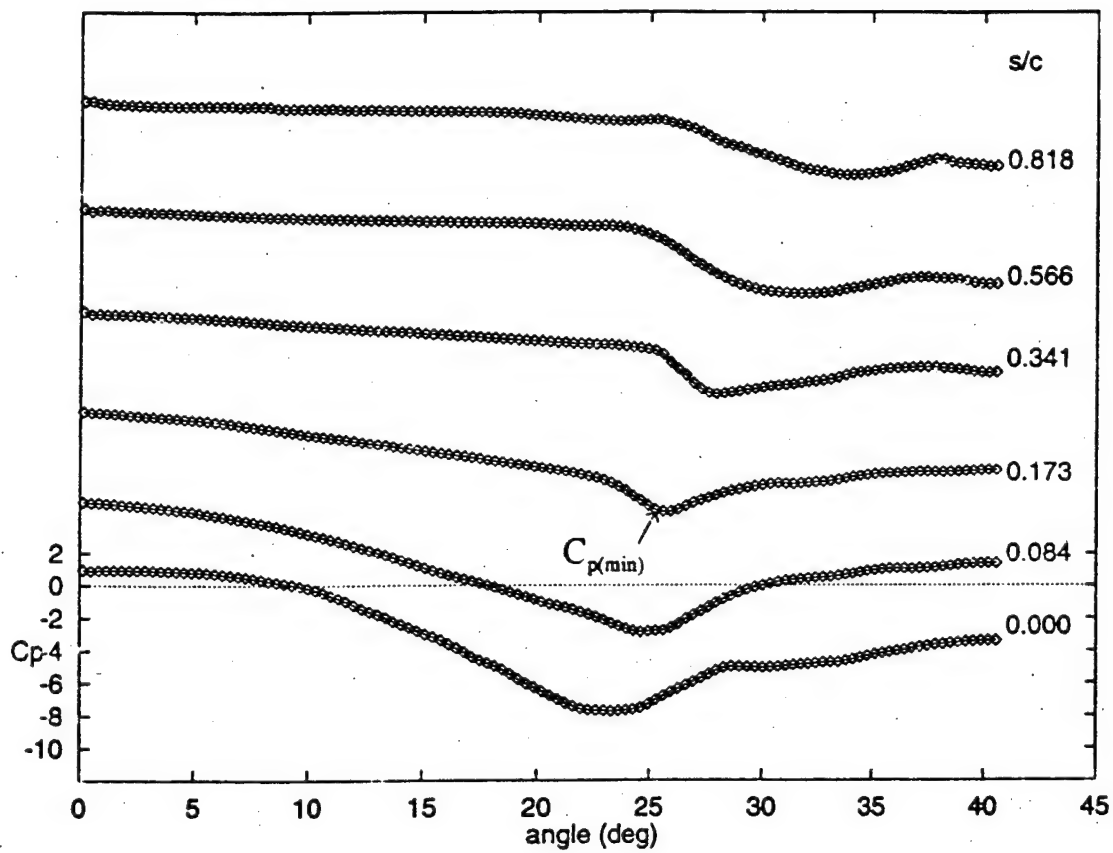
Figure 3. Typical pressure-angle traces at selected pressure tap locations. z/c=0; α^+ =0.075
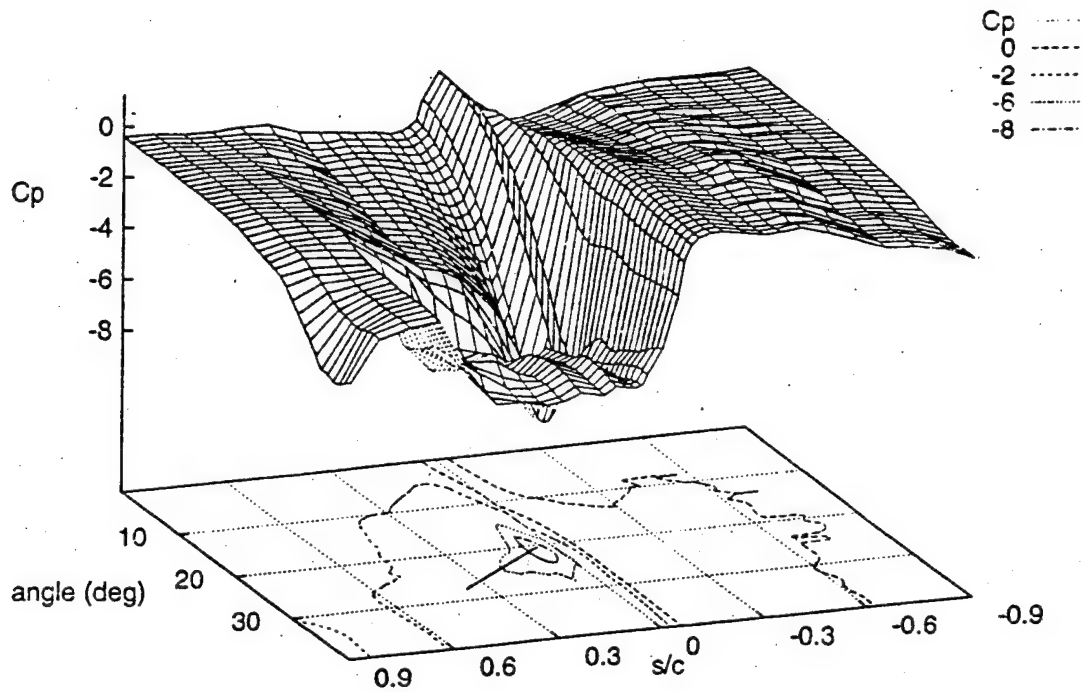
Figure 4. Three-dimensional plots of Pressure-angle history. $z/c=0$; $\alpha^+=0.075$. The lower plot shows C_p contours. The full line in this contour map indicates the locus of α_{min} in the s/c- α plane.
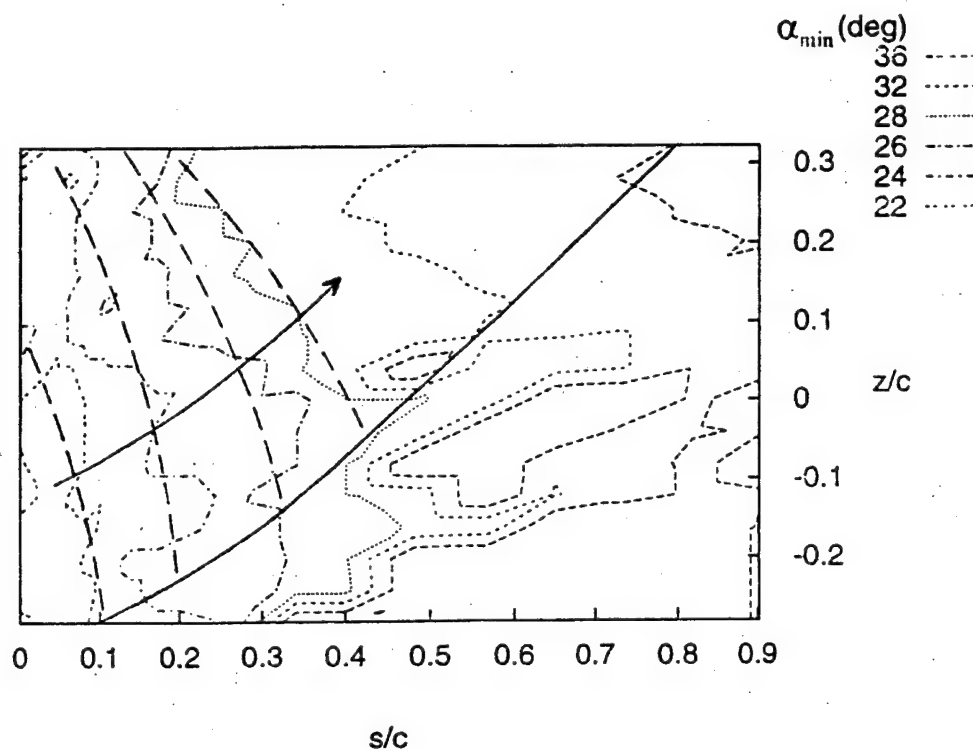
Figure 5. Lines of constant α_{min} in the s-z plane. $\alpha^+=0.075$. The broken lines denote the location of the average $C_{p(min)}$ front at different incidences. The arrow indicates the direction of front motion. The full line represents the limit to the left of which pressure minima can be identified.
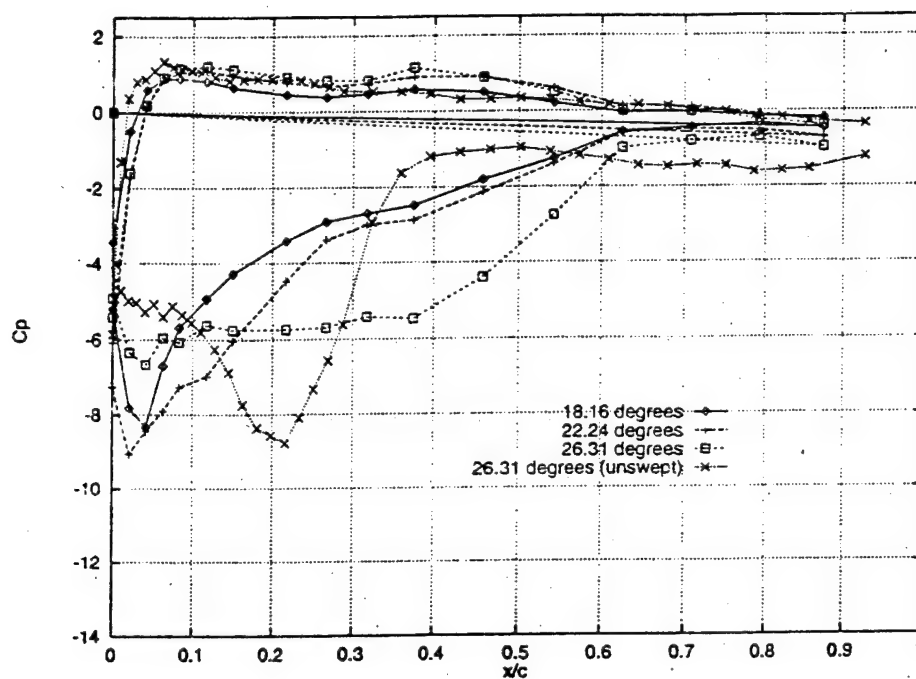
Figure 6. Typical phase-locked distributions at different incidences. $z/c=0$; $\alpha^+=0.075$. Unswept-wing data are from Ref.8.
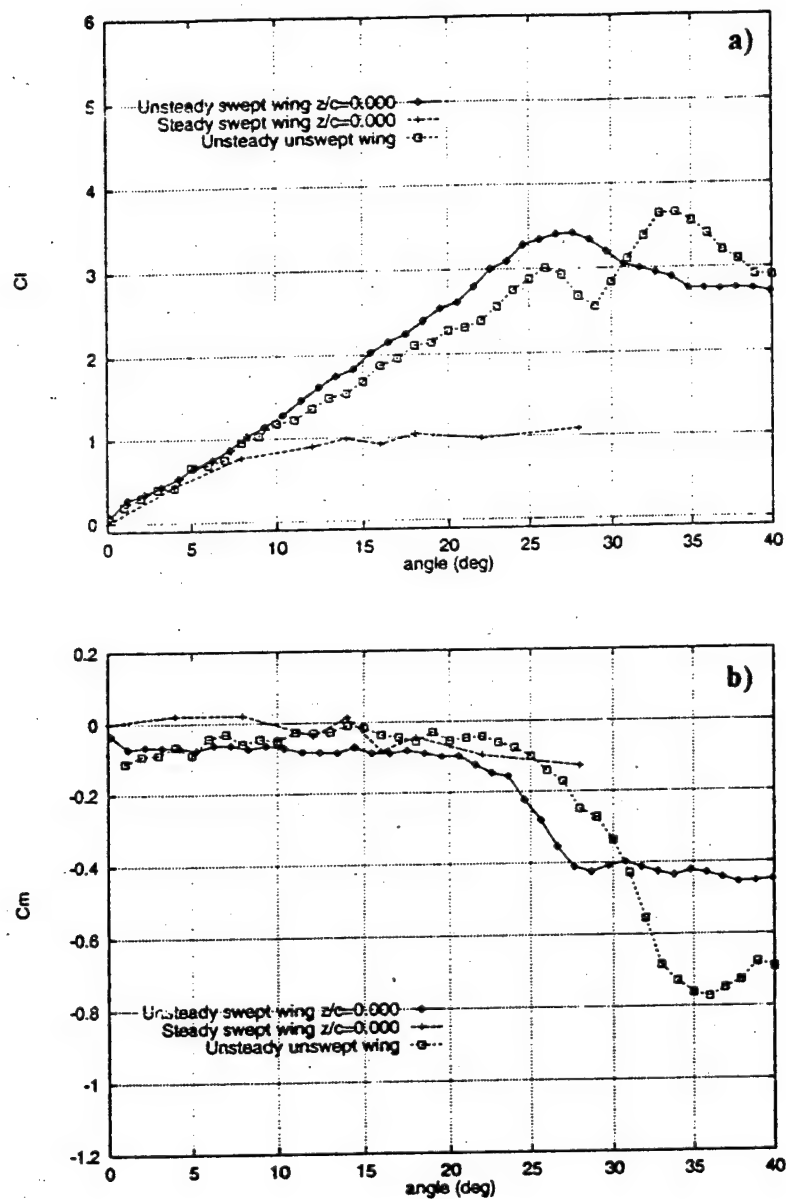
Figure 7. Lift and moment coefficient comparisons. Unswept wing data are from Ref.8. $\alpha^+=0.075$
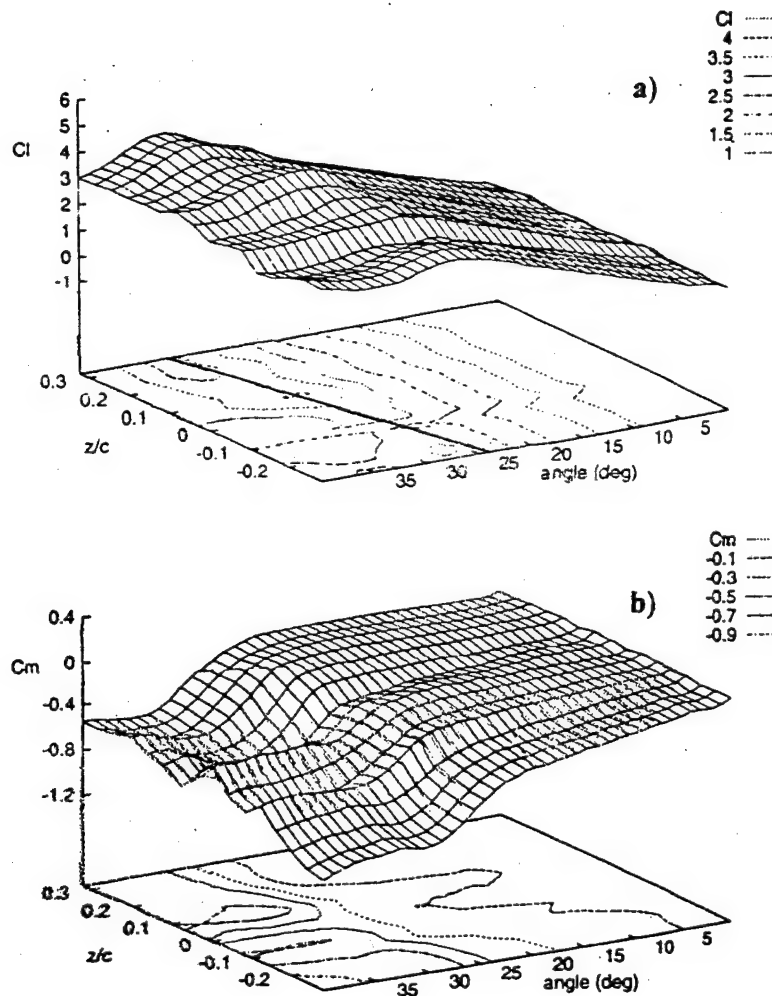
Figure 8. Variation of sectional lift and sectional pitching moment with incidence and spanwise location. $\alpha^+=0.075$
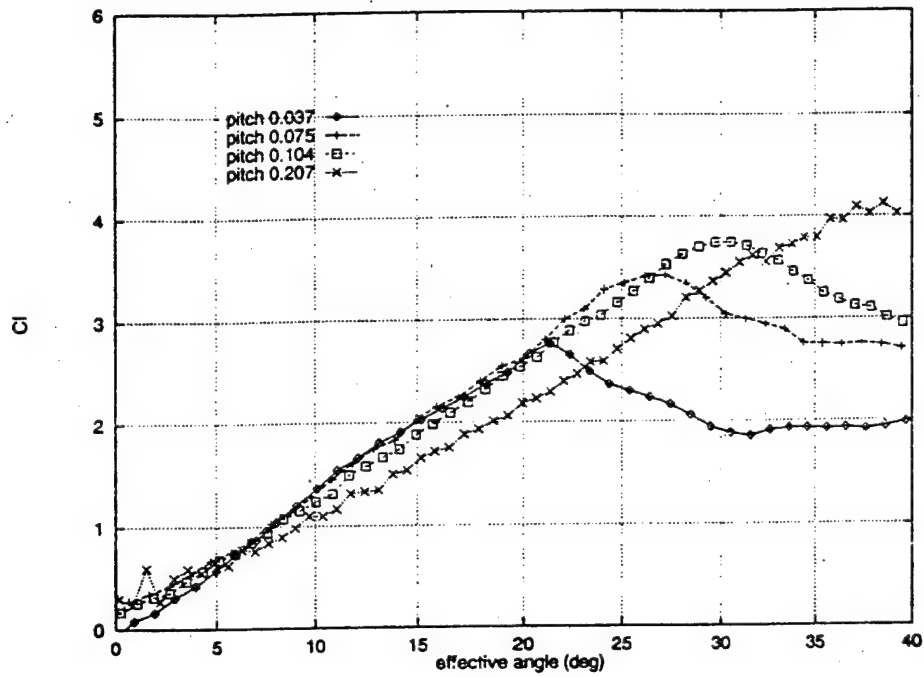
Figure 9. Effect of pitch rate on lift. z/c=0
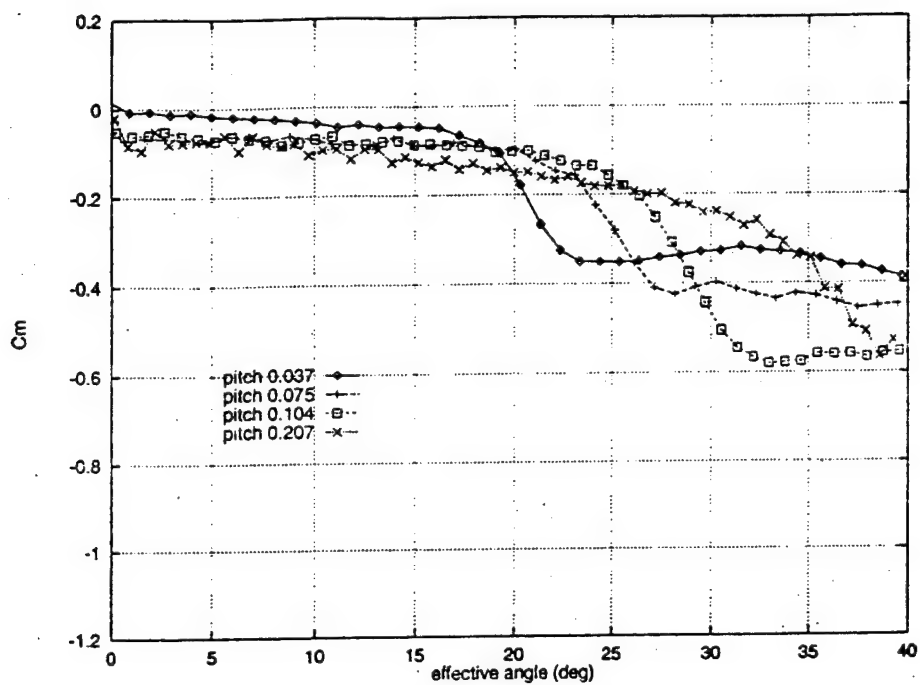
Figure 10. Effect of pitch rate on pitching moment. z/c=0
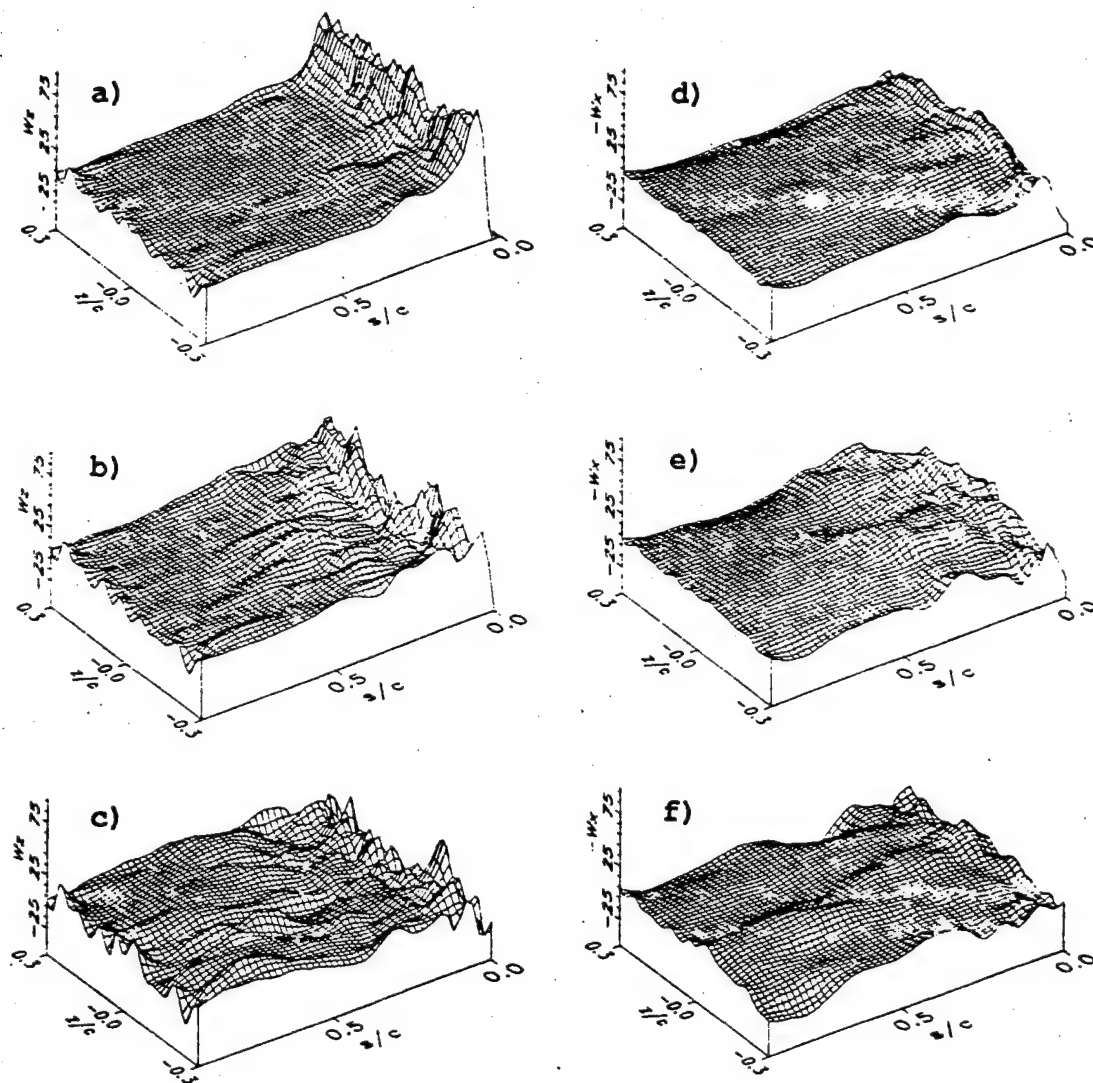
Figure 11. Vorticity fluxes W_z and W_x at the wing surface caused by pressure gradients in the x and z directions. $\alpha^+=0.075$. (a) and (d) are for $\alpha=20$ degrees, (b) and (e) are for $\alpha=24$ degrees, and (c) and (f) are for $\alpha=28$ degrees.
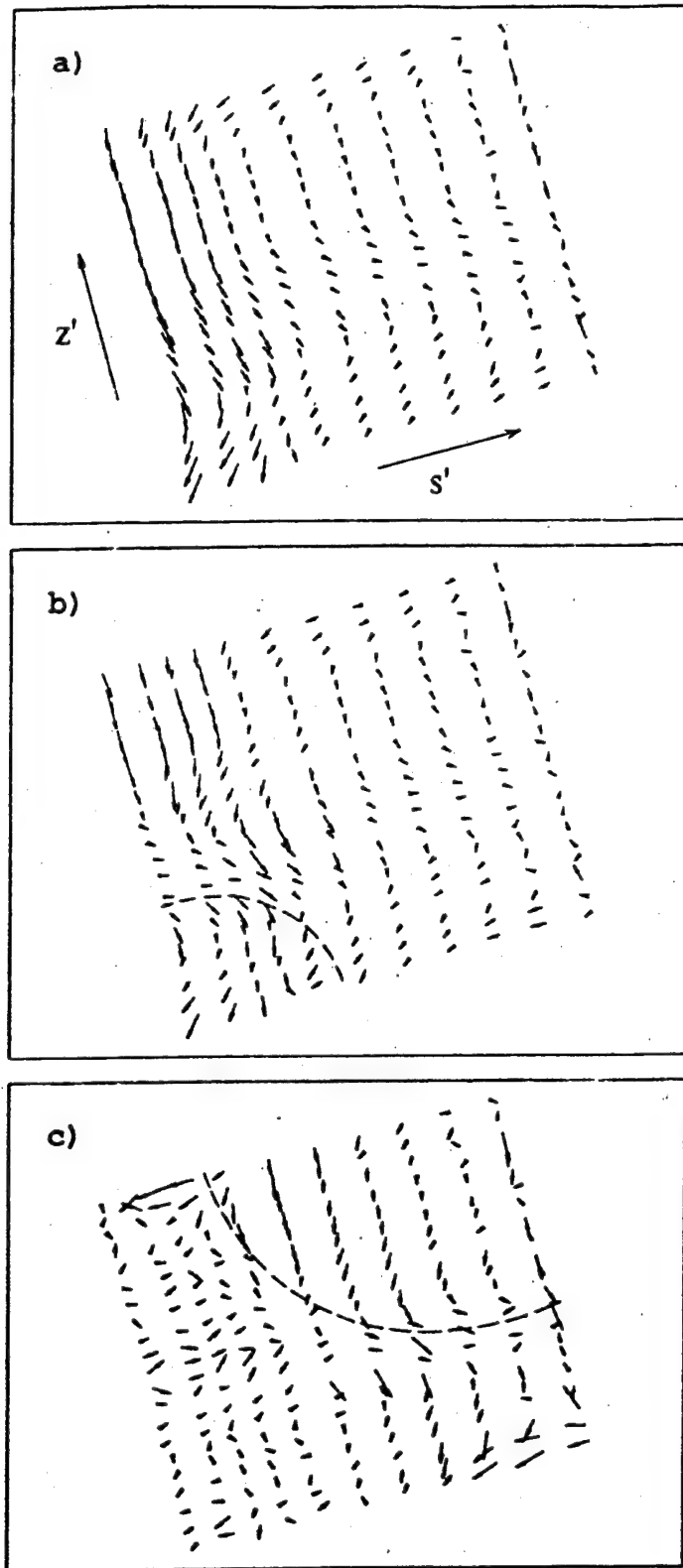
Figure 12. Vorticity flux vectors at the wing surface corresponding to the conditions in Fig.11.

AIAA 95-2161
Measurements of the Velocity and Vorticity Fields Around a Pitching Swept Wing

P.B. Rymarz and B.R. Ramaprian
Washington State University
Pullman, WA

26th AIAA Fluid Dynamics Conference
June 19-22, 1995/San Diego, CA

MEASUREMENTS OF THE VELOCITY AND VORTICITY FIELDS AROUND A PITCHING SWEPT WING

P.B. Rymarz[1] and B. R. Ramaprian[2]

Department of Mechanical and Materials Engineering
Washington State University, Pullman WA, 99164-2920

Abstract

This report presents measurements of the instantaneous velocity and vorticity fields around a pitching "infinite" swept wing of NACA 0015 profile and back sweep angle of 15 degrees. The experiments were performed in a water channel. The wing was pitched at a constant angular velocity α about an axis perpendicular to the free stream velocity U_∞. Velocity measurements were made using the technique of Particle Image Velocimetry (PIV). All measurements were made at a Reynolds number of 130,000 (based on chord c) and a non-dimensional pitch rate α^+ ($= \alpha c/U_\infty$) of 0.075. The objective of the study was to understand the fundamental aspects of vortex dynamics and lift production in three-dimensional flows, by studying a geometry which represents a *small* departure from two-dimensionality. The most significant observation is that even mild three-dimensional geometry causes both the dynamic stall and the accompanying loss of lift to be gradual rather than catastrophic. The detailed PIV data have also been used to study the vorticity transport in the flow. The basic experimental data have been archived and are available to any interested reader.

Nomenclature

c	chord measured along x
C_l	sectional lift coefficient, lift/$(1/2\ \rho U^2_\infty)$
C_p	Pressure coefficient, $(p-p_\infty)/(1/2\ \rho U^2_\infty)$
F_x	convective flux of spanwise vorticity per unit area along x
F_z	convective flux of spanwise vorticity per unit area along z
G_{accum}	rate of increase of accumulated vorticity per unit area
n	direction normal to the wing surface
p	local pressure
p_∞	freestream pressure
Re	Reynolds number $U_\infty c/\upsilon$
s	direction along the wing surface
t	time
U_∞	freestream velocity
v_s	s-component of local velocity
v_x	x-component of local velocity
v_y	y-component of local velocity
v_z	z-component of local velocity
W	rate of vorticity generation
x	freestream direction
y	direction normal to the x-z plane
z	spanwise direction (see Fig.2)
α	angular velocity of pitching
z	spanwise component of vorticity
ρ	density
υ	kinematic viscosity
ω_z	spanwise component of vorticity
overbar	denotes nondimensional quantity

Introduction

Numerous studies have been reported in recent years on the vortex dynamics and stall over pitching and oscillating airfoils. Most of these studies have been limited to two-dimensional flows. There have been some studies reported recently on three-dimensional unsteady vortex dynamics. These relate typically to

---

flows near wing tips, wing-body junctions, and flows over delta wings. However, the flows in these cases are extremely complex. The authors feel that an efficient initial approach to understand three-dimensional effects is to consider flow configurations which represent *small* departures from two-dimensional flows. Such a flow situation is produced when an "infinite" wing of small sweep is pitched about an axis perpendicular to the freestream. This flow is "quasi-two-dimensional" when the wing is stationary, but would be three-dimensional when the wing is pitched. The true three-dimensionality of the unsteady flow is a consequence of the pitch axis geometry, which causes the relative chordwise location of the pitch axis to vary in the spanwise direction. The configuration selected in the present studies approximates this situation.

Additionally, a swept wing with a pitch axis that varies in chordwise position along the spanwise direction, provides one a good opportunity to study the effect of pitch axis location. In their computational studies of two-dimensional flows, Visbal and Shang[1] concluded that a downstream displacement of the pitch axis resulted in delayed formation of the stall vortex but a lower maximum lift. Experimental studies on a swept wing will provide an opportunity to verify some of these computational results and further examine the effect of pitch axis.

Comprehensive studies of flows over pitching wings, both with and without sweep, have just been completed at Washington State University. In each case, the research effort was divided into three phases, namely, flow visualization, surface pressure measurements, and PIV measurements of the instantaneous flow field. Several of these studies have already been reported[2-5]. One of the distinguishing features of these studies is that both pressure and velocity/vorticity information has been obtained on the same model, in the same facility, and under the same flow conditions. The study reported in this paper represents the final phase of this overall research program. For a report on the surface pressure data of the swept wing, the reader is referred to Patterson, Rymarz, and Ramaprian[5].

Experimental Setup

The experiments were conducted in an open-surface water channel constructed specifically for this series of studies. The facility is schematically illustrated in Fig.1. It is constructed entirely of rust-proof materials like PVC, glass and stainless steel. It holds 5000 gallons of softened, filtered water, which is continuously recirculated by two 30-hp centrifugal pumps at test section velocities that can be varied from 0 to 0.5 m/s. The water is periodically monitored for pH level and chlorinated if necessary. The glass test section is 3.68 m long, 0.9 m wide, and 0.7 m deep. Flow in the test section has been measured to be uniform to within 1% and has a freestream turbulence level of about 1.2% at a test section velocity of 30 cm/s. More details of the flow facility can be found in Conger and Ramaprian[6].

The wing model is the same as was used earlier for flow visualization and pressure measurements. It has a 30-cm chord, a 61-cm span, and a back sweep angle of 15 degrees. It is assembled from 5-cm wide airfoil sections of NACA 0015 profile. These elements are machined from extruded aluminum stock on a numerically controlled milling machine. The wing is painted black to reduce reflection, and equipped with sacrificial anodes at the tip for corrosion protection. For more details of the model construction, see Patterson, Rymarz and Ramaprian[5].

The wing and mounting assembly form a single, removable unit as shown in Fig.2. The wing is sandwiched between two circular Plexiglas end plates, each of 1.2 cm thickness. The main support for the system is provided by a 1.2 meter square aluminum plate. The wing assembly is suspended vertically in the water channel such that the wing and the end plates can rotate about a vertical axis (the pitching axis), inside a 65-cm diameter ball bearing carried by the aluminum support plate. In order to keep vibration from the pumps to a minimum, the aluminum support plate is supported on a steel frame that is adjacent to but not in contact with the water channel. Placement of the wing assembly is such that the upper plexiglas plate just skims the free surface of the water. The presence of a constant water-plexiglas interface is needed to obtain distortion-free visualization of the flow field when viewed from the top.

Wing movement is provided by a computer-controlled stepper motor mounted on the aluminum support plate, but not directly over the pitching axis. The motor instead rotates the wing about the pitching axis via a chain drive. This design allows an unobstructed view of the flow field from above.

2

P.I.V. Setup

The entire water channel was seeded with polystyrene particles of 20 μm diameter and specific gravity of 1.04. These were used as the tracer particles for the PIV measurements. They were illuminated by a horizontal laser light sheet of approximately 1-2 mm thickness. The light source used was a pulsed copper vapor laser pulsing at a uniform rate of 6 kHz and operating at an average power of approximately 10 watts. The optical arrangement for the light sheet is shown in Fig.1. A Nikon F3 35-mm camera was mounted directly above the 65 cm bearing, as shown in Fig.2 and was focused through the top Plexiglas end plate onto the illuminated spanwise plane of interest. The camera moved with the rotating end plate, so that photographs were obtained in a frame moving with the wing. Multiple exposures of the tracer particles were produced by the use of a rotating slotted disk operating at 254 Hz and placed in the optical path of the laser (see Fig.1). The width of the slot was such as to provide an exposure period of about 1/2000 s. The camera shutter was set to remain open for 1/30 sec., thus making it possible to capture eight exposures of the particles in each picture. The above settings correspond to a maximum particle travel of about 4 mm in the streamwise direction between exposures, and an effective averaging time of 1/30 s. These can be compared with the chord length of 300 mm and the total pitching time of about 9s. The camera shutter itself was triggered by the computer to open at the rate of one frame per degree in the incidence interval of 0 to 33 degrees, so that 34 pictures could be obtained during one pitching realization.

It should be noted that the PIV system used can measure only two components of the velocity, in this case the streamwise (v_x) and cross-stream (v_y) components. The spanwise component of the velocity could not be measured. Also, the two-dimensional PIV system can, in principle, be used only in a two-dimensional flow. However, the mild spanwise flow present in the tests did not introduce any major difficulties in the measurement of the flow field using the two-dimensional PIV system.

Each photographic negative was digitized using a microscope objective, a CCD camera, and a digital image processor. A rectangular area 2.4 cm long and 1.85 cm high was analyzed on each negative. This represents an area of approximately 17 cm by 13 cm in the actual flow. This rectangular area was divided into a checkerboard pattern with 40 divisions per side, for a total of 1600 square segments to be analyzed. The velocity vector was computed at the center of each segment by evaluating the two-dimensional autocorrelation function of the digitized image of the particles, using a high-speed array processor installed inside the PC. The entire process was automated, and a computer controlled two-axis traverse moved the film from one position to another.

After the velocity vectors were obtained in the above manner, the results were examined for missing and spurious values, which were then either corrected (where possible), or interpolated from reliable neighboring values (where not possible). Such corrections/interpolations were usually limited to about 10% of the total number of vectors. The details of this procedure are reported in Oshima[7]. Also, after determining the velocity vectors, corresponding vorticity and stream function values were obtained using a series of post-processing programs developed and described in Oshima[7] and Rymarz[8].

Experimental Procedure

All the PIV data were obtained at a freestream velocity of about 32 cm/s (corresponding to a Reynolds number Re= 135,000) and a non-dimensional pitch rate α^+=0.075. Surface pressure data are available for this combination of Reynolds number and pitch rate from Ref.5. In order to achieve a higher spatial resolution of the velocity field, only 1/3 of the chord (forward, middle, or aft) was photographed during a pitching realization. The results thus obtained for the three regions from three separate pitching realizations were then combined to obtain the composite flow field over the entire wing.

Each realization consisted of a pitching maneuver from 0 to 33 degrees, with photographs being taken in one degree increments. Three spanwise planes of the wing were photographed in the midspan plane, as well as at two off-midspan planes, 5 cm above and 5 cm below the midspan plane. Although the somewhat small aspect ratio of the model does not allow it to truly represent an "infinite" airfoil, this region around the mid-span plane was judged to be nearly free from end effects, based on the results from the previous pressure measurements reported in Ref.9, and hence was considered to be satisfactory for studying the three-

3

dimensional effects introduced by sweep and pitch axis location.

A detailed discussion of the estimation of uncertainties associated with the present PIV measurements is provided in Ref.8. These estimates indicate that, v_x and v_y have an uncertainty of 4% over all the regions of the flow except in the immediate vicinity of the wall where the uncertainty is about 8%, and the vorticity and stream function values estimated from the velocity data have an uncertainty of 8% (16% immediately next to the wall) and 4% respectively.

Results and Discussion

The results for the mid plane of the wing will be presented first and compared with the corresponding results for an unswept wing under similar conditions of Reynolds number and pitch rate, the latter being taken from Oshima[7]. Note also that the location of the pitch axis for the mid plane of the swept wing is the same (c/4 from the leading edge) as for the unswept wing. The results will be shown for angles of incidence greater than 22 degrees, since no noteworthy changes occur at earlier incidences for both wings. It is however, important to note that in both cases, the flow would have stalled well before this incidence if the wing was stationary.

Figures 3 and 4 show a comparison of the velocity vectors and contours of spanwise vorticity on the suction side of the two wings. The flow fields for the two wings were found to be nearly similar at early angles of incidence. At an incidence of 20 degrees, both flows were found exhibit the presence of strong leading edge vorticity. These vortices were thin, stretched out, and stayed very close to the wing surface. Figure 3(a) and 4(a) show that as the angle of incidence increases to 22 degrees, the swept wing continues to exhibit nearly the same vorticity structure as described above. In the case of the unswept wing, however, a well-defined vortex has formed and has started to move away from the wall as the shear layer begins to separate.

The contrast between the two wings becomes stronger as the incidence increases to approximately 24 degrees. The shear layer over the unswept wing has definitely moved out and is about to leave the surface, while no major separation has occurred over the unswept wing. Finally, at the incidence of 26 degrees, the dynamic stall vortex has detached from the surface of the unswept wing and has, in fact, partially left the field of view. In comparison, the

dynamic stall vortex structure of the swept wing (essentially a rolled up shear layer with a large number of vortices) is still contained and remains near the wall at 26 degrees. In fact, the interesting features of the flow field over the swept wing are still completely within the field of view even at 28 degrees. Clearly, events at the leading edge seem to occur later in time for the case of the swept wing, particularly with regard to the shear layer detachment and the growth and lift-off of the dynamic stall vortex structure. These observations are consistent with the lift data for the two wings obtained in earlier studies, as seen in Fig.5 taken from Ref.5. It is seen that maximum lift occurs at 26 degrees in the case of the unswept wing, whereas, the lift continues to increase beyond 26 degrees in the case of the swept wing.

The trailing edge regions of both wings seem to have much more comparable development. Perhaps this is because the vorticity and velocity fields are typically not undergoing such rapid changes in comparison to the nose region, and therefore any differences in flow field constraints are not as immediately apparent.

The second major difference between the swept and unswept wing is the severity with which they seem to stall. Flow visualizations, pressure/lift measurements, and PIV measurements all strongly suggest that the stall process for the swept wing is much less abrupt. This is perhaps best supported by comparing the velocity and vorticity fields of the swept and unswept wings at approximately 26 degrees (Figures 3c and 4c). After separation, the flow over the leading edge of the unswept wing continues in a direction nearly perpendicular to the chord. This causes the dynamic stall vortex to leave much more abruptly and results in the more drastic loss of lift after stall as seen in Fig.5. The vortex structures of the swept wing, however, turn to follow a direction more nearly parallel to the chord of the wing after separation. Even at post stall angles, the shear layer of the swept wing has broken up into a large number of vortices, but the vortex structures are still moderately close to the wing surface. The gradual nature of the stall process over the swept wing was also evident from the vortex trajectory, computed and presented in Ref.8.

Streamline patterns at the midspan plane of the swept wing are shown in Figs.6(a)-(e) for α=26-30 degrees. Regularly shaped closed streamlines can first be detected at 26 degrees, where the dynamic stall vortex structure is clearly identifiable, along with

4

a significantly large reversed flow region at the nose of the wing. The closed streamlines representing the vortex structure move further downstream at 27 degrees, and the leading edge separation zone becomes larger, with less order to the streamlines. Two distinct and isolated vortical structures, one near the leading edge and the other nearer the trailing edgezare seen up to this incidence. At 28 degrees, the vortex structure seems much more spread out, and the more widely spaced streamlines indicate a less rapidly moving fluid in the leading edge separation zone, which now extends into the midchord region of the streamline plot. The isolation between trailing edge and leading edge flow structures gradually begins to blur beyond this incidence. Once the dynamic stall vortex structure gets large enough, it seems to draw in flow from the trailing edge. This feature was also apparent in the preliminary qualitative flow visualization studies.

The growth in the number of vortex structures and the break down of coherency continues in the post stall incidences of 29 and 30 degrees, but the structures still remain close to the surface. Therefore, the "washing away" of the dynamic stall vortex structures is quite slow. The difference between the vortex kinematics of the swept and unswept wingss can be further quantified by calculating the vortex trajectories in the two cases. These results are described in Ref.8. and will not be presented here for lack of space.

The less catastrophic loss of lift of the swept wing can be attributed to the fact that the flow has an additional possible direction of travel, in contrast with the two-dimensional flow over the unswept wing. When the three-dimensional flow no longer has the energy required to continue travel in the chordwise direction, it has the option of veering along the spanwise direction before separating. In a purely two-dimensional flow, however, the fluid particles have no where to go but away from the surface once they lack the necessary energy for chordwise motion.

Comparison Between Different Spanwise Planes

The work of Patterson *et al*[5] showed that in the case of the pitching swept wing, there was a significant variation of lift in the spanwise direction. This is seen from the three-dimensional plot of the sectional lift coefficient shown in Fig,7 taken from Ref.5. This figure shows that maximum lift occurs later and is slightly larger as z/c changes from -0.333 to +0.333. In order to supplement these lift data, PIV

data were obtained in the present experiments, as already mentioned, at two other planes in addition to the midplane. The spanwise spacing between the three planes corresponds to a change in pitch axis location (i.e. distance of the pitch axis from the leading edge) from $0.208c$ at $z=-5$cm to $0.292c$ at $z=+5$cm. Although this is a fairly small variation in pitch axis location, it was found that the contrast between the flow development in the three planes was quite striking.

Figures 8(a)-(c) show a comparison of the velocity vectors in the three different spanwise planes for three incidences. Within experimental error, the velocity fields at 24 degrees appear to be somewhat similar at all three planes, though the lowest plane $z=-5$cm exhibits a somewhat more advanced stage of evolution of the leading-edge vortex. The difference in the flow fields, was found to be more apparent at these early angles in the vorticity fields, which are not shown here for lack of space. Significant differences in flow development at the different planes become very apparent as the wing approaches stall. The velocity vector plots at 26 degrees indicate a more advanced vortex development as z goes from positive to negative values. The main vortex structure at the $z>0$ plane is completely contained within the leading edge region of the flow (i.e., within the first visualization frame), whereas the midplane vortex structure protrudes slightly into the midchord region, and the vortex structure at the $z<0$ plane has spread out over the entire wing. The contrast in stall development is even more spectacular at 28 degrees. In the $z>0$ plane, vorticity is still largely contained fairly near the surface of the wing, while in the midspan midplane, the vortex structures have evolved significantly more.

Although the flow evolution goes through essentially similar stages in all three planes, the leading-edge vortex appears first in the $z<0$ plane (with the pitch axis displaced most forward), slightly later in the $z=0$ plane, and last in the $z>0$ plane (with the pitch axis located most aftward). It appears that the wing stalls from negative z to positive z, or from planes with forward pitch axis location towards planes with aftward pitch axis location.

Since the flow stays attached longer in the latter regions, more circulation will be associated with the leading-edge shear layer vortex structure, since it is 'fed' by the high vorticity from the nose region for a longer period of time. One can hence expect that maximum lift will be higher and will occur later as z increases, as is indeed seen from the lift data in Fig.7.

This result, however, seems to be in contradiction with the numerical studies of unswept wings by Visbal and Shang[1], who found that maximum lift actually decreases as pitch axis moves aftward (although the computed flow does stay attached longer as observed in the present experiments).

Vorticity Balance

Following earlier studies[2,10] on unswept wings, the instantaneous conservation equation for vorticity in the unsteady flow over the pitching swept wing is examined in the light of the PIV data. Consider a control volume bounded by the side ds along the wing surface, faces a and b in the $n-z$ plane, faces c and d in the $s-n$ plane, and extending to ∞ in the n direction. For this control volume, we can write the integral equation for the conservation of the spanwise vorticity, on a unit area basis as

$$\frac{d}{dt}\int_0^\infty \omega_z \, dn = -\frac{d}{ds}\int_0^\infty v_s \omega_z \, dn - \frac{d}{dz}\int_0^\infty v_z \omega_z \, dn - \upsilon \frac{\partial \omega_z}{\partial n}\Big|_{n=0} \quad (1)$$

In writing eq.(1), we have neglected the effect of streamline curvature. Nondimensionalizing the terms in eq.(1) by using U_∞ and c as the relevant velocity and length scales, we can write

$$2\frac{d}{dt}\int_0^\infty \overline{\omega}_z \, d\overline{n} = \left(\frac{2}{\Delta s}\int_0^\infty \overline{v}_x \overline{\omega}_z \, d\overline{n}\Big|_a - \frac{2}{\Delta s}\int_0^\infty \overline{v}_x \overline{\omega}_z \, d\overline{n}\Big|_b\right)$$

$$+ \left(\frac{2}{\Delta z}\int_0^\infty \overline{v}_z \overline{\omega}_z \, d\overline{n}\Big|_c - \frac{2}{\Delta z}\int_0^\infty \overline{v}_z \overline{\omega}_z \, d\overline{n}\Big|_d\right) - \frac{2}{Re}\frac{d\overline{\omega}_z}{dn}\Big|_{\overline{n}=0} \quad (2)$$

The arbitrary factor of 2 has been used to make the last term on the right hand side equal to the nondimensional pressure gradient, as will be seen later. The term on the left side of eq.(2) represents the time rate of increase of accumulated vorticity (G_{accum}) within the control volume. On the right hand side of the equation, the first two terms in parentheses represent the net influx of spanwise vorticity into the control volume by convection in the chordwise direction (F_x), and the second two terms in parentheses represent the net influx of spanwise vorticity into the control volume by convection in the spanwise direction (F_z). The last term represents the rate of production of spanwise vorticity at the wall (W). This term can also be regarded as influx of spanwise vorticity by viscous diffusion from the wall

in to the control volume. From applying the Navier-Stokes equations at the wall ($n=0$), we can write

$$\frac{\partial p}{\partial s} = \mu\Big|\frac{\partial^2 u}{\partial n^2}\Big|_{n=0} \quad (3)$$

Using the definition of spanwise vorticity and introducing the pressure coefficient C_p, we can finally write

$$\frac{2}{Re}\frac{\partial \overline{\omega}_z}{\partial n}\Big|_{\overline{n}=0} = -\frac{\partial C_p}{\partial(s/c)} \quad (4)$$

Thus the last term on the right side of eq.(2) is also equal to the instantaneous nondimensional pressure gradient along the surface. Therefore, we have

$$G_{accum} = F_x + F_z + W \quad (5)$$

Two out of the four terms in eq.(5), namely, G_{accum} and F_x can be calculated from the PIV data. The third term W can be calculated from the pressure data obtained earlier under identical conditions in Ref.5. The fourth term F_z can then be estimated as the closing term in eq.(5). Since F_z represents the net convection of spanwise vorticity in the spanwise direction, through the plane of interest, it can provide some insight into the three-dimensional nature of the flow. It is important to note, however, that the terms in eq.(5) estimated from the PIV measurements have larger uncertainties than the velocity and vorticity data. Estimated uncertainties are: G_{accum}, 15%; F_x, 15%; and W, 10%. The term F_z obtained as the closing term has an uncertainty of 25%. These accuracy limitations have to be kept in mind while attempting to interpret the results.

Figures 9-11 show the distributions of G_{accum}, F_x and W at several angles of incidence in the range 20-30 degrees. These results pertain to the midspan plane. First, referring to G_{accum} (Fig.9), it is seen that at 20 and 22 degrees, the change in vorticity is fairly small everywhere over the wing. As the angle increases to 24 degrees however, negative vorticity begins to accumulate rapidly, especially near the leading edge. This leads to the inception and growth of the so-called leading-edge vortex with center around $x/c \approx 0.12$ at an angle of incidence of about 24

6

As the angle of incidence increases, the peak in G_{accum} moves downstream. This is consistent with the observed convection of the vortex center downstream. It is also significant that other peaks begin to appear along the wing. In fact, the distribution of G_{accum} along the wing becomes substantially periodic at higher angles of incidence. This periodic accumulation of vorticity along the wing can be attributed to one or both of two factors - (i) longitudinal periodicity in the rate of production of vorticity at the wall (W), (ii) longitudinal periodicity in the net influx of vorticity by convection in the x and/or z directions (i.e., periodicity in F_x and/or F_z). Figure 10 shows the flux through the wall (W), as calculated from the surface pressure data of Patterson[9]. Most of the negative vorticity flux through the wall seems to be originating very near the nose, with the region immediately downstream contributing to the generation (and infusion) of positive vorticity. This is a direct consequence of the nature of the pressure gradient along the wall. The wall vorticity flux, however, is clearly not periodic in the longitudinal direction and hence is not responsible for the periodic accumulation of vorticity seen in Fig.9.

In contrast to the above result, the plots of F_x shown in Fig.11 are clearly periodic along the wing. This periodic behavior is apparent as early as 20 degrees, and continues up to post-stall angles. It therefore appears that the convection is primarily responsible for the wavy nature of the accumulation of vorticity.

The convection of spanwise vorticity in the spanwise direction (F_z), obtained as the closing term of eq.(5) is shown in Fig.12. As was the case with F_x, there is a significant periodic variation in the distribution of F_z. In contrast with F_x, however, F_z is slightly less periodic at the lower angles of attack. At twenty degrees, the modulation in spanwise flux along the chord is quite small, and even approaches zero near the trailing edge. F_z does not seem to display significant modulation until 24 degrees. As the angle of attack increases, this periodicity grows in magnitude and spreads more and more uniformly across the chord toward the trailing edge. It should be noted that negative peaks in these spanwise vorticity plots correspond to transport of vorticity from positive to negative z values (i.e., from the top towards the bottom of the wing model in the experimental set-up) and that non-zero values of F_z are, in general, indicators of three dimensionality of the flow.

Conclusions

Even though the geometry studied represented a small departure from two-dimensionality, significant three-dimensional and pitch-axis location effects were observed in the present experiments. These are summarized below.

1)   The vortex structures remained close to the surface of the swept airfoil. In fact, the dynamic stall vortex was never actually washed away from the swept wing even at the highest post-stall incidence of 34 degrees studied in the present experiments. Hence, post-stall loss of circulation and lift was gradual rather than catastrophic.

2)   The dynamic stall "vortex" at the larger incidences over the swept wing is really a conglomeration of a number of smaller vortex structures that spread out over the entire wing surface. The swept wing stalls as the vortical structures begin to move away one by one from the surface. The unswept wing, in contrast, stalls after the dynamic stall vortex is abruptly swept away as a single structure. The distributed vortex structure, as well as the noncatastrophic nature of stall are believed to be the general characteristics of all three dimensional flows.

3)   The trailing edge flow of the swept wing does not seem to influence the lift-off of the leading-edge vortex structure. Rather, the leading-edge vortex seems to be pushed away from the surface of the wing by a localized build-up of low energy fluid. While this feature can be observed over the unswept wing also, it is more clearly observed over the swept wing.

4)   A strong spatial periodicity was observed in the rate of accumulation of vorticity along the swept wing. This periodicity is caused essentially by periodic convection of vorticity in both the chordwise and spanwise directions. The origin of this periodicity is unknown. It is also not clear whether this periodicity is peculiar to the specific mildly three-dimensional geometry studied in the present experiments, or whether it is a characteristic feature of all three-dimensional flows.

5)   There is strong evidence that aftward movement of the pitch axis delays the dynamic stall process, as well as slightly increasing the maximum lift produced by the wing. The present data trend (strong monotonic variation with z) suggest that this is primarily a pitch-axis location effect, and should be observable in two-dimensional flows also.

7

Acknowledgments

References

1. Visbal, M.R., and Shang J.S., "Investigation of the Flow Structure Around a Rapidly Pitching Airfoil", *AIAA Journal*, vol. 27 no. 8, 1988, p 1044.

2. Oshima, H., and Ramaprian, B.R., "Measurements of the Velocity and Vorticity Fields over a Pitching Airfoil," AIAA Paper No. 92-226, 1992.

3. Conger, R.N., Oshima, H., and Ramaprian, B.R., "Experimental Studies of the Unsteady Vortex Dynamics of a Two-Dimensional Pitching Airfoil", Proc. of the *11th Australasian Fluid Mechanics Conference*, University of Tasmania, Hobart, Australia, 14-18, Dec. 1992, p 1117.

4. Conger, R.N., and Ramaprian, B.R., "Pressure Measurements on a Pitching Airfoil in a Water Channel," *AIAA Journal*, Vol.32, No.1, Jan 1994, pp.108-115.

5. Patterson, A.K., Rymarz, P.B., and Ramaprian, B.R., "Surface Pressure Measurements on a Pitching Swept Airfoil in a Water Channel", to appear in the *AIAA Journal*, April 1994.

6. Conger, R,N, and Ramaprian, B.R., "The WSU-MME 1m x .7m Water Channel", Report No. MME-TF-92-1, Department of Mechanical and Materials Engineering, Washington State University, Pullman, WA, May 1992.

7. Oshima, H. " The Use of Particle Image Velocimetry for the Study of the Vortex Dynamics of a Pitching Airfoil", Ph.D. Thesis, Mechanical and Materials Engineering Department, Washington State University, Pullman, WA, July 1994.

8. Rymarz, P.B., " Measurements of Velocity and Vorticity Fields around a Pitching Swept Wing," M.S. Thesis, Mechanical and Materials Engineering Department, Washington State University, Pullman, WA, June 1995

9 .Patterson, A.K., "Surface Pressure Measurements on a Pitching Swept Airfoil in a Water Channel," M.S. Thesis, Department of Mechanical and Materials Engineering, Washington State University, Pullman, WA, Dec 1993.

10. Shih, C., Lourenco, L., Van Dommelen, L., and Krothapalli, A., "Unsteady Flow Past an Airfoil Pitching at a Constant Rate", *AIAA Journal*, May 1992, p.1153.
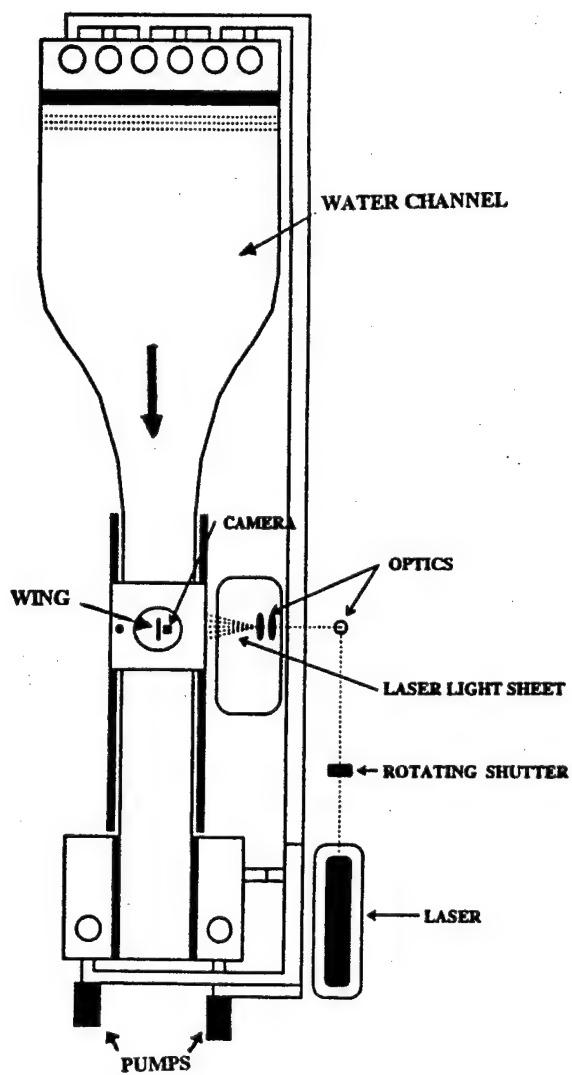
Fig.1. Schematic of the experimental setup and optical arrangement for light sheet.
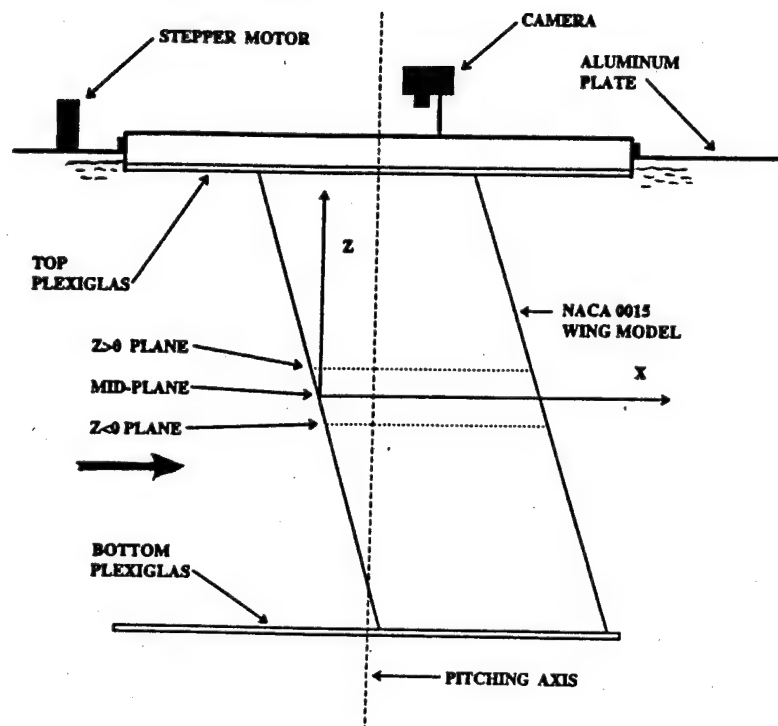
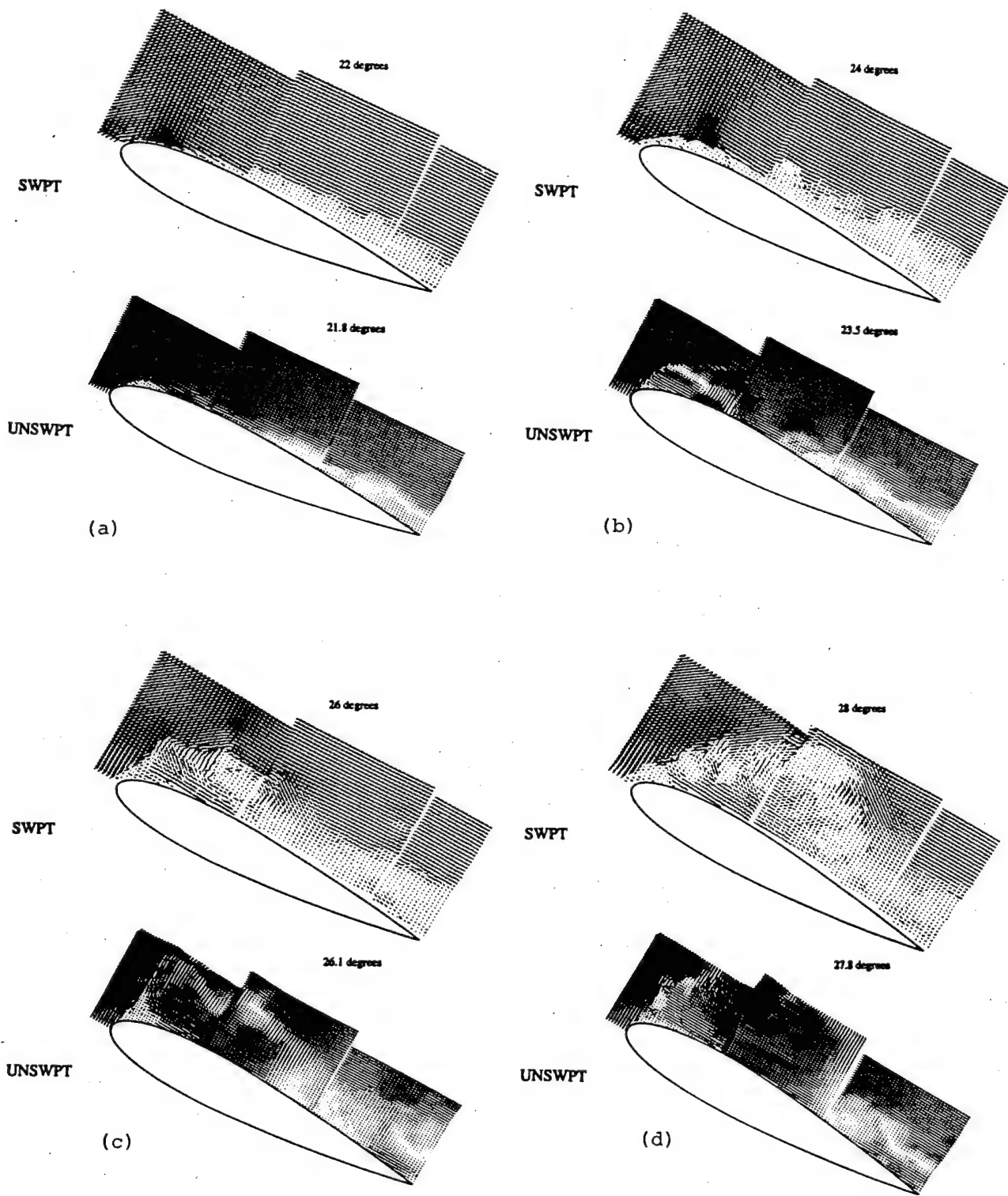Fig.2. Details of wing mounting and flow visualization.

Fig.3. Instantaneous Velocity vectors in the midspan plane (z=0) over the suction side of the swept wing. Comparison with unswept wing data from Ref.7.
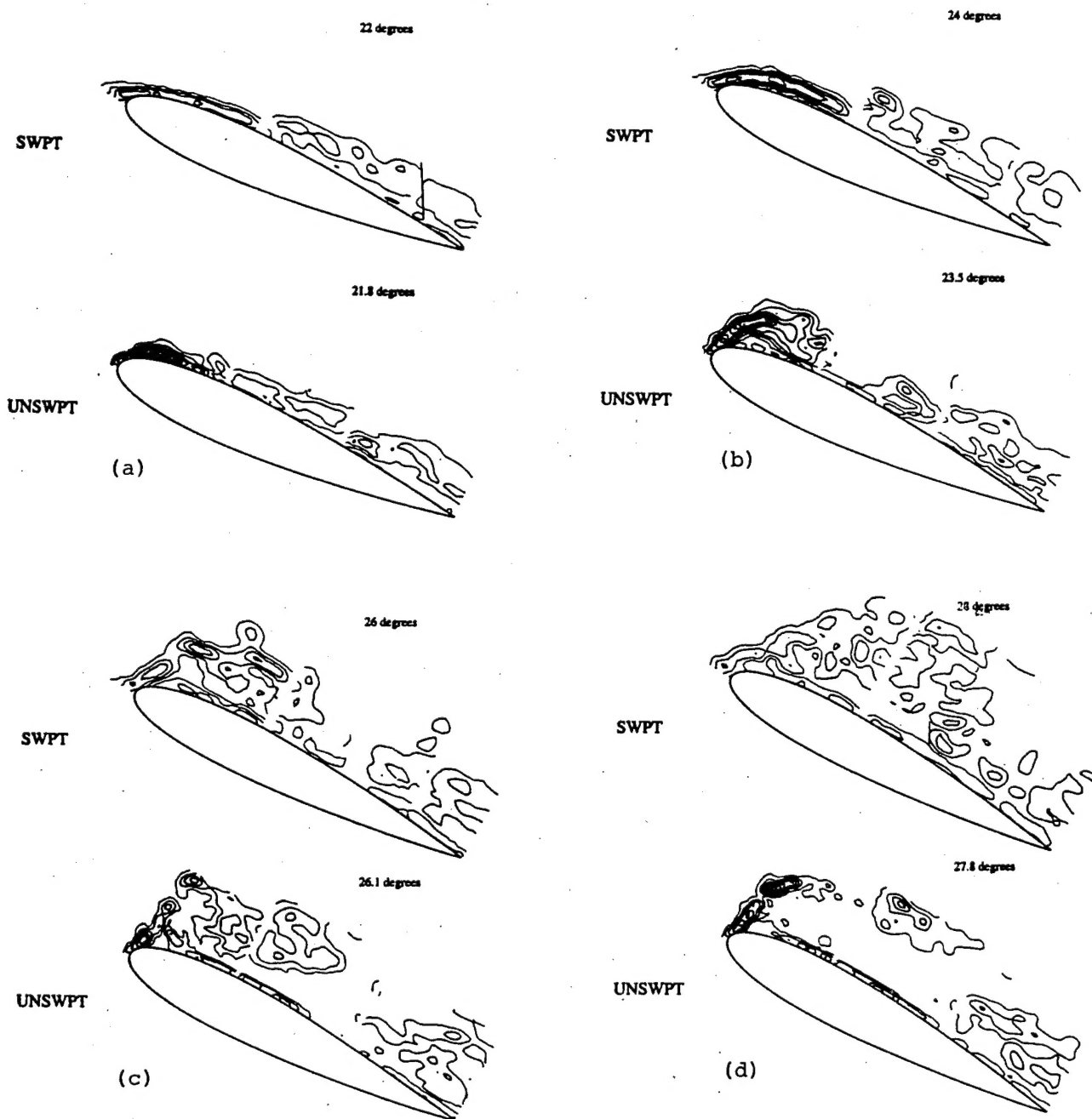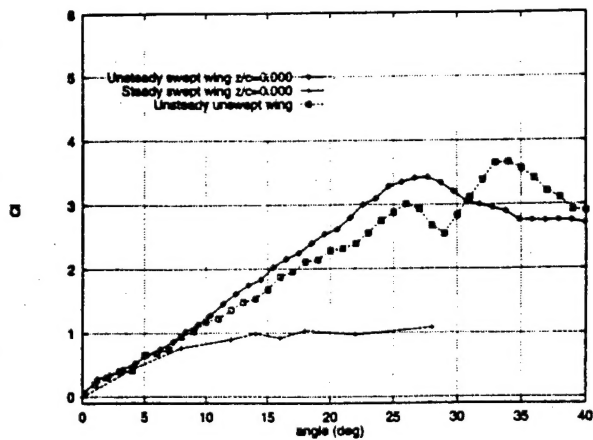
22 degrees

SWPT

21.8 degrees

UNSWPT

(a)

24 degrees

SWPT

23.5 degrees

UNSWPT

(b)

26 degrees

SWPT

26.1 degrees

UNSWPT

(c)

28 degrees

SWPT

27.8 degrees

UNSWPT

(d)

Fig.4.   Instantaneous contours of ω_z in the midspan plane (z=0) over the suction side of the swept wing. Comparison with unswept wing data from Ref.7.

11

Fig.5. Lift data for swept and unswept wings (from Ref.5).
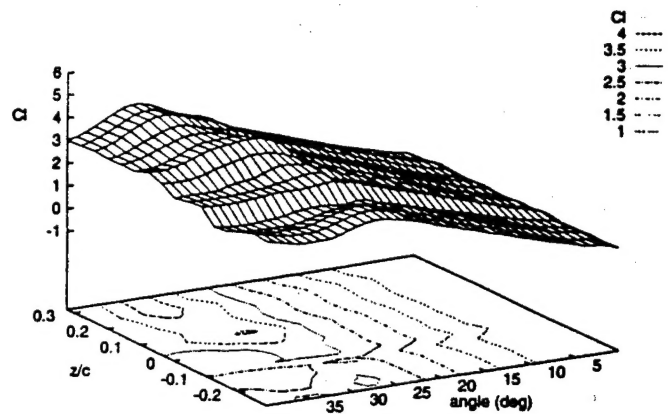
Fig.7. Sectional lift coefficient for the swept wing (from Ref.5)
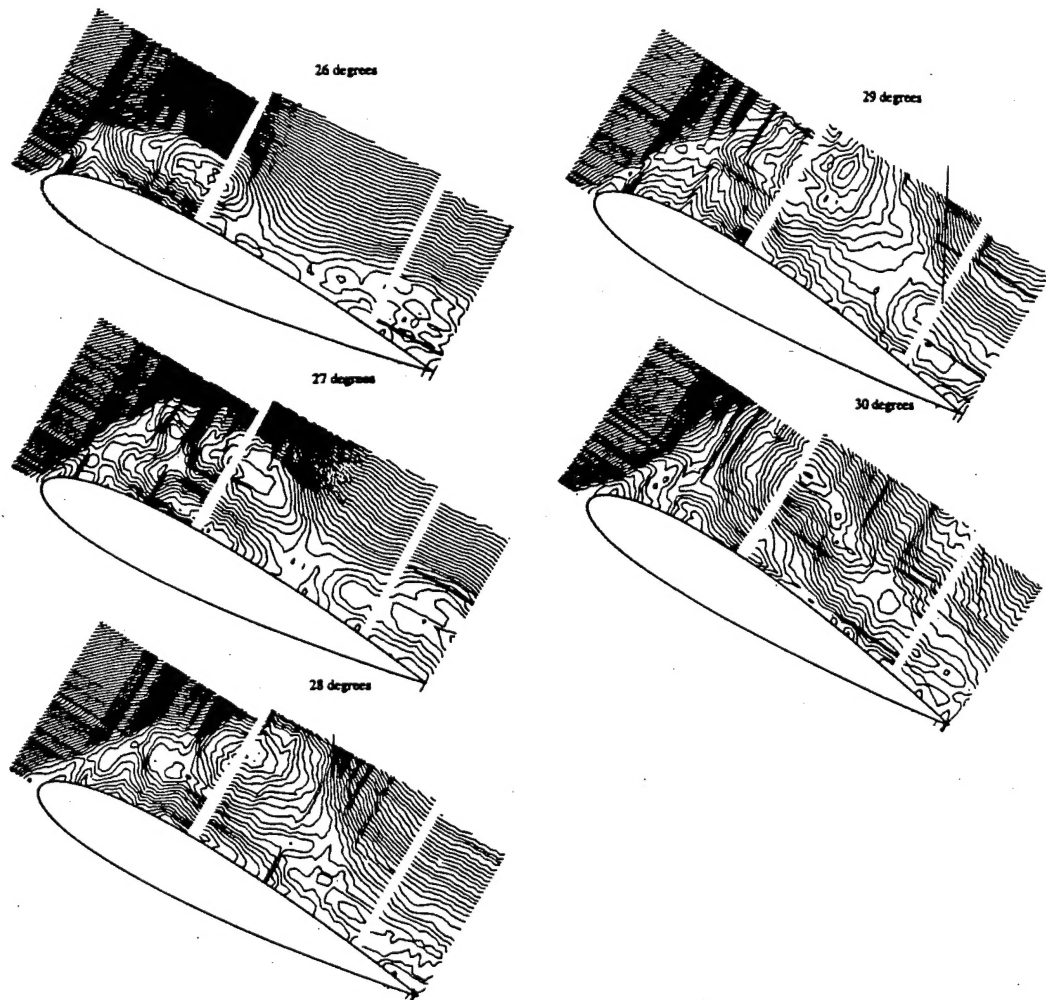
Fig.6. Instantaneous streamline pattern in the midspan plane (z=0) over the suction side of the swept wing.

12

(a)

(b)

(c)

Z > 0

Z = 0

Z < 0

24 degrees

26 degrees

28 degrees
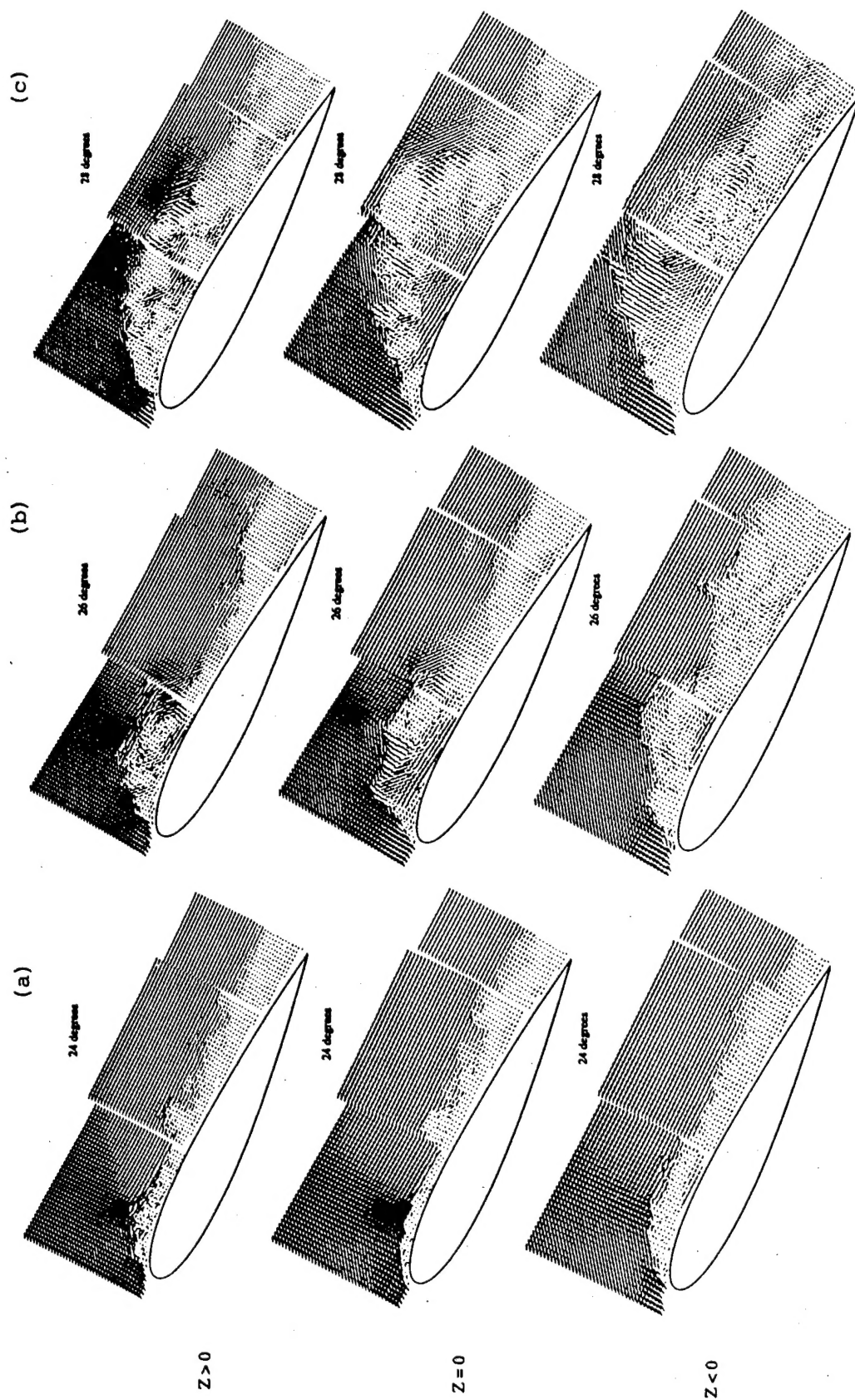
Fig.8. Comparison of the instantaneous vectors in the three planes z=+5 cm, z=0, z=-5 cm.

13
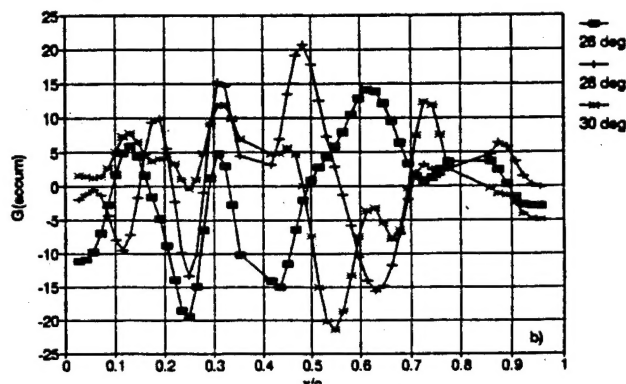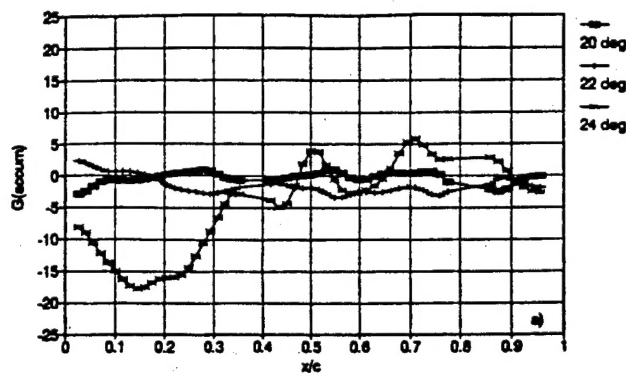
Fig.9. Instantaneous distributions of G_{accum} along the wing surface
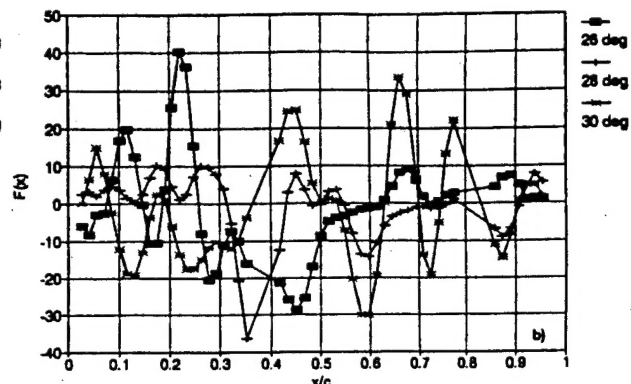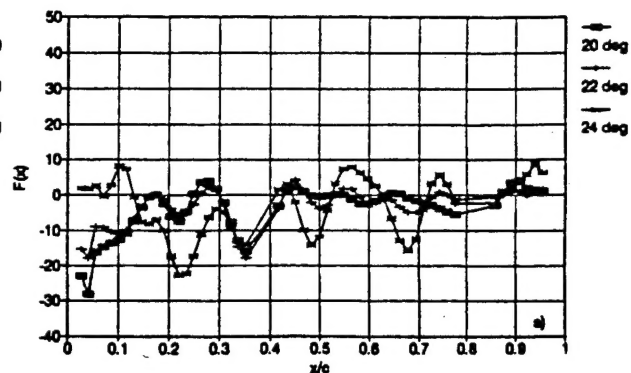
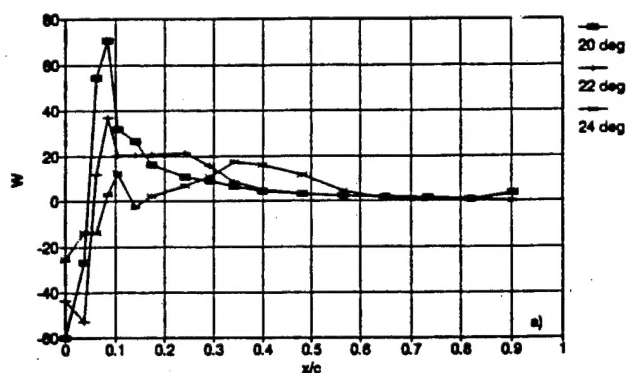Fig.11. Instantaneous distributions of F_x along the wing surface.
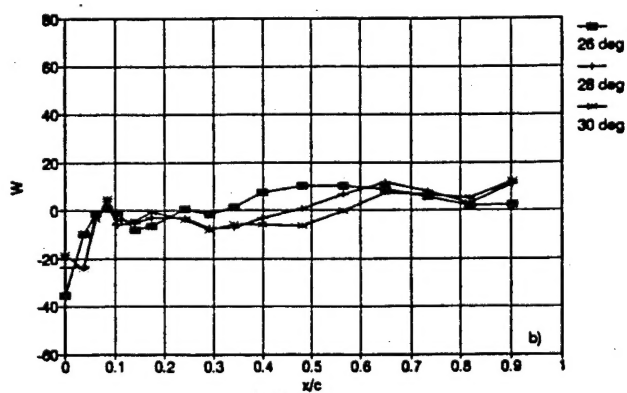
Fig.10. Instantaneous distributions of W along the wing surface, as calculated from eq.(4) using the pressure data of Ref.5.
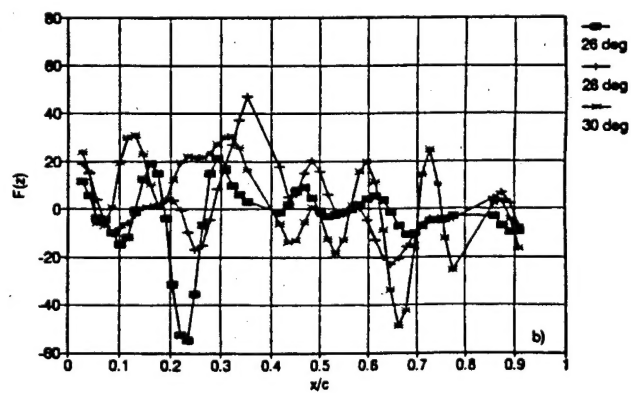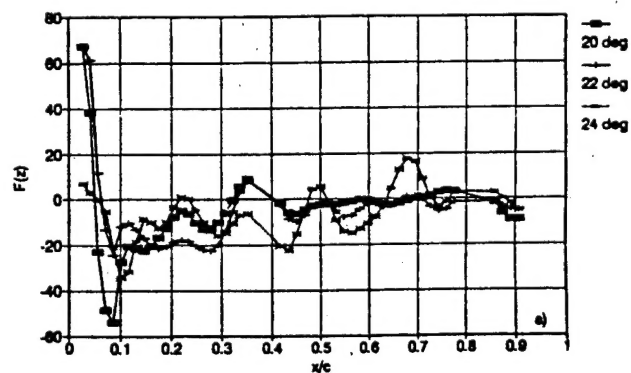

Fig.12. Instantaneous distributions of F_z along the wing surface, obtained as the closing term in eq.(2).

14